THE UNIVERSITY OF
SYDNEY

Dynamics of Bragg Grating Solitons In Coupled Bragg Gratings With Dispersive Reflectivity

by

BABAK HAJI BARATALI

A thesis submitted in fulfillment of the requirements for the degree of Doctor of Philosophy

THE UNIVERSITY OF SYDNEY

Faculty of Engineering and Information Technologies

University of Sydney

2014

Abstract

We study properties and dynamics of Bragg grating solitons in a system of linearly coupled Bragg gratings equipped with Kerr nonlinearity. The effects of dispersive reflectivity on the behaviour of gap solitons in the system are also investigated. To this end, nonlinear coupled mode equations are solved numerically.

Gap solitons, whether quiescent or moving are found to exist throughout the bandgap of the structure. We show that the system supports two types of symmetric and asymmetric gap solitons that can have any velocities from zero to the speed of light in the medium. At given soliton parameters a critical coupling coefficient, bifurcation point, is found above which only symmetric solitons exist. Below the bifurcation point however, both types of gap solitons may exist at the same time.

Linear forms of coupled mode equations are solved analytically. We show that these solutions are in excellent agreement with the gap soliton tails. This is done in both cases of quiescent and moving gap solitons. Interestingly, dispersive reflectivity results in the change of soliton profiles. Also, using the linear analysis a condition is found for the gap solitons to have sidelobes in their tails.

Stability of gap solitons are investigated using systematic numerical simulations. A general rule for the stability of both quiescent and moving gap solitons is concluded: it is found that when dispersive reflectivity is zero, asymmetric solitons are stable for $\omega \gtrsim 0$. While with increase of dispersive reflectivity the stable region expands into the negative frequencies. Symmetric solitons on the other hand are found to be

stable where they exist on their own.

Interactions of quiescent gap solitons in the model are studied numerically. Through various simulations we found that interactions of quiescent solitons generally depend on the initial separation (Δx) and phase difference ($\Delta\varphi$). However, when the dispersive reflectivity parameter is small, Δx-dependence is very weak. Depending on the parameters, interactions are found to result in a number of outcomes including merger into a single quiescent soliton, destruction of solitons, formation of a bound state that eventually breaks up into two separating solitons, formation of two moving and one quiescent soliton and repulsion of solitons. A key finding is that destruction and $2 \rightarrow 3$ transformation can occur even if dispersive reflectivity is absent.

In the case of moving solitons, collisions of counter-propagating gap solitons are investigated. In-phase collisions are studied and several outcomes are identified among which merger of the solitons into a single quiescent and $2 \rightarrow 3$ transformation are the most interesting ones. On the contrary, out-of-phase collisions generally result in the repulsion of the pulses.

Acknowledgements

I would like to thank Associate Professor Javid Atai for his excellent supervision of this research project and for all of his help and advice during my PhD. Not only he guided me in conducting the research but also taught me other aspects of being in a scientific community.

I would also like to thank my friends and colleagues in Fiber Optic and Photonic Laboratory (FPL) for their assistance and fruitful discussions about solitons; particularly Sahan, Saddam, Jahed, Tony, Xudong, and Weiwei.

Last but not least, I appreciate the support from my beautiful wife and my dedicated parents without whom I couldn't get this far.

List of Publications

Journal Papers

1. B. H. Baratali and Javid Atai, "Properties of moving gap solitons in dual core Bragg gratings with dispersive reflectivity," to be submitted.

2. B. H. Baratali and J. Atai, "Dynamics of interacting solitons in dual core Bragg gratings with dispersive reflectivity," *J. Appl. Phys.* **115**, 153112 (2013).

3. B. H. Baratali and J. Atai, "Gap solitons in Dual-Core Bragg Gratings with Dispersive Reflectivity," *J. Opt.* **14**, 065202 (2012).

Conference Papers

1. B. H. Baratali and Javid Atai, "Moving Gap Solitons in Coupled Bragg Gratings with Dispersive Reflectivity," Photonics Conference (IPC), USA, 2013 IEEE.

2. B. H. Baratali and Javid Atai, "Interactions of gap solitons in linearly coupled Bragg gratings with dispersive reflectivity," Photonics Conference (IPC), USA, 2012 IEEE.

3. B. H. Baratali and Javid Atai, "Gap solitons in coupled Bragg gratings with dispersive reflectivity," Photonics Conference (PHO), USA, 2011 IEEE.

Contents

List of Figures

Chapter 1

Introduction

1.1 Optical Communications: Overview

High-speed long-distance communication is an essential part of today societies. Every year the rate at which digital information is carried over telecommunication networks increases exponentially. This demands for new technologies that offer higher bandwidth, more reliability, better management, more versatility, and more importantly less cost. Optical communication specially fiber-based networks play a vital role in connecting today's users across the world. Theoretically, the optical carrier offers low-loss transmission over a wide range of frequencies of about 50 THz. In addition, other advantages such as low cost, easy installation, signal security compared to many other media, life more than 25 years, wider bandwidth i.e. accommodation of more channels, no electromagnetic interference (EMI), and abundant availability of raw material makes fiber the ideal communication medium among all other types of transmission media [1].

Historically, the field of fiber optics developed rapidly starting from 1960s when Light Amplification by Stimulated Emission of Radiation, i.e. LASER, was invented. It soon exploded during 1970s with the development of new fiber fabrication tech-

nologies [2] and became a communication revolution with the invention of low loss fibers in 1979 [3]. The fast-paced development of the field of optics, and generally communications, has been due to the exponentially-increasing need for transmitting digital data, which initially was in the form of voice signals but soon digitized images came into play which demanded for transmission of huge volume of data in the backbone networks altogether. This was not possible with the use of traditional copper cables which were the main medium.

With significant decrease in fiber loss by using 1550 nm band, there were still other effects preventing long-distance communication channels: dispersion and nonlinearity. This led to the invention of dispersion-shifted fibers and discovery of many nonlinear effects such as birefringence, Self-phase modulation, stimulated Raman scattering (SRS) and stimulated Brillouin scattering (SBS) [4]. It was a result of the advancements of nonlinear optics during 1970s and 80s that optical solitons were developed and later on observed experimentally.

The advancements of fiber optics continued at even a faster pace with the invention of Erbium-dopped fiber amplifiers (EDFA) in 1987 which allowed amplification in the 1550 nm wavelength region and reduction in cost and amplifier noise compared to the existing optical or electro-optical amplifiers. In a 1998 study various transmission experiments are reviewed in which transmission capacities of up to 1 Tb/s and greater are achieved over a single fiber using different techniques [5]. With the use of fiber amplifiers and incorporating gratings, which were first made in 1987, the field of optical solitons also became a hot topic among researchers and scientists which continues to date. In the next section we will briefly review optical solitons history and their importance in today's communication network.

1.2 History of Optical Solitons

Optical solitons are one of the most enchanting phenomena found in optical fibers which occur as a result of the balance between the fiber nonlinearity and dispersion. Solitons, being special types of waves that can propagate undistorted over long distances, have been discovered in many branches of physics. Historical records show that the first observation of solitons date back in 1834 when John Scott Russell accidentally watched the motion of water heaps in a narrow channel [6]. The waves propagated for long distances keeping their shape and speed, as he stated in his report.

In 1965 Norman Zabusky and Martin Kruskal demonstrated solitary waves in plasmas subject to the Korteweg–de Vries equation (known as KdV equation) via computational techniques using a finite difference method [7]. They coined the term "soliton" to point out the particle-like behavior of such waves specially during collisions. In contrast to solitons, water waves change their amplitude when interact with each other, which is why they are not solitons; sometimes called solitary waves in the literature to differentiate their properties from solitons. Nonetheless, scientists have used the term soliton to refer to any types of waves that are of permanent form and can interact with one another without change of shape.

KdV equation was first derived in 1895 to explain soliton-like waves in shallow waters. In its simplest form KdV equation can be expressed as,

$$\frac{\partial u\left(z,t\right)}{\partial t}+6u\frac{\partial u\left(z,t\right)}{\partial z}+\frac{\partial^{3}u\left(z,t\right)}{\partial z^{3}}=0, \tag{1.1}$$

where $u\left(z,t\right)$ represent the amplitude of the field envelope, propagating along z. Analytical solutions of KdV were not found only until 1967 when inverse-scattering method was discovered by Gardner, Greene, Kruskal and Miura [8]. It was shown

that Eq. (1.1) supports solutions of the form

$$u(z,t) = \frac{v}{2}\,\mathrm{sech}^2\left[\frac{\sqrt{v}}{2}(z - vt)\right], \tag{1.2}$$

where v is the soliton velocity, and sech () is the secant hyperbolic function. Since then, the inverse-scattering method have been applied to various nonlinear evolution equations. The discovery of inverse-scattering method was a great mathematical step forward particularly in explaining solitary waves in other branches of physics such as hydrodynamics, and quantum mechanics [9].

In optics, one equation that is commonly used to describe the propagation of the waves through a nonlinear medium is the well-known nonlinear Schrödinger equation (NLSE). The equation models many nonlinearity effects in a fiber, including but not limited to self-phase modulation (SPM), four-wave mixing, second harmonic generation, and stimulated Raman scattering (SRS) [10]. In simple form it is expressed as [4],

$$i\frac{\partial u}{\partial z} - \frac{\beta_2}{2}\frac{\partial^2 u}{\partial T^2} + \gamma\,|u|^2\,u = 0, \tag{1.3}$$

where $u(z,t)$ is the field envelope, β_2 is the group velocity dispersion (GVD) parameter which is positive for normal dispersion and negative in the anomalous dispersion region. γ is the nonlinear parameter responsible for SPM. Equation (1.3) has been referred to as the master equation for information transfer in optical fibers [1].

NLSE is an integrable system meaning that it is possible to solve Eq. (1.3) analytically using inverse-scattering method. This was done in 1972 by Zakharov and Shabat which resulted in the soliton solutions of the NLSE. It was shown that based on the sign of the GVD parameter being positive or negative, dark or bright solitons can exist in the fiber, respectively. It was also shown that first order bright solitons maintain their shape while propagating along the fiber. In contrast higher order solitons, whose amplitudes are integer-multiples of the fundamental soliton,

change shape in a periodic fashion.

In 1973, Hasegawa and Tappert demonstrated the stability of picosecond optical pulses in the form of solitons in glass fibre, by performing various computer simulations [11, 12]. It was the first time that the use of solitons in optical communications was theoretically suggested. Their work, eventually led to the experimental observation of solitons in optical fiber in 1980 [13].

The number of papers that were published in the area of nonlinear optics during 1970s and 1980s is so large that it is not possible to list them here. Solitons among other topics were of particular interest as they found to be suitable candidates for potential all-optical and slow-light applications. The research efforts around solitons particularly intensified after the discovery of solitons in periodic guide structures such as nonlinear Bragg gratings [14]. Taking advantage of strong dispersion of Bragg grating, it was possible to generate solitons in distances as short as a few centimeters; the grating length. By late 1990s it was shown both numerically and experimentally that Bragg grating solitons can have any velocities between zero to the speed of light. This opened the gate to a whole new research area and seeded the idea of optical buffers and memories or in a more general sense optical signal processing specially slow light.

1.3 Thesis Outline

In this thesis we study properties of Bragg grating solitons in a system of linearly coupled Bragg gratings. To this end, this work is structured as follow: due to their importance, in Chapter 2 we will briefly review fiber Bragg gratings and generation of optical solitons in the photonic bandgap of the gratings. Properties of Bragg grating solitons or gap solitons are then reviewed through coupled mode equations. Properties of directional couplers and their use in nonlinear applications, particularly

grating-assisted couplers, are then investigated and described. An in-depth derivation of nonlinear coupled mode equations, describing two linearly coupled gratings, starting from Maxwell's equations is given in Chapter 3. Coupled mode equations are generalised at the end of Chapter 3 by inclusion of dispersive reflectivity parameter that takes into account nonuniformities in gratings.

Chapter 4 deals with numerical techniques and methods that are used in computer simulations to find soliton solutions and also to propagate the solitons in the structure. The results are then divided into two subsequent chapters. Chapter 5 is dedicated to the study of zero-velocity or quiescent solitons in the model. Chapter 6 deals with the existence, stability and interactions of moving solitons in the structure. The thesis is summarized in Chapter 7 where also a few ideas are outlined to further extend the research in this area.

Chapter 2

Optical Waveguides

2.1 Fibre Bragg Gratings

Gap solitons were originally introduced in the framework of superlattices [15]. This discovery has led to extensive research, focusing on their characteristics and experimental observation in nonlinear optical media [16, 17, 19–25] and, more recently, Bose–Einstein condensation (BEC) [26–30]. An optical medium that has been at the center of activity is the fiber Bragg grating (FBG). FBGs are produced by varying the refractive index along an optical fiber. Their compactness, ease of fabrication and the ability to design their spectral response have made them the device of choice for various applications both in the linear and nonlinear regimes such as dispersion compensation, pulse compression, filtering, add-drop multiplexing (ADM) and sensing [14, 31–36].

There are various techniques to make fiber gratings. Four of which have been commonly used are known as the single-beam internal technique, the dual-beam holographic technique, the phase-mask technique, and the point-by-point fabrication technique [37]. The fabrication of fiber Bragg gratings typically involves the illumination of the core material which is photosensitive with ultraviolet laser light,

which induces some structural changes i.e. permanent variations of the refractive index. In addition the photosensitivity of the fiber is strongly dependent on the chemical composition of the core as well as the laser wavelength. For instance silica glass has a very weak photosensitivity, whereas Germanosilicate glass exhibits a much stronger effect, making a refractive index modulation depth of up to $\Delta n \sim 10^{-3}$ possible [31, 37, 38].

A schematic diagram of the periodic refractive index inside a FBG core is shown in Figure 2.1(a) where $\overline{n}$ is the average refractive index of the core, and Λ is the grating period. An important feature of FBGs is that, due to the periodic (or aperiodic) perturbation of refractive index, their linear spectrum contains a photonic bandgap, centered at the Bragg wavelength $\lambda_0 = 2\overline{n}\Lambda$, in which low-intensity light experiences high reflectivity. Physically, when the wavelength of the incident light is equal to λ_0, exactly half the wavelength fits in one grating period causing the reflected waves off the local nonuniformities to be in-phase, thus giving rise to a strong backward-propagating wave [19]. At wavelengths far from the phase-matching condition, reflected waves are not constructive and the light can pass through the structure, making the grating an optical band-stop filter. Additionally, cross-coupling between the forward- and backward- propagating waves leads to a strong effective dispersion which may be six orders of magnitude larger than the underlying material dispersion of the fiber [19, 22, 25].

Wave propagation in FBGs, and generally periodic media, is usually governed by coupled mode theory. Here, we briefly review the features of FBGs described mathematically using the coupled mode equations. Detailed derivation of the general case of nonlinear coupled mode equations is given in the next chapter.

In coupled mode theory it is assumed that the guided modes of the structure can be expressed in terms of the modes of the unperturbed waveguide. In the case of a single mode fiber equipped with gratings, it has been shown that electromagnetic

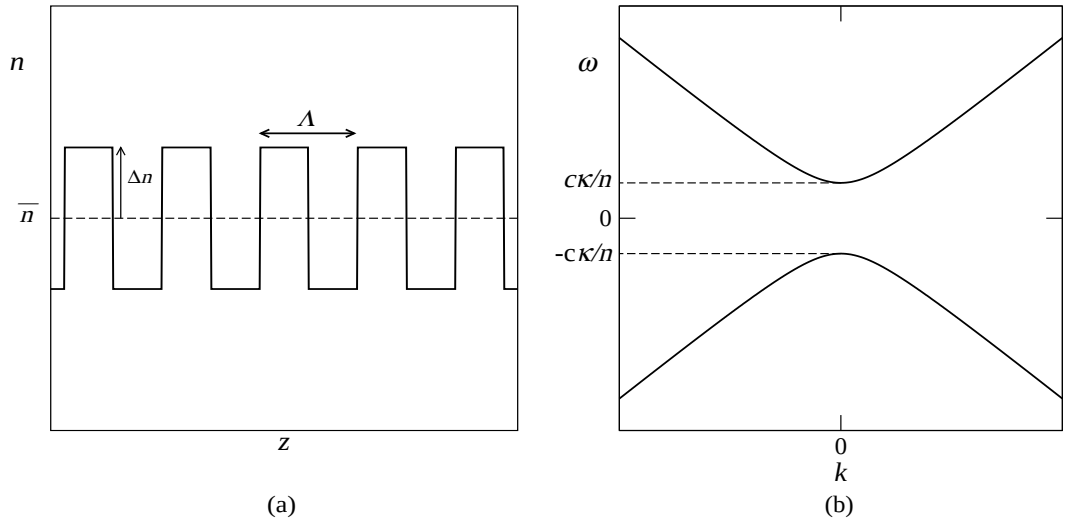

Figure 2.1: (a) Refractive index variation along the length of a uniform fiber Bragg grating, and (b) dispersion relation of the uniform FBG in the plane of (k, ω).

waves admit the following equations [19],

$$i\frac{\partial E^+}{\partial z} + i\frac{\overline{n}}{c}\frac{\partial E^+}{\partial t} + \kappa E^- = 0, \tag{2.1a}$$

$$-i\frac{\partial E^-}{\partial z} + i\frac{\overline{n}}{c}\frac{\partial E^-}{\partial t} + \kappa E^+ = 0, \tag{2.1b}$$

where c is the speed of light in vacuum, and $E^+$and E^- are the forward- and backward- propagating waves, respectively. κ is the grating coupling coefficient defined as below,

$$\kappa \equiv \frac{\omega_0 \Delta\varepsilon}{2\overline{n}c}. \tag{2.2}$$

It should be noted that κ in general is more complex and includes transverse variations of refractive index (cf. Ref. [37] page 12), however in the uniform case it simplifies to Eq. (2.2). Equations (2.1) are the linear coupled mode equations that can be generalized to include nonlinear and higher order effects. Before explaining the generalization of the equations, it is useful to look at the dispersion relation associated with the structure. To this end, we look for envelope functions of the

form,

$$E^{\pm}(z,t) = A^{\pm} e^{-i(\omega t - kz)}, \tag{2.3}$$

where $A^{\pm}$ are constants. Substituting (2.3) into (2.1b), the following equations in the matrix form are obtained,

$$\begin{bmatrix} \frac{\overline{n}}{c}\omega - k & \kappa \\ \kappa & \frac{\overline{n}}{c}\omega + k \end{bmatrix} \begin{bmatrix} A^{+} \\ A^{-} \end{bmatrix} = 0, \tag{2.4}$$

which leads to the following dispersion relation:

$$\omega = \pm \frac{c}{\overline{n}} \sqrt{k^2 + \kappa^2}. \tag{2.5}$$

Equation (2.5) is plotted in Figure 2.1(b) where clearly shows that there is a gap in the spectrum for the frequencies in the range $|\omega| < c\kappa/\overline{n}$. It should be noted that the gap is centered at (k_0, ω_0) and ω in Eq. (2.5) can be thought of as detuning from the Bragg frequency; this can be shown by translating the coordinates introducing $\omega \equiv \omega' - \omega_0$ and $k \equiv k' - k_0$ (cf. Ref. [19]).

The reflection bandwidth, from Eq. (2.5) is obtained as $\Delta\omega = 2c\kappa/\overline{n}$, which may be expressed in the form of filter Q-factor, i.e.

$$\frac{\omega_0}{\Delta\omega} \approx \frac{\overline{n}}{\Delta n}. \tag{2.6}$$

The latter shows that reflection bandwidth depends on the modulation depth. Also tells us that standard gratings with typical $\Delta n \sim 10^{-4}$ have quality factors of the order of $\gtrsim 10^4$.

First and second order dispersion, representing the group velocity and group velocity dispersion, are obtained from the first and second order derivatives of Eq. (2.5), respectively. It is obvious that near bandgap edges the structure exhibits

strong dispersion which, as mentioned earlier, dominate the material dispersion.

2.2 Kerr-type Nonlinear Gratings

All the materials that are found in nature are nonlinear. That is their response to electromagnetic waves depends on the intensity of the waves and may even change over time. The origin of this behavior in physics is described through the nonlinear relationship between the electromagnetic field and its induced material polarization [4], i.e.

$$\mathbf{P} = \varepsilon_0 \left(\chi^{(1)} \cdot \mathbf{E} + \chi^{(2)} \vdots \mathbf{EE} + \chi^{(3)} \vdots \mathbf{EEE} + \cdots \right), \tag{2.7}$$

where $\chi^{(m)}$ is the m-th order susceptibility which in general is a $m+1$ rank tensor. In silica fiber the effects of $\chi^{(2)}$ are negligible due to symmetrical molecules of silica [4]. Therefore the lowest-order nonlinear response is due to $\chi^{(3)}$ which causes effects such as third-harmonic generation, four-wave mixing, self-phase modulation, and cross-phase modulation, of which we only consider the last two in this work. The intensity dependence of the refractive index of the fiber is a direct result of the above polarization relation. In simple form,

$$n = n_0 + n_2 \left| E \right|^2, \tag{2.8}$$

where $|E|^2$ is the intensity of light inside the fiber and n_2 is the nonlinear index or Kerr coefficient related to $\chi^{(3)}$. The values of n_2 are typically small, on the order of $\sim 10^{-20} m^2 W^{-1}$.

Taking Kerr-type nonlinearity into account the linear coupled mode Eqs. (2.1)

takes the form (for detailed derivation refer to Section 3.2) [19, 39],

$$i\frac{\partial E^+}{\partial z} + i\frac{\overline{n}}{c}\frac{\partial E^+}{\partial t} + \kappa E^- + \gamma\left(\left|E^+\right|^2 + 2\left|E^-\right|^2\right)E^+ = 0, \tag{2.9a}$$

$$-i\frac{\partial E^-}{\partial z} + i\frac{\overline{n}}{c}\frac{\partial E^-}{\partial t} + \kappa E^+ + \gamma\left(\left|E^-\right|^2 + 2\left|E^+\right|^2\right)E^- = 0, \tag{2.9b}$$

where the nonlinear parameter γ is obtained as

$$\gamma = \frac{n_2\omega_0}{cA_{eff}}, \tag{2.10}$$

where A_{eff} is the effective mode area of the unperturbed fiber (cf. Ref. [4] page 35). Equations (2.9) are the nonlinear coupled mode equations (NLCMEs). Fourth and fifth terms in Eqs. (2.9) account for self-phase modulation (SPM) and cross-phase modulation (XPM) contributions, respectively.

Coupled mode equations are often expressed in dimensionless form which reduce the number of parameters that must be investigated. It is straightforward to show that Eqs. (2.9) remain the same for the following rescaling,

$$z \to \frac{z}{\kappa},\ t \to \frac{\overline{n}}{\kappa c}t, \tag{2.11}$$

$$E^+ = \sqrt{\frac{\kappa}{2\gamma}}u,\ E^- = \sqrt{\frac{\kappa}{2\gamma}}v, \tag{2.12}$$

which results in the following normalized nonlinear coupled mode equations,

$$i\frac{\partial u}{\partial z} + i\frac{\partial u}{\partial t} + v + \left(\frac{1}{2}\left|u\right|^2 + \left|v\right|^2\right)u = 0, \tag{2.13a}$$

$$-i\frac{\partial v}{\partial z} + i\frac{\partial v}{\partial t} + u + \left(\frac{1}{2}\left|v\right|^2 + \left|u\right|^2\right)v = 0. \tag{2.13b}$$

It has been shown that Eqs. (2.13) have traveling-wave solutions whose frequencies are well inside the photonic bandgap of the structure which would normally be Bragg reflected; the so-called Gap Solitons. One of the striking features of gap solitons is

that they can propagate undistorted through the grating at any velocities in the range of zero to the speed of light in the medium. This feature was first described theoretically in Refs. [20, 21]. Gap solitons had not been observed until 1996 when moving solitons were experimentally verified for the first time by Eggleton *et al.* [24].

In the next section analytical soliton solutions of the nonlinear coupled mode equations (2.13) are discussed with the objective of giving the reader an overview of the characteristics of gap soliton solutions in periodic media.

2.3 Bragg Grating Solitons

Analytical solutions of the nonlinear coupled mode equations (2.13) have been well studied in many references before [14, 20, 21]. The model admits a two-parameter family of gap solitons that fill the entire bandgap whose velocity may range from zero (quiescent) to the speed of light in the medium. Solutions of Eqs. (2.13) i.e. gap solitons may be expressed in the following form [17]

$$u = +\alpha W(X) \exp\left[\frac{y}{2} + i\varphi(X) - iT\cos(\theta)\right], \tag{2.14a}$$

$$v = -\alpha W^*(X) \exp\left[-\frac{y}{2} + i\varphi(X) - iT\cos(\theta)\right], \tag{2.14b}$$

where X and T are given by

$$X = \frac{x - Vt}{\sqrt{1-V^2}}, \quad T = \frac{t - Vx}{\sqrt{1-V^2}}, \tag{2.15}$$

where V is the group velocity of the soliton. Also,

$$\alpha^{-2} = 1 + \frac{1}{2}\cosh(2y), \tag{2.16}$$

$$\varphi(X) = \alpha^2 \sinh(2y) \arctan\left[\tanh(X\sin(\theta)) \tan\left(\frac{\theta}{2}\right)\right], \tag{2.17}$$

$$W(X) = \sin(\theta)\,\mathrm{sech}\left[X\sin(\theta) - i\frac{\theta}{2}\right]. \tag{2.18}$$

Thus, the two parameters of the gap solitons are rapidity y and the detuning parameter θ. The former is related to the soliton group velocity through $V = \tanh(y)$ while the later determines the frequency detuning inside the gap spectrum [17].

Experimental studies have confirmed the existence of gap solitons in nonlinear FBGs. To date, gap solitons with velocities as low as 23% of the speed of light in the medium have been experimentally observed [18]. Numerical and analytical studies of the stability of gap solitons have led to the conclusion that nearly half of the gap soliton family, whose frequency detuning falls in the range $-1 < \cos\theta < 0$, are unstable against oscillatory perturbations [16, 17, 23]. It is worth pointing out here that Eqs. (2.13) are a non-integrable system that can explain special features of gap solitons that do not exist in the case of nonlinear Schrodinger (NLS) solitons described through Eq. (1.3). More specifically, gap solitons exhibit feature rich collisions in both co- and contra-propagating cases which do not happen for the NLS solitons. For example based on the relative phase of the colliding solitons, the fundamental properties of both solitons such as frequency, velocity or even the number of solitons may change after the collision. This is further investigated in Chapters 5 and 6 where interactions and collisions of quiescent and moving gap solitons are studied, respectively.

2.4 Directional Couplers

Optical couplers, often called directional couplers, are one of the most commonly used devices in optical networks that split the light into two or more physically separated parts [37]. While they have been extensively studied in linear applications, optical couplers in nonlinear regime play an essential role in all-optical applications such as switching, amplification and logic operations [40–42]. Directional couplers can be made using planar waveguides or fibers. Our focus in this thesis is on fiber-

based couplers. When two fibers are placed (fused) next to each other so that the cores are close enough, the fundamental modes propagating in each core may overlap partially in the cladding region between the two cores resulting in the power transfer between the two cores. This means that the coupling coefficient of a coupler depends on the spacing of the cores as well as the mode distributions. To have an in-depth understanding of the characteristics of couplers, following the approaches in Refs. [37] and [43], in this section we derive the equations describing a nonlinear coupler using coupled mode theory.

In coupled mode theory, as mentioned also in Section 2.1, it is assumed that the variations of dielectric constant (or refractive index) are so small that can be taken into account as perturbations of the modes of the unperturbed waveguide. Therefore the dielectric tensor representing the compound structure can be written as [43],

$$\varepsilon(x,y,z) = \varepsilon_r(x,y) + \tilde{\varepsilon}(x,y,z) + \varepsilon_{NL}(x,y,z) \tag{2.19}$$

where the first, second and third terms account for the unperturbed, periodic along z direction, and nonlinear parts of the dielectric tensor, respectively. The modes of the unperturbed structure can be expressed in the form

$$F_m(x,y)\, e^{-i(\omega t - \beta_m z)} \tag{2.20}$$

where m is the core index, β_m is the mode propagation constant, and $F_m(x,y)$ is the transverse mode distribution in m-th core which is in the form of Bessel functions in the case of fiber couplers. Note that we study the case of coupled single mode fibers where only one mode is confined within each core. Each mode is known to satisfy the wave equation,

$$\left[\nabla_T^2 + \omega^2 \mu \varepsilon_r(x,y) - \beta_m^2\right] F_m(x,y) = 0. \tag{2.21}$$

It is assumed that the electric field in the coupler can be expressed in the form

$$E(x,y,z,t) = \left[E_1(z)\,F_1(x,y)\,e^{-i\omega t} + E_2(z)\,F_2(x,y)\,e^{-i\omega t}\right] e^{i\beta z}, \tag{2.22}$$

where $E_m(z)$ are field envelopes in the m-th core, and β is the propagation constant to be determined. In fact in Eq. (2.22) the variables are separated which is a common method in solving the wave equation and generally ordinary differential equations. Here we also assume that the two cores are identical (a more general derivation for asymmetric couplers are available in Ref. [37]). Substituting (2.22) into the wave equation

$$\left[\nabla_T^2 + \omega^2\mu\varepsilon(x,y,z) - \beta^2\right] E = 0, \tag{2.23}$$

and using Eqs. (2.19) and (2.21) the nonlinear coupled mode equations are obtained as,

$$i\frac{\partial E_1}{\partial z} + \frac{\overline{n}}{c}\frac{\partial E_1}{\partial t} + \frac{\beta_2}{2}\frac{\partial^2 E_1}{\partial t^2} = KE_2 + \gamma\left(|E_1|^2 + \sigma|E_2|^2\right)E_1, \tag{2.24a}$$

$$i\frac{\partial E_2}{\partial z} + \frac{\overline{n}}{c}\frac{\partial E_2}{\partial t} + \frac{\beta_2}{2}\frac{\partial^2 E_2}{\partial t^2} = KE_1 + \gamma\left(|E_2|^2 + \sigma|E_1|^2\right)E_1, \tag{2.24b}$$

where β_2 is the group velocity dispersion parameter, K is the linear coupling coefficient defined as,

$$K = \frac{k_0}{2\beta}\int\int_{-\infty}^{\infty}\left(\overline{n}^2 - n_1^2\right)F_1^* F_2 dxdy, \tag{2.25}$$

where $n_1^2 = \varepsilon_r$ and the nonlinear coefficient γ is defined in Eq. (2.10). The cross-phase modulation (XPM) parameter σ is defined as

$$\sigma = \frac{\int\int_{-\infty}^{\infty}|F_1|^2|F_2|^2\,dxdy}{2\int\int_{-\infty}^{\infty}|F_1|^4\,dxdy}. \tag{2.26}$$

It should be noted that the denominator in Eq. (2.26) can also be $2\int\int_{-\infty}^{\infty}|F_2|^4\,dxdy$, because the two cores are identical. From Eq. (2.26) it is clear that σ is generally

very small and negligible, because it accounts for the overlap of the transverse mode distributions in the cladding region.

It is often convenient to assume that the cores of the couplers are identical, as we did above. However, in practice there are many reasons that couplers may become asymmetric. For instance, couplers composed of cores with different nonlinear properties have been studied before [45, 46]. It has been shown that such devices may have interesting properties that do not exist in simple couplers. For example couplers may be equipped with Bragg gratings which leads to striking features discussed in the next subsection.

2.4.1 Grating-Assisted Couplers

First studied in planar waveguides, grating-assisted couplers make use of periodic variation of refractive index to improve the power transferred between the two cores of the coupler, even though the cores are weakly coupled or highly mismatched [44]. Periodic refractive index, which in the case of planar waveguides means periodic coupling constant, is made by periodic changes in the dielectric slab thickness. However in the case of fiber-based couplers it is not feasible to perturb the diameter of the core, instead fibers can be equipped with Bragg gratings. Therefore the coupling coefficient remains almost constant along the coupler length. In either of the cases, the period of the gratings is selected in such a way that the mismatch between the propagation constants of the two unperturbed cores equals the grating wave vector, i.e.

$$\beta_1 - \beta_2 = \frac{2\pi}{\Lambda}, \tag{2.27}$$

which is known as the Bragg or phase matching or resonant coupling condition [37, 43]. It has been shown that under the phase matching condition complete power transfer between the modes of each core is possible [47–49]. It has been shown that a symmetric Kerr-type nonlinear grating-assisted coupler can be described via the

following set of nonlinear coupled mode equations [37],

$$i\frac{\partial E_1^+}{\partial z}+\frac{\overline{n}}{c}\frac{\partial E_1^+}{\partial t}+\kappa E_1^-+\gamma\left(\left|E_1^+\right|^2+2\left|E_1^-\right|^2\right)E_1^++KE_2^+=0, \tag{2.28a}$$

$$-i\frac{\partial E_1^-}{\partial z}+\frac{\overline{n}}{c}\frac{\partial E_1^-}{\partial t}+\kappa E_1^++\gamma\left(\left|E_1^-\right|^2+2\left|E_1^+\right|^2\right)E_1^-+KE_2^-=0, \tag{2.28b}$$

$$i\frac{\partial E_2^+}{\partial z}+\frac{\overline{n}}{c}\frac{\partial E_2^+}{\partial t}+\kappa E_2^-+\gamma\left(\left|E_2^+\right|^2+2\left|E_2^-\right|^2\right)E_2^++KE_1^+=0, \tag{2.28c}$$

$$-i\frac{\partial E_2^-}{\partial z}+\frac{\overline{n}}{c}\frac{\partial E_2^-}{\partial t}+\kappa E_2^++\gamma\left(\left|E_2^-\right|^2+2\left|E_2^+\right|^2\right)E_2^-+KE_1^-=0. \tag{2.28d}$$

It should be noted that GVD is neglected which is an accurate assumption because the dispersion length in such a structure is much larger than the grating length. Equations (2.28) are derived in details in Section 3.2.

The fiber-based grating-assisted couplers have been studied and used widely in Wavelength Division Multiplexing (WDM) systems [48,50,51]. In linear regime, when a broadband WDM signal is launched inside one core of a coupler, the channel whose wavelength falls within the stop band of the grating is reflected back and appears at the unused input port of the second core while the remaining channels appear at the output end (cf. Figure 1 in Ref. [48]). Also a signal at the same specific wavelength can be added by injecting it from the output port of the core without the grating. Such grating-assisted fiber couplers have been fabricated and exhibit large add–drop efficiency ($> 90\%$) with low losses [50]. These devices can also act as a switch such that the channel is dropped only if its power exceeds a certain value: At low power, the coupler couples the power from one normal mode to the other at resonance. At high power, the nonlinearity-induced refractive index change detunes the resonance, leaving all the power in the mode initially excited [47]. Applied to WDM signals, the intensity-dependent shift of the Bragg frequency affects the channel to be dropped. As a result, the device can act as a nonlinear switch. Complete discussions regarding the principle of operation and design criteria of grating-assisted couplers can be found in Ref. [37] (Section 2.4.3) and references mentioned therein.

Chapter 3

Theoretical Background

3.1 Introduction

Propagation of light as electromagnetic waves in a medium is in general governed by Maxwell's equation [52],

$$\nabla \times \mathbf{E} = -\frac{\partial \mathbf{B}}{\partial t} \tag{3.1a}$$

$$\nabla \times \mathbf{H} = \mathbf{J} + \frac{\partial \mathbf{D}}{\partial t} \tag{3.1b}$$

$$\nabla \cdot \mathbf{D} = \rho \tag{3.1c}$$

$$\nabla \cdot \mathbf{B} = 0, \tag{3.1d}$$

where $\mathbf{E}$ and $\mathbf{H}$ are electric and magnetic field vectors, $\mathbf{D}$ and $\mathbf{B}$ are electric and magnetic flux density vectors, ρ and $\mathbf{J}$ are charge density and current density vectors, respectively. Also,

$$\mathbf{D} = \varepsilon_0 \mathbf{E} + \mathbf{P}, \tag{3.2a}$$

$$\mathbf{B} = \mu_0 \left(\mathbf{H} + \mathbf{M} \right), \tag{3.2b}$$

where $\mathbf{P}$ and $\mathbf{M}$ are polarization and magnetization vectors, $\varepsilon_0 = 8.854 \times 10^{-12} F/m$ and $\mu_0 = 4\pi \times 10^{-7} H/m$ are the vacuum permittivity and permeability, respectively. In a non-magnetic material ($\mathbf{M} = 0$) such as optical fiber where charge and current densities are zero, i.e. $\rho = 0$ and $J = 0$, by taking the curl of Eq. (3.1a) and using (3.1b) it obtains

$$\nabla \times \nabla \times \mathbf{E} = -\frac{1}{c^2}\frac{\partial \mathbf{E}^2}{\partial t^2} - \mu_0 \frac{\partial \mathbf{P}^2}{\partial t^2}, \tag{3.3}$$

where the speed of light c, permittivity ε_0 and permeability μ_0 in vacuum are related through

$$c = \frac{1}{\sqrt{\varepsilon_0 \mu_0}}. \tag{3.4}$$

Substituting the left side of Eq. (3.3) by the curl of curl identity

$$\nabla \times \nabla \times \mathbf{E} = \nabla \left(\nabla . \mathbf{E}\right) - \nabla^2 \mathbf{E}, \tag{3.5}$$

and using Eq. (3.1c), the general wave equation is obtained,

$$\nabla^2 \mathbf{E} - \frac{1}{c^2}\frac{\partial \mathbf{E}^2}{\partial t^2} = \mu_0 \frac{\partial \mathbf{P}^2}{\partial t^2}. \tag{3.6}$$

The induced polarization in Eq. (3.6) accounts for both linear and nonlinear effects and can be splitted into two parts, $\mathbf{P} = \mathbf{P}_L + \mathbf{P}_{NL}$, where $\mathbf{P}_L$ and $\mathbf{P}_{NL}$ are the linear and nonlinear terms of polarization, respectively. They are expressed in terms of electric field using the following well-known relations [4],

$$\mathbf{P}_L \left(\mathbf{r}, t\right) = \varepsilon_0 \int_{-\infty}^{t} \chi^{(1)} \left(t - \tau\right) \cdot \mathbf{E} \left(\mathbf{r}, \tau\right) d\tau, \tag{3.7}$$

$$\mathbf{P}_{NL} \left(\mathbf{r}, t\right) = \varepsilon_0 \int_{-\infty}^{t} \int_{-\infty}^{t} \int_{-\infty}^{t} \chi^{(3)} \left(t - t_1, t - t_2, t - t_3\right) \vdots \mathbf{E} \left(\mathbf{r}, t_1\right) dt_1 dt_2 dt_3, \tag{3.8}$$

where $\chi^{(1)}$ and $\chi^{(3)}$ are first and third order electrical susceptibility. Equations (3.6)-(3.8) can be used to explain most of the nonlinear effects in optical fiber such

as third-harmonic generation, four-wave mixing, and nonlinear refraction [4]. It should be noted that only third order nonlinearity is included in Eq. (3.8) because in this thesis we study the systems with cubic or Kerr-type nonlinearity. Higher order nonlinearities may become prominent in cases that are not dealt with in this work, such as pulse propagation in Chalcogenide glass which is a highly-nonlinear material [53] where including the fifth order susceptibility $\chi^{(5)}$ results in non-trivial quintic nonlinearity terms [54].

In deriving the NLCMEs in standard fiber, it is valid to assume that $\mathbf{E}(\mathbf{r},t)$ does not have any components along the direction of propagation z and is polarized along one direction in the transverse plane, i.e. $\mathbf{E}(\mathbf{r},t) = E(\mathbf{r},t)\,\hat{x}$ and as a result $\mathbf{P}(\mathbf{r},t) = P(\mathbf{r},t)\,\hat{x}$. This means we assume that the polarization does not change as the pulse propagates in the fiber, hence fiber birefringence is neglected, which is a good approximation for soliton propagation in Bragg gratings. The wave equation in (3.6) then takes the scalar form

$$\nabla_T^2 E + \frac{\partial^2 E}{\partial z^2} - \frac{1}{c^2}\frac{\partial E^2}{\partial t^2} = \mu_0 \frac{\partial P^2}{\partial t^2}, \tag{3.9}$$

where ∇_T is the transverse operator. In linear and homogenous material with instantaneous polarization response wave equation simplifies to

$$\nabla_T^2 E + \frac{\partial^2 E}{\partial z^2} - \frac{\varepsilon_r}{c^2}\frac{\partial E^2}{\partial t^2} = 0, \tag{3.10}$$

where $\varepsilon_r = 1 + \chi^{(1)}$ is the relative permittivity of the material. Electric field distribution in a single mode fiber (SMF) in low intensities ($\mathbf{P}_{NL} = 0$) can be derived by solving Eq. (3.10) which leads to the Bessel function solutions. The solutions appear in many text books [4, 55, 56] and we do not include them here.

The problem of interest in this thesis is to study the effects of grating nonuniformities on the characteristics of a system of two linearly coupled Kerr-type nonlinear

fibers with gratings written on both cores. This involves solving the NLCMEs for soliton solutions in the system. In Section 3.2, starting from the wave equation (3.9), the mathematical model describing such a system is derived. Grating nonuniformities are then added to the obtained NLCMEs through the introduction of dispersive reflectivity in Section 3.3. We emphasize here that the inclusion of these equations are solely for the completeness of this thesis and they are not author's original work. Excellent derivations and thorough discussions about the approximations made in the derivations can be found in [1, 4, 37, 43, 57, 58].

3.2 Nonlinear Coupled Mode Equations (NLCMEs)

Pulse propagation in the system of two linearly coupled nonlinear Bragg gratings involves finding the electric fields E_1 and E_2 in cores 1 and 2. The electric fields are sought for in the form

$$E_1(\mathbf{r},t) = \frac{1}{2}F_1(x,y)\left[E_1^+(z,t)\,e^{-i(\omega_0 t - k_0 z)} + E_1^-(z,t)\,e^{-i(\omega_0 t + k_0 z)} + c.c.\right], \quad (3.11a)$$

$$E_2(\mathbf{r},t) = \frac{1}{2}F_2(x,y)\left[E_2^+(z,t)\,e^{-i(\omega_0 t - k_0 z)} + E_2^-(z,t)\,e^{-i(\omega_0 t + k_0 z)} + c.c.\right], \quad (3.11b)$$

where $E_{1,2}^+$ are the slowly varying electric field envelopes of the forward-propagating waves in core 1 and 2, respectively. Similarly $E_{1,2}^-$ are the slowly varying envelopes of the backward-propagating waves which are induced as the result of grating reflections. The abbreviation *c.c.* stands for complex conjugates. It is assumed that the nonlinear effects and presence of grating do not affect the unperturbed fiber modes. $F_{1,2}(x,y)$ are the transverse distribution of the fundamental modes in core 1 and 2 in the absence of grating that satisfy wave equation (3.10), i.e.

$$\frac{\partial^2 F_{1,2}}{\partial x^2} + \frac{\partial^2 F_{1,2}}{\partial y^2} + \left(\frac{\varepsilon_{r1,2}(x,y)\,\omega_0^2}{c^2} - \beta_{1,2}^2\right) F_{1,2} = 0, \quad (3.12)$$

where $\beta_{1,2}$ are the fundamental mode propagation constants and $\varepsilon_{r1,2}(x,y)$ are the dielectric coefficients of core 1 and 2, respectively. In equations (3.11) pulses are assumed to propagate along z axis, ω_0 and k_0 are the frequency and wave number at the Bragg condition

$$\omega_0 = \frac{\pi c}{\overline{n}\Lambda}, \tag{3.13}$$

$$k_0 = \frac{\pi}{\Lambda}, \tag{3.14}$$

where Λ is the grating period and $\overline{n}$ is the average refractive index inside the cores.

For simplicity, the medium is assumed to be isotropic, i.e. the nonlinear properties of the medium are uniform in all the directions. The nonlinear response of the medium is also assumed to be instantaneous. The latter means we neglect the Raman effect which is a valid assumption as long as the pulse width is approximately greater than 1 ps [4]. Under these assumptions, and in the presence of uniform gratings, polarization can be expressed using Eqs. (3.7) and (3.8) in the following form,

$$P(\mathbf{r},t) = \varepsilon_0 \left(\varepsilon_r(x,y) - 1 + \tilde{\varepsilon}(x,y,z)\right) E(\mathbf{r},t) + \varepsilon_0 \chi^{(3)} E^3(\mathbf{r},t), \tag{3.15}$$

where for simplicity the susceptibility component $\chi^{(3)}_{xxxx}$ is shown with the same notation as the susceptibility tensor. It should be noted that susceptibility in general is a tensor of complex vector components but in an isotropic medium takes the form of a symmetric diagonal tensor of complex scalars. In a Kerr-type material the real and imaginary parts of the susceptibility account for linear and nonlinear refractive index (i.e. $\overline{n} = n_0 + n_2 |E|^2$ where n_2 is the nonlinear refractive index) and loss coefficient (i.e. $\overline{\alpha} = \alpha + \alpha_2 |E|^2$ where α_2 is the two-photon absorption coefficient), respectively. Loss components are usually negligible in fiber couplers equipped with gratings [47, 48, 51]. Therefore from here onward we treat the susceptibility as a real number. One implicit assumption in Eq. (3.15) is that high frequency terms, i.e.

third-harmonic terms, are neglected.

$\tilde{\varepsilon}(x,y,z)$ in Eq. (3.15) accounts for the spatial changes of refractive index because of the grating and is a periodic function of z with the period of Λ, the grating period. It is useful to expand $\tilde{\varepsilon}(x,y,z)$ into Fourier series [19],

$$\tilde{\varepsilon}(x,y,z) = \sum_m \varepsilon_m(x,y)\, e^{2ik_0 mz}, \tag{3.16}$$

where m is a non-zero integer. Only frequencies near the Bragg frequency ω_0 take part in the interaction of the waves ($m = \pm 1$) and higher order effects are neglected for simplicity. It is known that the higher order effects can be incorporated into the equations separately [4, 37]. Letting $m = \pm 1$ in Eq. (3.16), it follows,

$$\tilde{\varepsilon}(x,y,z) = \varepsilon_1(x,y)\, e^{2ik_0 z} + \varepsilon_{-1}(x,y)\, e^{-2ik_0 z} = 2\Delta\varepsilon(x,y)\cos(2k_0 z), \tag{3.17}$$

where $\varepsilon_1 = \varepsilon_{-1} = \Delta\varepsilon$. Substituting Eqs. (3.17) and (3.15) into Eq. (3.9) it yields,

$$\nabla_T^2 E + \frac{\partial^2 E}{\partial z^2} - \frac{\varepsilon_r(x,y)}{c^2}\frac{\partial E^2}{\partial t^2} - \frac{\tilde{\varepsilon}(x,y,z)}{c^2}\frac{\partial E^2}{\partial t^2} - \frac{\chi^{(3)}}{c^2}\frac{\partial^2}{\partial t^2}\left(E^3\right) = 0. \tag{3.18}$$

Noting that the total electric field in the compound structure is $E = E_1 + E_2$, we substitute Eqs. (3.11) into (3.18). Here we evaluate each term of Eq. (3.18) separately:

$$\nabla_T^2 E_{1,2} = \frac{1}{2}\nabla_T^2 F_{1,2}(x,y)\left[E_{1,2}^{+} e^{-i(\omega_0 t - k_0 z)} + E_{1,2}^{-} e^{-i(\omega_0 t + k_0 z)} + c.c.\right], \tag{3.19}$$

$$\begin{aligned}\frac{\partial^2 E_{1,2}}{\partial z^2} &= \frac{1}{2}F_{1,2}(x,y)\left[\frac{\partial^2 E_{1,2}^{+}}{\partial z^2} + 2ik_0\frac{\partial E_{1,2}^{+}}{\partial z} - k_0^2 E_{1,2}^{+}\right] e^{-i(\omega_0 t - k_0 z)} \\ &\quad + \frac{1}{2}F_{1,2}(x,y)\left[\frac{\partial^2 E_{1,2}^{-}}{\partial z^2} - 2ik_0\frac{\partial E_{1,2}^{-}}{\partial z} - k_0^2 E_{1,2}^{-}\right] e^{-i(\omega_0 t + k_0 z)} + c.c.,\end{aligned} \tag{3.20}$$

$$\begin{aligned}\frac{\partial^2 E_{1,2}}{\partial t^2} &= \frac{1}{2}F_{1,2}(x,y)\left[\frac{\partial^2 E_{1,2}^{+}}{\partial t^2} - 2i\omega_0\frac{\partial E_{1,2}^{+}}{\partial t} - \omega_0^2 E_{1,2}^{+}\right] e^{-i(\omega_0 t - k_0 z)} \\ &\quad + \frac{1}{2}F_{1,2}(x,y)\left[\frac{\partial^2 E_{1,2}^{-}}{\partial t^2} - 2i\omega_0\frac{\partial E_{1,2}^{-}}{\partial t} - \omega_0^2 E_{1,2}^{-}\right] e^{-i(\omega_0 t + k_0 z)} + c.c.,\end{aligned} \tag{3.21}$$

We then replace the transverse derivative terms in Eq. (3.19) using Eq. (3.12), which yields

$$\nabla_T^2 E_{1,2} = \frac{1}{2}\left(\beta_{1,2}^2 - \frac{\varepsilon_{r1,2}\omega_0^2}{c^2}\right) F_{1,2}\left[E_{1,2}^{+} e^{-i(\omega_0 t - k_0 z)} + E_{1,2}^{-} e^{-i(\omega_0 t + k_0 z)} + c.c.\right], \quad (3.22)$$

It is assumed that the dielectric perturbations are weak giving rise to the slowly varying envelope approximation (SVEA) that satisfies the following conditions,

$$\left|\frac{\partial E}{\partial z}\right| \ll |k_0 E|, \quad (3.23a)$$

$$\left|\frac{\partial E}{\partial t}\right| \ll |\omega_0 E|, \quad (3.23b)$$

$$\left|\frac{\partial^2 E}{\partial z^2}\right| \ll \left|k_0 \frac{\partial E}{\partial z}\right|, \quad (3.23c)$$

$$\left|\frac{\partial^2 E}{\partial t^2}\right| \ll \left|\omega_0 \frac{\partial E}{\partial t}\right|. \quad (3.23d)$$

Under SVEA the second-order derivative terms in Eqs. (3.20) and (3.21) are all eliminated, taking the form

$$\frac{\partial E_{1,2}^2}{\partial z^2} = \frac{1}{2} F_{1,2}(x,y) \left[\left(2ik_0 \frac{\partial E_{1,2}^{+}}{\partial z} - k_0^2 E_{1,2}^{+}\right) e^{-i(\omega_0 t - k_0 z)} - \left(2ik_0 \frac{\partial E_{1,2}^{-}}{\partial z} + k_0^2 E_{1,2}^{-}\right) e^{-i(\omega_0 t + k_0 z)}\right] + c.c. \quad (3.24)$$

$$\frac{\partial E_{1,2}^2}{\partial t^2} = \frac{1}{2} F_{1,2}(x,y) \left[-\left(2i\omega_0 \frac{\partial E_{1,2}^{+}}{\partial t} + \omega_0^2 E_{1,2}^{+}\right) e^{-i(\omega_0 t - k_0 z)} - \left(2i\omega_0 \frac{\partial E_{1,2}^{-}}{\partial t} + \omega_0^2 E_{1,2}^{-}\right) e^{-i(\omega_0 t + k_0 z)}\right] + c.c., \quad (3.25)$$

The fourth term in Eq. (3.18) takes the form

$$-\frac{\tilde{\varepsilon}(z)}{c^2}\frac{\partial E_{1,2}^2}{\partial t^2} = \frac{\omega_0^2 \tilde{\varepsilon}(z)}{2c^2} F_{1,2}(x,y)\left[E_{1,2}^{+} e^{-i(\omega_0 t - k_0 z)} + E_{1,2}^{-} e^{-i(\omega_0 t + k_0 z)}\right], \quad (3.26)$$

in which we substitute Eqs. (3.17):

$$-\frac{\tilde{\varepsilon}(z)}{c^2}\frac{\partial E_{1,2}^2}{\partial t^2} = \frac{\Delta\varepsilon\omega_0^2}{2c^2}F_{1,2}(x,y)\left[E_{1,2}^- e^{-i(\omega_0 t - k_0 z)} + E_{1,2}^+ e^{-i(\omega_0 t - k_0 z)}\right], \tag{3.27}$$

where only phase-matched terms are included. Equation (3.27) accounts for the linear coupling of the counter-propagating modes which is a result of the refractive index modulation.

The last term in Eq. (3.18), the nonlinear term, is evaluated by substituting the electric field with Eqs. (3.11a) and (3.11b). The result includes many of higher order terms and terms which do not satisfy the phase matching criteria. Keeping the phase-matched terms we obtain

$$\begin{aligned} E_{1,2}^3 = {} & \frac{3}{4}\left|F_{1,2}\right|^2 F_{1,2}\left(\frac{1}{2}\left|E_{1,2}^+\right|^2 + \left|E_{1,2}^-\right|^2\right)E_{1,2}^+ e^{-i(\omega_0 t - k_0 z)} \\ & + \frac{3}{4}\left|F_{1,2}\right|^2 F_{1,2}\left(\frac{1}{2}\left|E_{1,2}^-\right|^2 + \left|E_{1,2}^+\right|^2\right)E_{1,2}^- e^{-i(\omega_0 t + k_0 z)} + c.c.. \end{aligned} \tag{3.28}$$

The second derivative of $E_{1,2}^3$ is simplified by neglecting the higher order effects and applying the SVEA and it takes the form

$$\begin{aligned} -\frac{\chi^{(3)}}{c^2}\frac{\partial^2}{\partial t^2}\left(E_{1,2}^3\right) = {} & \frac{3\chi^{(3)}\omega_0^2}{4c^2}\left|F_{1,2}\right|^2 F_{1,2}\left(\frac{1}{2}\left|E_{1,2}^+\right|^2 + \left|E_{1,2}^-\right|^2\right)E_{1,2}^+ e^{-i(\omega_0 t - k_0 z)} \\ & + \frac{3\chi^{(3)}\omega_0^2}{4c^2}\left|F_{1,2}\right|^2 F_{1,2}\left(\frac{1}{2}\left|E_{1,2}^-\right|^2 + \left|E_{1,2}^+\right|^2\right)E_{1,2}^- e^{-i(\omega_0 t + k_0 z)} + c.c.. \end{aligned} \tag{3.29}$$

We now replace the terms in Eq. (3.18) by what we obtained from Eqs. (3.22),

(3.24), (3.25), (3.27), and (3.29). It then follows,

$$\sum_{m=1,2}\left[\frac{\varepsilon_r-\varepsilon_{rm}}{2c^2}\omega_0^2E_m^+ + \frac{1}{2}\left(\beta_m^2-k_0^2\right)E_m^+ + ik_0\frac{\partial E_m^+}{\partial z} + i\frac{\varepsilon_r\omega_0}{c^2}\frac{\partial E_m^+}{\partial t} + \frac{\Delta\varepsilon\omega_0^2}{2c^2}E_m^- + \frac{3\chi^{(3)}\omega_0^2}{4c^2}\left|F_m\right|^2\left(\frac{1}{2}\left|E_m^+\right|^2+\left|E_m^-\right|^2\right)E_m^+\right]F_me^{-i(\omega t-k_0z)}$$
$$+\sum_{m=1,2}\left[\frac{\varepsilon_r-\varepsilon_{rm}}{2c^2}\omega_0^2E_m^- + \frac{1}{2}\left(\beta_m^2-k_0^2\right)E_m^- - ik_0\frac{\partial E_m^-}{\partial z} + i\frac{\varepsilon_r\omega_0}{c^2}\frac{\partial E_m^-}{\partial t} + \frac{\Delta\varepsilon\omega_0^2}{2c^2}E_m^+ + \frac{3\chi^{(3)}\omega_0^2}{4c^2}\left|F_m\right|^2\left(\frac{1}{2}\left|E_m^-\right|^2+\left|E_m^+\right|^2\right)E_m^-\right]F_me^{-i(\omega t+k_0z)}+c.c.=0. \quad (3.30)$$

We note that $\varepsilon_r = n^2(x,y) = n_0^2$ everywhere except in the two cores, and $\varepsilon_{rm} = n_m^2(x,y) = n_0^2$ everywhere except in the m-th core. Letting $\beta_m^2 - k_0^2 \approx 2k_0\Delta\beta$ where $\Delta\beta = \beta_m - k_0$, the corresponding terms in Eq. (3.30) mean detuning from the Bragg condition. Multiplying Eq. (3.30) by F_1^* (or F_2^*) and taking the integral over all transverse plane, the following coupled system of equations is obtained,

$$i\frac{\partial E_1^+}{\partial z} + \frac{\overline{n}}{c}\frac{\partial E_1^+}{\partial t} + \kappa E_1^- + \gamma\left(\left|E_1^+\right|^2+2\left|E_1^-\right|^2\right)E_1^+ + KE_2^+ = 0, \quad (3.31a)$$
$$-i\frac{\partial E_1^-}{\partial z} + \frac{\overline{n}}{c}\frac{\partial E_1^-}{\partial t} + \kappa E_1^+ + \gamma\left(\left|E_1^-\right|^2+2\left|E_1^+\right|^2\right)E_1^- + KE_2^- = 0, \quad (3.31b)$$
$$i\frac{\partial E_2^+}{\partial z} + \frac{\overline{n}}{c}\frac{\partial E_2^+}{\partial t} + \kappa E_2^- + \gamma\left(\left|E_2^+\right|^2+2\left|E_2^-\right|^2\right)E_2^+ + KE_1^+ = 0, \quad (3.31c)$$
$$-i\frac{\partial E_2^-}{\partial z} + \frac{\overline{n}}{c}\frac{\partial E_2^-}{\partial t} + \kappa E_2^+ + \gamma\left(\left|E_2^-\right|^2+2\left|E_2^+\right|^2\right)E_2^- + KE_1^- = 0, \quad (3.31d)$$

where κ, γ, and K are given in Eqs. (2.2), (2.10), and (2.25) respectively. We emphasize that in obtaining (3.31) and all the the coefficient it is assumed that the two cores are identical. Otherwise (3.31) takes the form of Eqs. 2.4.12-15 of Ref. [37].

Last, the method used above in obtaining NLCMEs is a general approach because we started from Maxwell's equations, even though many terms due to SVEA and phase-matching conditions were neglected. It is possible to incorporate all the neglected higher-order and phase-mismatched terms into Eqs. (3.31) separately. Al-

ternative approaches may be used in obtaining Eqs. (3.31) which are simpler: One approach is to start from Eqs. (2.9) and assume that modes of the individual gratings are perturbed as a result of coupling. Alternatively, it is valid to start from the nonlinear coupled mode equations (2.24) and assume that gratings written on the nonlinear coupler result in mode perturbations.

It is often convenient to normalize Eqs. (3.31) and express them in dimensionless form. Rescaling variables of Eqs. (2.11) and (2.12) we obtain,

$$iu_{1t} + iu_{1x} + \left(\frac{1}{2}|u_1|^2 + |v_1|^2\right)u_1 + v_1 + \lambda u_2 = 0, \tag{3.32a}$$

$$iv_{1t} - iv_{1x} + \left(\frac{1}{2}|v_1|^2 + |u_1|^2\right)v_1 + u_1 + \lambda v_2 = 0, \tag{3.32b}$$

$$iu_{2t} + iu_{2x} + \left(\frac{1}{2}|u_2|^2 + |v_2|^2\right)u_2 + v_2 + \lambda u_1 = 0, \tag{3.32c}$$

$$iv_{2t} - iv_{2x} + \left(\frac{1}{2}|v_2|^2 + |u_2|^2\right)v_2 + u_2 + \lambda v_1 = 0, \tag{3.32d}$$

where the rescaled linear coupling between the two cores is now,

$$\lambda = K\sqrt{\frac{\kappa}{2\gamma}}. \tag{3.33}$$

In terms of physical units $\Delta x = 1$ and $\Delta t = 1$ correspond to 1 mm and 10 ps respectively. Also, Bragg reflection length (L_B) and Coupling length (L_c) should be of the same order (e.g. ~ 1 mm) in order for the system to support soliton generation. Existing gratings have typical Bragg length of ~ 1 mm which is feasible for L_c, too. Also the Silica fiber nonlinear coefficient is $\sim 2\,(kmW)^{-1}$, therefore a peak power of 1 MW is required for the gap solitons to form in the structure. It is worth noting that this is an upper bound and experimental studies have demonstrated that significantly less power is needed to observe gap solitons [24, 25, 59, 60]. Using these parameters the required total length of the dual-core structure is ~ 10 cm [61].

3.3 Dispersive Reflectivity

Uniform gratings have been extensively studied and are commercially available for a variety of applications (cf. Section 2.1). Their nonuniform counterparts such as chirped gratings, apodized gratings, phase-shifted gratings, and superstructure gratings have been used in various applications such as signal processing and tunable fibre lasers [37,62–65]. For example, due to the sudden change of refractive index at the ends of a uniform grating, light is reflected back into the grating, forming a cavity that stops the pulses at lower or higher frequencies (compared to Bragg frequency) to pass through the grating. These are seen as sidebands in the grating spectrum. It has been shown experimentally that apodization not only increases the efficiency of coupling of light into the grating but also by removing the weak reflections at the grating ends, results in the grating spectrum sidebands to shrink [66].

In general, grating nonuniformities may be in the form of the grating period and/or the grating strength variations along the direction of propagation. Hence, nonuniform gratings can be generated by a nonuniform modulation of the refractive index, i.e.

$$n(x) = \overline{n} + \Delta n(x) \cos\left(\frac{2\pi x}{\Lambda} + \theta(x)\right), \tag{3.34}$$

where $\Delta n(x)$ and $\theta(x)$ are the amplitude and phase of the modulation. x-dependence of depth and phase modulation gives rise to the apodization and chirping of the grating, respectively, both of which result in the change of the photonic bandgap. Such effects may not be characterised accurately through the standard coupled mode equations that were derived in the previous section. A method has been put forward in Ref. [67] that takes into regard certain types of grating nonuniformities by introducing dispersive reflectivity. The phenomenological generalization of the standard model presented in Ref. [67] is able to predict light propagation in non-standard gratings and may be applicable to Bragg superstructures of various types [63,68,69],

gratings written on photonic wires [70], or semi-discrete Bragg gratings [71] and generally to structures in which the Bandgap in reflection spectra becomes broader and/or inhomogeneous. A common situation that may occur in an experiment is that the grating may have weak local variations in its refractive index (what one may call weakly disordered grating) due to the variations in the intensity of the ultraviolet laser beam used to make the grating or incoherence of the laser beams [31]. This may lead to random variations of $\theta(x)$ in Eq. (3.34) on a large scale.

The generalization has been applied to a variety of models such as the standard single-core fiber Bragg gratings [72], gratings equipped with cubic-quintic nonlinearity [54] and symmetric coupled fiber Bragg gratings [73, 74]. Due to its practical importance, in this section we derive the modified coupled mode equation incorporating the dispersive reflectivity term.

It is assumed that the local refractive index varies randomly along the grating length which may be accounted for by introducing a locally disturbed coordinate $\hat{x} = x + (2\pi/\Lambda)\,\theta(x)$, while taking the modulation depth Δn constant [67]. It should be noted that the linear coupling between the two cores is also assumed to be constant for simplicity. Substituting the refractive index from Eq. (3.34) into the wave equation, in order to evaluate the second and third terms in Eq. (3.18) one needs to deal with the terms

$$\left[\varepsilon_r + 2\Delta\varepsilon\cos\left(\frac{2\pi}{\Lambda} + \theta(x)\right)\right] E_{1,2} = \left[\overline{n} + \Delta n\cos\left(\frac{2\pi x}{\Lambda} + \theta(x)\right)\right]^2 E_{1,2}, \quad (3.35)$$

where we used the following relation,

$$\sqrt{\varepsilon_r + 2\Delta\varepsilon\cos\left(\frac{2\pi}{\Lambda} + \theta(x)\right)} \simeq \overline{n} + \Delta n\cos\left(\frac{2\pi x}{\Lambda} + \theta(x)\right), \quad 2\Delta\varepsilon \ll \varepsilon_r \quad (3.36)$$

The physical meaning of Eq. (3.35) is a phase mismatch in the exponential terms of Eq. (3.27) which results in the x-dependence of the grating coupling coefficient.

Following the method of Ref. [67] and Taylor expanding Eq. (3.35) and replacing the randomly varying values with their average, correction terms of $m\frac{\partial^2 v_{1,2}}{\partial x^2}$ and $m\frac{\partial^2 u_{1,2}}{\partial x^2}$ appear in the coupled mode equations,

$$iu_{1t} + iu_{1x} + \left(\frac{1}{2}\left|u_1\right|^2 + \left|v_1\right|^2\right) u_1 + v_1 + \lambda u_2 + m v_{1xx} = 0, \tag{3.37a}$$

$$iv_{1t} - iv_{1x} + \left(\frac{1}{2}\left|v_1\right|^2 + \left|u_1\right|^2\right) v_1 + u_1 + \lambda v_2 + m u_{1xx} = 0, \tag{3.37b}$$

$$iu_{2t} + iu_{2x} + \left(\frac{1}{2}\left|u_2\right|^2 + \left|v_2\right|^2\right) u_2 + v_2 + \lambda u_1 + m v_{2xx} = 0, \tag{3.37c}$$

$$iv_{2t} - iv_{2x} + \left(\frac{1}{2}\left|v_2\right|^2 + \left|u_2\right|^2\right) v_2 + u_2 + \lambda v_1 + m u_{2xx} = 0. \tag{3.37d}$$

where dispersive reflectivity parameter is defined as,

$$m \equiv 0.5\left(\frac{\Lambda}{2\pi}\right)\left\langle \theta^2(x)\right\rangle, \tag{3.38}$$

where $\langle \cdots \rangle$ representing the spatial average.

A similar approach is to assume that the spatial variations of refractive index are translated to the spatial variations of amplitudes of the coupled modes in each core. Taylor expanding the coupled term in say Eq. (3.31a) the following equation is obtained,

$$\kappa E_1^- = \kappa\left[E_1^- + \Delta x\frac{\partial E_1^-}{\partial x} + \frac{1}{2}(\Delta x)^2\frac{\partial^2 E_1^-}{\partial x^2} + O\left((\Delta x)^3\right)\right], \tag{3.39}$$

where E_1^- is a randomly varying function. Replacing the randomly varying function with its spatial average and noting that the average of Δx is zero due to its random nature, one obtains

$$\left\langle \kappa E_1^-\right\rangle \approx \kappa\left[E_1^- + \frac{1}{2}\left\langle(\Delta x)^2\right\rangle\frac{\partial^2 E_1^-}{\partial x^2}\right]. \tag{3.40}$$

Therefore defining dispersive reflectivity parameter as $m \equiv \frac{1}{2}\left\langle (\Delta x)^2 \right\rangle$ one arrives at Eq. (3.37). We also note that this correction term is consistent with the SVEA, as long as $m \gtrsim 10^{-4}$, which is the case in our simulations [75].

Chapter 4

Numerical Techniques

4.1 Introduction

Analytical expressions of solutions of the nonlinear coupled mode equations (NLCMEs) exist in some models such as the single-core standard Bragg grating with Kerr nonlinearity, as explained in Section 2.3, or in the special case of quiescent cubic-quintic solitons where NLCMEs are solved analytically by separation of variables [76]. However analytical solutions to the model of Eqs. (3.37) are not known to this date. In the case of $m = 0$, i.e. two uniform coupled Bragg gratings, approximate analytical solutions have been derived using variational techniques for stationary solitons [77]. However, it was shown that the obtained solutions deviate significantly from the exact numerical solutions in the case of moving solitons. That is why in this thesis we base our study on the numerical techniques presented in this chapter, to directly solve the NLCMEs for both quiescent and moving soliton solutions in the general case of non-uniform gratings. The obtained soliton solutions are then propagated numerically in the model to investigate the properties of the system. All the computer programs in this work were written in FORTRAN 95 programing language for better efficiency.

In Section 4.2 we explain the relaxation method used to solve the NLCMEs in details. In Section 4.3 the interpolation technique used in this work is explained. Lastly, Section 4.4 is dedicated to the well-known split-step Fourier method that is often utilized to propagate the soliton pulses in fiber-based structures.

4.2 Relaxation Method

The system of NLCMEs in (3.37) can be categorized as a nonlinear coupled Partial Differential Equation (PDE). One common approach in solving PDEs is to transform them into ordinary differential equations (ODE) with the use of separation of variables. Similarly in the case of coupled PDEs it may be possible to decouple the equations into ODEs. The obtained ODEs are then solved numerically or analytically where possible. In the case of Eqs. (3.37) solitons are searched for in the form of stationary solutions that maintain their shape while propagating along the fiber. The following separation of variables may be used,

$$\begin{aligned} u_{1,2}(x,t) &= exp(-i\Omega t)\, U_{1,2}(X), \\ v_{1,2}(x,t) &= exp(-i\Omega t)\, V_{1,2}(X), \end{aligned} \tag{4.1}$$

where $X = x - vt$ is the coordinate in the reference frame moving with the solitons velocity v. Substituting Eqs. (4.1) into Eqs. (3.37) we arrive at the following set of coupled nonlinear ODEs,

$$\begin{aligned} &\Omega U_1 + i(1-v)\, U_{1X} + \left(\frac{1}{2}|U_1|^2 + |U_1|^2\right) U_1 + V_1 + \lambda U_2 + mV_{1XX} = 0 \\ &\Omega V_1 - i(1+v)\, V_{1X} + \left(\frac{1}{2}|V_1|^2 + |U_1|^2\right) V_1 + U_1 + \lambda v_2 + mU_{1XX} = 0 \\ &\Omega U_2 + i(1-v)\, U_{2X} + \left(\frac{1}{2}|U_2|^2 + |V_2|^2\right) U_2 + V_2 + \lambda u_1 + mV_{2XX} = 0 \\ &\Omega V_2 - i(1+v)\, V_{2X} + \left(\frac{1}{2}|V_2|^2 + |U_2|^2\right) V_2 + U_2 + \lambda V_1 + mU_{2XX} = 0, \end{aligned} \tag{4.2}$$

where the subscript X stands for d/dX. Equations (4.2) form a one-dimensional boundary value problem with the boundary conditions of $U_{1,2}(\pm\infty) = V_{1,2}(\pm\infty) = 0$. As inferred from Eqs. 4.2, it is not possible to decouple Eqs. (3.37) by separation of variables and therefore it is required to solve the equations numerically. For this purpose a relaxation algorithm, which is explained in this section, has been used throughout this thesis to obtain soliton solutions.

The relaxation method that we use in this thesis to solve the ODEs in Eqs. (4.2) is based on a deferred correction technique and Newton iteration [78]. The iterative method starts with an initial guess which may be the soliton solution to a simpler model such as that of Nonlinear Schrodinger Equations (NLS) or even single-core standard grating with Kerr nonlinearity. The algorithm then corrects the approximate solution at each iteration using Newton iteration and deferred corrections with the objective of making the error everywhere less than the defined tolerance (10^{-8} in this thesis). The computational window needs to be carefully chosen in order for the algorithm to converge accurately. As a rule of thumb it needs to be an order of magnitude greater than the width of the approximate solution.

There are cases that the initial guessed solution deviates substantially from the exact solution which causes the iterations to diverge (the error in each iteration becomes larger), specially in the presence of strong dispersive reflectivity. For instance to obtain the asymmetric soliton solutions near the bifurcation points, as shown in Figure 4.1(a), for given ω, m, and v, it is required to apply relaxation algorithm recursively. More specifically, to find the asymmetric solitons for point D where $|\lambda_D| \sim |\lambda_c|$, it is necessary to set the initial guess to the solution obtained for point C where $|\lambda_C| < |\lambda_D|$. Sometimes this process has to be repeated several times, i.e. to obtain the solutions at point D solutions of points A, B, and C need to be obtained respectively, as shown in Figure 4.1(a) . Similar approach is needed in obtaining symmetric solution at point B near the bandgap edge, as shown in Figure 4.1(b).

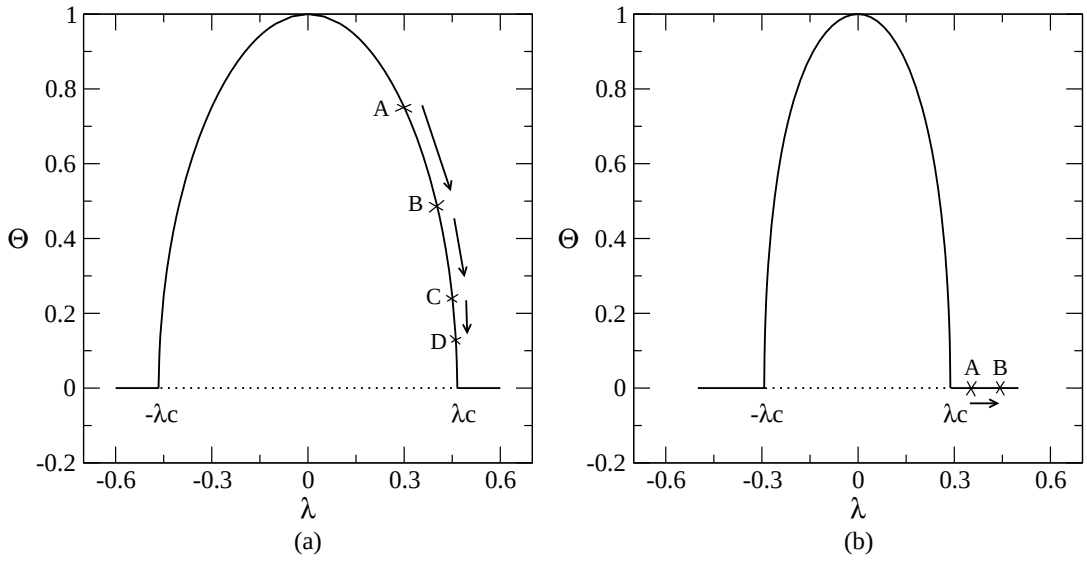

Figure 4.1: Schematic diagram showing the application of relaxation algorithm recursively to Eqs. (4.2) in order to obtain (a) asymmetric soliton solutions near bifurcation points, and (b) symmetric soliton solutions near bandgap edges. Bifurcation graphs are explained in Chapter 5.

4.3 Interpolation

The relaxation algorithm described in Section 4.2 requires a large mesh for the resulted finite-difference equation to have an accurate solution (cf. [78]). We used 50,000 (and 100,000 where needed) points in our simulations. However propagating the obtained solutions using such large number of points is not feasible nor efficient. Therefore a Lagrange interpolation is used to first reduce the number of points [79]. The mapped mesh uses 2^n points to improve the efficiency of the Fast Fourier Transform (FFT) algorithm, where n is an integer. In our work n is set to 11 or 12 where more accuracy is needed, for instance where a larger computational window is used. In analyzing the interaction and collisions of solitons it is required to change the size of the computational window for which interpolation is also used.

4.4 Numerical Pulse Propagation

Pulse propagation in optical domain often involves solving PDEs for given initial values. For instance propagation of solitons along a nonlinear optical fiber involves solving NLS equation to obtain the field envelopes and distributions in the cross section of the fiber, over time. This is an initial value problem because the field amplitudes along the fiber depend on the initial field distribution. Another example is of course propagation of solitons in gratings using NLCMEs. Generally nonlinear optical waveguides whose governing equations posses solutions in an analytical form are very rare [80], thus analytical approaches are limited to special cases such as solving NLS in cases where inverse scattering method can be applied [81]. On the contrary, very complicated pulse propagation problems can be solved using a numerical procedure. Even if an analytical form does exist, the solutions may be hard to interpret without the use of numerical computations.

Much effort have been put towards developing more efficient numerical techniques for solving soliton propagation problems. These techniques fall under two categories of finite difference and spectral domain or pseudospectral methods. Finite difference methods, such as the Crank-Nicolson method, approximate the partial derivatives by finite difference equations. There are known disadvantages for finite difference methods such as slow convergence, large memory requirement and low stability. With the help of current computers large memory is not an issue however computation time can be long if high spatial and temporal resolution is required to ensure accurate results. Yet they may be the preferred method for some nonlinear equations [82].

Spectral methods on the other hand, such as Fourier methods, solve equations in the Fourier domain. Spectral methods are sometime called pseudospectral methods because these methods only partially involve evaluating frequency domain terms. Pseudospectral methods are generally faster by an order of magnitude than time domain methods to obtain the same accuracy due to the speed of FFT algorithm

[83,84]. As mentioned in the previous section, the efficiency of the FFT is maximized by using 2^n simulation points, where n is an integer. Numerical simulations in this thesis are done using a symmetrised split-step Fourier method [85, 86]. The name arises for two reasons. First, the method relies on computing the solution in small steps, and treating the linear and the nonlinear steps separately (see below). Second, it is necessary to transform field components between time and frequency domains successively because the linear step is done in the frequency domain while the nonlinear step is made in the time domain [4].

4.4.1 Split-step Fourier Method

Split-step Fourier method is one of the most widely used methods in soliton propagation problems specially in solving NLS equation and NLCMEs [86,87]. This method has been elaborated in Ref. [4]. Due to its importance in this thesis, in what follows we repeat the same procedure. The method is then applied to the model of Eqs. (3.37) in the next section to propagate soliton solutions in the model.

It is possible to write a PDE such as NLS equation in the following form,

$$\frac{\partial A}{\partial t} = \left(\hat{D} + \hat{N}\right) A, \tag{4.3}$$

where $\hat{D}$ and $\hat{N}$ are the spatial dispersion and nonlinear operators, respectively. Assuming $A(x, t_0)$ is the initial boundary condition, field distribution at $t = t_0 + \Delta t$, where Δt is the step size, may be written as

$$A\left(x, t_0 + \Delta t\right) = \exp\left(\Delta t \left(\hat{D} + \hat{N}\right)\right) A\left(x, t_0\right), \tag{4.4}$$

which can be approximated by

$$A\left(x, t_0 + \Delta t\right) \approx \exp\left(\Delta t \hat{D}\right) \exp\left(\Delta t \hat{N}\right) A\left(x, t_0\right). \tag{4.5}$$

We say approximated because the two operators do not commute. More specifically,

in obtaining Eq. (4.5) from (4.4) we have neglected the commutators in Baker-Hausdorff expansion [4],

$$\exp\left(\Delta t\hat{D}\right)\exp\left(\Delta t\hat{N}\right) = \exp\left(\Delta t\hat{D}+\Delta t\hat{N}+\frac{1}{2}\left[\Delta t\hat{D},\Delta t\hat{N}\right]+\frac{1}{12}\left[\Delta t\hat{D}-\Delta t\hat{N},\left[\Delta t\hat{D},\Delta t\hat{N}\right]\right]+\cdots\right), \tag{4.6}$$

where $\left[\Delta t\hat{D},\Delta t\hat{N}\right] = \Delta t\hat{D}\Delta t\hat{N} - \Delta t\hat{N}\Delta t\hat{D}$ is a commutator.

Nonlinear term in Eq. (4.5), i.e. $\exp\left(\Delta t\hat{N}\right)A(x,t)$, is evaluated using finite difference method, while the dispersion term can be easily calculated in spectral domain using the following relation:

$$\exp\left(\Delta t\hat{D}\right)A(x,t_0) = F^{-1}\left\{\exp\left(\Delta t\tilde{D}\right)\tilde{A}(x,t_0)\right\}, \tag{4.7}$$

where F^{-1} is the inverse Fourier transform, and $\tilde{D}$ and $\tilde{A}$ are dispersion operator and pulse envelope in Fourier domain, respectively. So by repeating the procedure the field envelope at any time can be obtained.

The accuracy of the method through Baker-Hausdorff formula is found to be in orders of $(\Delta t)^2$. That is an accuracy of 6 decimal places for increments of $\Delta t = 0.001$ which is not satisfactory. This can be improved by taking two half dispersion steps and compute the nonlinear term at the middle of the segment,

$$A(x,t_0+\Delta t) \approx \exp\left(\frac{\Delta t}{2}\hat{D}\right)\exp\left(\Delta t\hat{N}\right)\exp\left(\frac{\Delta t}{2}\hat{D}\right)A(x,t_0). \tag{4.8}$$

The latter is called symmetrised split-step Fourier method [88]. In Eq. (4.8) (and (4.5)) it is assumed that nonlinearity is constant over the segment. By including the nonlinearity over the whole segment the accuracy of the method can be further

improved, i.e.

$$A\left(x,t_0+\Delta t\right)\approx\exp\left(\frac{\Delta t}{2}\hat{D}\right)\exp\left(\int_{t_0}^{t_0+\Delta t}\hat{N}\left(\tau\right)d\tau\right)\exp\left(\frac{\Delta t}{2}\hat{D}\right)A\left(x,t_0\right), \quad (4.9)$$

where the accuracy is on the order of $(\Delta t)^3$. When applying the method over N consecutive segments, Eq. (4.8) can be written as

$$A\left(x,t_0+N\Delta t\right)\approx \exp\left(-\frac{\Delta t}{2}\hat{D}\right)\left[\prod_{n=1}^{N}\exp\left(\Delta t\hat{D}\right)\exp\left(\int_{t_0}^{t_0+\Delta t}\hat{N}\left(\tau\right)d\tau\right)\right]\exp\left(\frac{\Delta t}{2}\hat{D}\right)A\left(x,t_0\right) \quad (4.10)$$

where the number of required FFTs are halved, resulting in the evaluation time to be twice as fast.

4.4.2 Runge-Kutta Method

The accuracy of split-step Fourier method, as mentioned in the previous subsection, depends greatly on how the nonlinear step is evaluated. Iterative methods may be used to directly evaluate the nonlinear operator in each step. There is trade off between the total computation time and the accuracy of the iterative method used. The one iterative method that suits our purpose is 4th order Runge-Kutta method or shortly RK4 which is briefly explained in this subsection.

Let's consider a general linear ODE such as

$$\frac{\partial y}{\partial t}=f\left(t,y\left(t\right)\right). \quad (4.11)$$

The value of $y\left(t_0+\triangle t\right)$ (the next value) can then be approximated by $y\left(t_0\right)$ (present value) as

$$y\left(t+\triangle t\right)=y\left(t\right)+\frac{\triangle t}{6}\left(K_1+2K_2+2K_3+K_4\right), \quad (4.12)$$

where,

$$
\begin{aligned}
K_1 &= f\left(t_0, y\left(t_0\right)\right) \\
K_2 &= f\left(t_0 + \frac{\triangle x}{2}, y\left(t_0\right) + \frac{\triangle x}{2} K_1\right) \\
K_3 &= f\left(t_0 + \frac{\triangle x}{2}, y\left(t_0\right) + \frac{\triangle x}{2} K_2\right) \\
K_4 &= f\left(t_0 + \triangle x, y\left(t_0\right) + \triangle x K_3\right).
\end{aligned} \tag{4.13}
$$

The total accumulated error of RK4 is on the order of $(\triangle t)^4$ [79, 89].

4.5 Application to the Model

In this section we apply the split-step Fourier method to the problem of linearly coupled Bragg gratings with dispersive reflectivity, utilizing RK4 in evaluating the nonlinear step.

We start by rewriting Eqs. (3.37),

$$
\begin{aligned}
u_{1t} &= i\, m v_{1xx} - u_{1x} + i\left(\frac{1}{2}\left|u_1\right|^2 + \left|v_1\right|^2\right) u_1 + i v_1 + i\lambda u_2, \\
v_{1t} &= i\, m u_{1xx} + v_{1x} + i\left(\frac{1}{2}\left|v_1\right|^2 + \left|u_1\right|^2\right) v_1 + i u_1 + i\lambda v_2, \\
u_{2t} &= i\, m v_{2xx} - u_{2x} + i\left(\frac{1}{2}\left|u_2\right|^2 + \left|v_2\right|^2\right) u_2 + i v_2 + i\lambda u_1, \\
v_{2t} &= i\, m u_{2xx} + v_{2x} + i\left(\frac{1}{2}\left|v_2\right|^2 + \left|u_2\right|^2\right) v_2 + i u_2 + i\lambda v_1.
\end{aligned} \tag{4.14}
$$

We now note that to write Eqs. (4.14) in the form of Eq. (4.3), dispersion and

nonlinear operators can be written in the matrix form as follow,

$$\hat{D} \equiv \begin{bmatrix} -\frac{\partial}{\partial x} & im\frac{\partial^2}{\partial x^2} & 0 & 0 \\ im\frac{\partial^2}{\partial x^2} & \frac{\partial}{\partial x} & 0 & 0 \\ 0 & 0 & -\frac{\partial}{\partial x} & im\frac{\partial^2}{\partial x^2} \\ 0 & 0 & im\frac{\partial^2}{\partial x^2} & \frac{\partial}{\partial x} \end{bmatrix}, \tag{4.15a}$$

$$\hat{N} \equiv \begin{bmatrix} i\left(\frac{1}{2}\left|u_1\right|^2+\left|v_1\right|^2\right) & i & i\lambda & 0 \\ i & i\left(\frac{1}{2}\left|v_1\right|^2+\left|u_1\right|^2\right) & 0 & i\lambda \\ i\lambda & 0 & i\left(\frac{1}{2}\left|u_2\right|^2+\left|v_2\right|^2\right) & i \\ 0 & i\lambda & i & i\left(\frac{1}{2}\left|v_2\right|^2+\left|u_2\right|^2\right) \end{bmatrix}, \tag{4.15b}$$

where the field envelop $A(x,t)$ is the following matrix,

$$A(x,t) = \begin{bmatrix} u_1(x,t) \\ v_1(x,t) \\ u_2(x,t) \\ v_2(x,t) \end{bmatrix}. \tag{4.16}$$

It should be noted that the last two linear terms in each of the Eqs. (4.14) are calculated in the nonlinear step to make dispersion step, which is calculated in frequency domain, simpler and more efficient.

As explained in Section 4.4.1 the dispersion and nonlinear steps are evaluated separately. The nonlinear step involves calculating the RK4 coefficients according to Eqs. (4.13), where $f(x) = \hat{N}A(x,t_0)$, to find the four field components at $t = t_0 + \triangle t$ (note that the right side of Eqs. (4.14) are independent of time in each step). The dispersion step on the other hand involves solving four ODEs in Fourier domain, i.e.

solving the following matrix form equations,

$$\begin{bmatrix} \tilde{u}_{1t} \\ \tilde{v}_{1t} \\ \tilde{u}_{2t} \\ \tilde{v}_{2t} \end{bmatrix} = \begin{bmatrix} -i\omega & -im\omega^2 & 0 & 0 \\ -im\omega^2 & i\omega & 0 & 0 \\ 0 & 0 & -i\omega & -im\omega^2 \\ 0 & 0 & -im\omega^2 & i\omega \end{bmatrix} \begin{bmatrix} \tilde{u}_1 \\ \tilde{v}_1 \\ \tilde{u}_2 \\ \tilde{v}_2 \end{bmatrix}, \tag{4.17}$$

where $\tilde{u}_{1,2}$ and $\tilde{v}_{1,2}$ are Fourier domain counterparts. As inferred from Eq. (4.17), the two cores do not interact in the dispersion step which makes it possible to evaluate the dispersion step in two easy steps: First, we note that equations take the following form

$$\begin{aligned} \tilde{u}_{1,2t} &= -i\omega\tilde{u}_{1,2} - im\omega^2\tilde{v}_{1,2}, \\ \tilde{v}_{1,2t} &= \quad i\omega\tilde{v}_{1,2} - im\omega^2\tilde{u}_{1,2}. \end{aligned} \tag{4.18}$$

We can treat Eqs. (4.18) in two sub-steps as follows: the first step involves the following

$$\left.\begin{array}{rcl} \tilde{u}_{1,2t} & = & -i\omega\tilde{u}_{1,2} \\ \tilde{v}_{1,2t} & = & i\omega\tilde{v}_{1,2} \end{array}\right\} \Longrightarrow \left\{\begin{array}{rcl} \tilde{u}_{1,2}(t) & = & \tilde{u}_{1,2}(0)\, e^{-i\omega\triangle t} \\ \tilde{v}_{1,2}(t) & = & \tilde{v}_{1,2}(0)\, e^{i\omega\triangle t} \end{array}\right. , \tag{4.19}$$

while in the second step we take the second terms in Eqs. (4.18) separately. It follows,

$$\begin{aligned} \tilde{u}_{1,2}(t) &= \tilde{u}_{1,2}(0)\cos\left(m\omega^2 t\right) - i\tilde{v}_{1,2}(0)\sin\left(m\omega^2 t\right), \\ \tilde{v}_{1,2}(t) &= \tilde{v}_{1,2}(0)\cos\left(m\omega^2 t\right) - i\tilde{u}_{1,2}(0)\sin\left(m\omega^2 t\right). \end{aligned} \tag{4.20}$$

Combining (4.19) and (4.20) and letting $t = t_0 + \triangle t$ leads to

$$\begin{aligned} \tilde{u}_{1,2}(t_0+\triangle t) &= \left[\tilde{u}_{1,2}(t_0)\cos\left(m\omega^2\triangle t\right) - i\tilde{v}_{1,2}(t_0)\sin\left(m\omega^2\triangle t\right)\right] e^{-i\omega\triangle t}, \\ \tilde{v}_{1,2}(t_0+\triangle t) &= \left[\tilde{v}_{1,2}(t_0)\cos\left(m\omega^2\triangle t\right) - i\tilde{u}_{1,2}(t_0)\sin\left(m\omega^2\triangle t\right)\right] e^{i\omega\triangle t}. \end{aligned} \tag{4.21}$$

The latter was implemented as

$$\tilde{u}_{1,2}(t_0+\triangle t) = \frac{1}{2}\left[\left(\tilde{u}_{1,2}(t_0)+\tilde{v}_{1,2}(t_0)\right)e^{-im\omega^2\triangle t} + \left(\tilde{u}_{1,2}(t_0)-\tilde{v}_{1,2}(t_0)\right)e^{im\omega^2\triangle t}\right]e^{-i\omega\triangle t},$$
$$\tilde{v}_{1,2}(t_0+\triangle t) = \frac{1}{2}\left[\left(\tilde{u}_{1,2}(t_0)+\tilde{v}_{1,2}(t_0)\right)e^{-im\omega^2\triangle t} - \left(\tilde{u}_{1,2}(t_0)-\tilde{v}_{1,2}(t_0)\right)e^{im\omega^2\triangle t}\right]e^{i\omega\triangle t}. \tag{4.22}$$

The propagation parameters in this thesis were $\Delta t = 0.001$, and 2^{10} or 2^{11} mesh points depending on the size of computational window. More specifically, analyzing interactions and collisions of solitons require a wider computational window of typically 140 (dimensionless units of length) which requires a larger mesh, while stability analysis are done using a computational window in the range $60 \sim 100$ units, depending on the soliton width (which in turn depends on soliton frequency).

So far, we have discussed pulse propagation in the laboratory reference frame. Using this method in propagating moving pulses for long times requires a wider computational window which requires a larger mesh for the same accuracy. For example for $v = 0.2$ approximately a minimum window of $260 \sim 300$ is required (the window size depends on the pulse width) to propagate the pulse for $t = 1000$, for which a minimum of 2^{11} points are necessary for acceptable accuracy. Such simulation takes about 15 minutes on the machine that was used for our simulations. In cases that $t = 3000$ is required the method is clearly inefficient, taking up to a few hours for one propagation to complete; often tens of simulations are needed to characterize soliton propagation within a region.

To solve this problem, a method is adopted in this thesis which involves transforming the equations into the moving frame. The method is explained in details in Chapter 6. This enables us to use a smaller computational window (in the range $60 \sim 100$), simply because the pulse does not move in the moving frame. Consequently, smaller number of points are required (2^{10} or 2^{11} points depending on the window size).

Split-step Fourier method in the moving frame can then be applied by following the same procedure explained in Eqs. (4.17)-(4.22). The nonlinear step is identical to the lab frame, however starting from Eqs. (4.2) the dispersion step takes the form

$$\tilde{u}_{1,2}\left(t_0+\triangle t\right)= \frac{1}{2}\left[\left(\tilde{u}_{1,2}\left(t_0\right)+\tilde{v}_{1,2}\left(t_0\right)\right)e^{-im\omega^2\triangle t}+\left(\tilde{u}_{1,2}\left(t_0\right)-\tilde{v}_{1,2}\left(t_0\right)\right)e^{im\omega^2\triangle t}\right]e^{-i\omega(1-v)\triangle t},$$

$$\tilde{v}_{1,2}\left(t_0+\triangle t\right)= \frac{1}{2}\left[\left(\tilde{u}_{1,2}\left(t_0\right)+\tilde{v}_{1,2}\left(t_0\right)\right)e^{-im\omega^2\triangle t}-\left(\tilde{u}_{1,2}\left(t_0\right)-\tilde{v}_{1,2}\left(t_0\right)\right)e^{im\omega^2\triangle t}\right]e^{i\omega(1-v)\triangle t}. \tag{4.23}$$

Last, the computational window must be equipped with absorbing boundaries to absorb not only the reflections of noise from the boundaries but also the pulses that reach the window ends. Otherwise due to the FFT algorithm both the noise and pulses will re-enter the computational window. The absorbing boundaries that were used in this thesis are very similar in principle of operation to uniaxial perfectly matched layers (UPML) [90]. More specifically, they construct the conditions under which reflections of the incident waves off the boundaries are minimized.

Chapter 5

Quiescent Gap Solitons

In this chapter we investigate the existence and stability of quiescent gap solitons in a system of coupled Bragg gratings with dispersive reflectivity. The starting point is Eqs. (3.37). As explained in Chapter 4, generally there are no known analytical solutions for the NLCMEs describing dual-core FBGs with or without dispersive reflectivity. Therefore we rely on numerical methods to solve the NLCMEs for soliton solutions. The obtained solutions are then propagated using the split-step Fourier method, which was described in Chapter 4, to characterize the stability and interactions of quiescent gap solitons in the system.

In the next section, we first analyze the photonic bandgap of the structure in which solitons may exist. The types of soliton solutions that may exist in the bandgap are then investigated. In Section 5.2 analytical forms of the quiescent soliton tails are derived. Section 5.3 addresses the stability of quiescent solitons in detail followed by Section 5.4 which is dedicated to the study of quiescent soliton interactions.

5.1 Quiescent Solutions

To characterize the spectral gap within which gap solitons may exist, it is necessary to analyze the linear spectrum of the system. Substituting plane wave solutions,

i.e. $u_{1,2}, v_{1,2} \sim exp\,(ikx - i\omega t)$ where ω is the frequency detuning and k is the wave number, into the linearized form of Eqs. (3.37), i.e.

$$\begin{aligned} iu_{1t} + iu_{1x} + v_1 + \lambda u_2 + mv_{1xx} &= 0, \\ iv_{1t} - iv_{1x} + u_1 + \lambda v_2 + mu_{1xx} &= 0, \\ iu_{2t} + iu_{2x} + v_2 + \lambda u_1 + mv_{2xx} &= 0, \\ iv_{2t} - iv_{2x} + u_2 + \lambda v_1 + mu_{2xx} &= 0, \end{aligned} \tag{5.1}$$

we arrive at the the following equations in the matrix form,

$$\begin{bmatrix} \omega - k & 1 - mk^2 & \lambda & 0 \\ 1 - mk^2 & \omega + k & 0 & \lambda \\ \lambda & 0 & \omega - k & 1 - mk^2 \\ 0 & \lambda & 1 - mk^2 & \omega + k \end{bmatrix} \begin{bmatrix} u_1 \\ v_1 \\ u_2 \\ v_2 \end{bmatrix} = 0. \tag{5.2}$$

For Eq. (5.2) to have non-trivial solutions, the determinant of the coefficients matrix must be zero. This gives rise to the following dispersion relation,

$$\omega^2 = \left(1 - mk^2\right)^2 + \lambda^2 + k^2 \pm 2\lambda\sqrt{(1 - mk^2)^2 + k^2}. \tag{5.3}$$

Positive and negative signs account for the upper and lower branches of the dispersion relation, respectively. Four branches of Eq. (5.3) are plotted in Figures 5.1(a)-(c) for different values of λ and m. The dispersion relation for $m = 0$, i.e. standard model, is shown with doted lines. Figure 5.1(c) shows that no soliton solution exist for $\lambda = 1$ because the bandgap closes.

To find the bandgap we look for the roots of $\partial\omega^2/\partial k^2 = 0$. The following bandgap is obtained,

$$\omega^2 \;<\; \omega_0^2 = \begin{cases} (1 - |\lambda|)^2 & m \leq 0.5 \\ \left(\frac{\sqrt{4m-1}}{2m} - |\lambda|\right)^2 & m > 0.5 \end{cases} \tag{5.4}$$

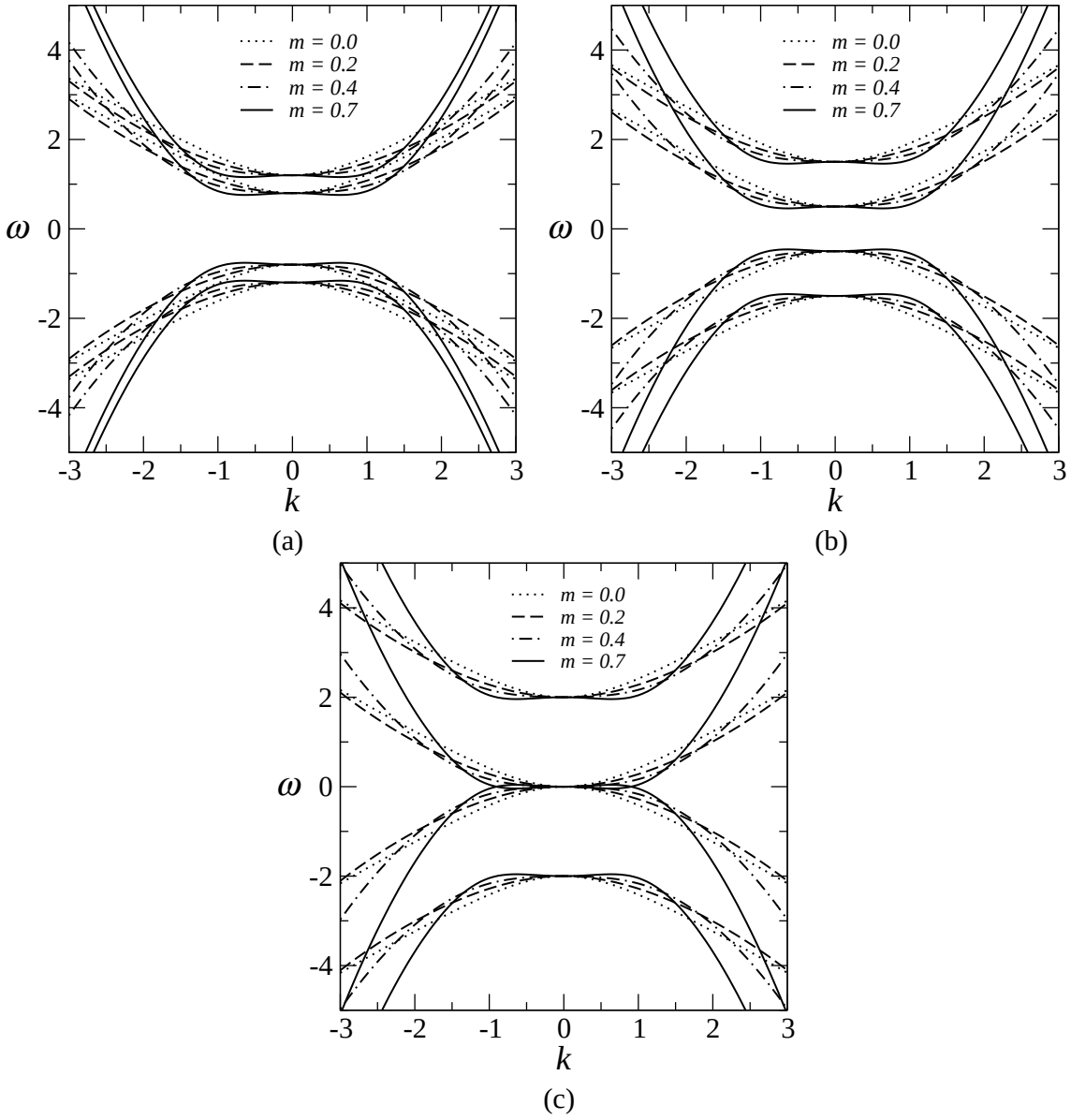

Figure 5.1: Dispersion curves for $m = 0$, 0.2, 0.4, and 0.7 and (a) $\lambda = 0.2$, (b) $\lambda = 0.5$, and (c) $\lambda = 1$.

where ω_0^2 is the minimum value of $\omega^2(k^2)$, i.e. where group velocity is zero, and is found at $k^2 = 0$ if $m \leq 0.5$ and $k^2 = (2m-1)/2m^2$ if $m > 0.5$. Equation (5.4) shows that the bandgap does not exist for $|\lambda| \geq 1$ when $m \leq 0.5$ and $|\lambda| \geq \frac{\sqrt{4m-1}}{2m}$ when $m > 0.5$.

It is worth noting that for $\lambda = 0$, the dispersion relation in (5.4) takes the

following form,

$$\omega^2 = \left(1 - mk^2\right)^2 + k^2, \tag{5.5}$$

which leads to the bandgap of $|\omega| \leq 1$; same as the bandgap in a single non-uniform grating found in Ref. [67]. Another finding is that for the range of $m \leq 0.5$ the size of the bandgap in (5.4) does not depend on m. However, as shown in Figures 5.1(a)-(c), the bandgap becomes smaller as m increases in the range $m > 0.5$. Since the values of $m > 0.5$ may not be of physical significance, without loss of generality, we restrict our analysis to $m \leq 0.5$ [67, 72].

Stationary soliton solutions are sought for in the following form,

$$\{u_{1,2}(x,t), v_{1,2}(x,t)\} = \{U_{1,2}(x), V_{1,2}(x)\} exp(i\omega t). \tag{5.6}$$

Substituting Eq. (5.6) into (3.37) and invoking the symmetry condition for quiescent solutions, i.e.

$$v_{1,2} = -u^*_{1,2}, \tag{5.7}$$

we arrive at the following system of nonlinear differential equations,

$$\begin{aligned} \omega U_1 + iU_1' + \frac{3}{2}|U_1|^2 U_1 - U_1^* + \lambda U_2 - mU_1^{*''} &= 0, \\ \omega U_2 + iU_2' + \frac{3}{2}|U_2|^2 U_2 - U_2^* + \lambda U_1 - mU_2^{*''} &= 0, \end{aligned} \tag{5.8}$$

where the prime represents a derivative with respect to x. We solved Eqs. (5.8) for various values of parameters and found that gap solitons exist everywhere within the bandgap. Also, Eqs. (5.8) readily show that the system supports symmetric solutions, i.e. by replacing $U_1 \rightarrow U_2$ and $U_2 \rightarrow U_1$ we arrive at the same equations. This is similar to the case of $m = 0$ that have been studied in Ref. [77].

In general, the system of Eqs. (5.8) supports two types of symmetric ($U_1 = U_2$) and asymmetric solitons ($U_1 \neq U_2$). A key finding is that for given ω and m there exists a critical linear coupling coefficient λ_c at which the two types of solutions

bifurcate. To explain this further it may be useful to define an asymmetry parameter as follow,

$$\Theta = \frac{U_{1m}^2 - U_{2m}^2}{U_{1m}^2 + U_{2m}^2}, \tag{5.9}$$

where $U_{1m,2m}$ are the maximum amplitudes of the forward-propagating waves in the two cores. It is worth noting that the above relation can also be defined using backward-propagating waves $V_{1,2}$ which leads to the same values of asymmetry parameter.

Asymmetry parameter is illustrated in Figure 5.2 in the plane of (λ, Θ) for different values of ω and m. The horizontal lines in Figures 5.2(a)-(d) account for $\Theta = 0$, i.e. symmetric solutions. It should be noted that $|U_{1m}|$ may be smaller than $|U_{2m}|$ resulting in negative values of Θ. Figure 5.2 only shows the positive branches of Θ simply because the negative branches are the mirror images of the positive branches. Also according to Eq. (5.4) the gap closes at $\pm(1 - |\lambda|)$. This is why for example in Figure 5.2(c) the horizontal lines stop at ± 0.5.

As Figure 5.2 show, at any given ω and m and for values of $|\lambda| < \lambda_c$ both symmetric and asymmetric solutions are found while for the range $|\lambda| \geq \lambda_c$ the system of Eqs. (5.8) only supports symmetric solutions. The dotted horizontal lines in Figure 5.2 depicts symmetric solutions that coexist with asymmetric ones. A striking finding is that λ_c, as Figure 5.2 shows, varies with m. More specifically, as m increases λ_c decreases. In Section 5.4 we will explain how this feature translates to the broadening of the stability region.

Figures 5.3(a)-(f) show examples of the solutions of Eqs. (5.8). Figures 5.3(a), (b) and (f) show examples of asymmetric and symmetric solutions for $\omega = 0.5$, $\lambda = 0.2$, and $m = 0.4$, respectively (for these parameters $\Theta = 0.7885$).

As shown in Figures 5.3(c)-(e) with increase of the dispersive reflectivity parameter, soliton profiles change significantly. More specifically, they develop sidelobes for larger values of m. Similar results have been reported in the single core

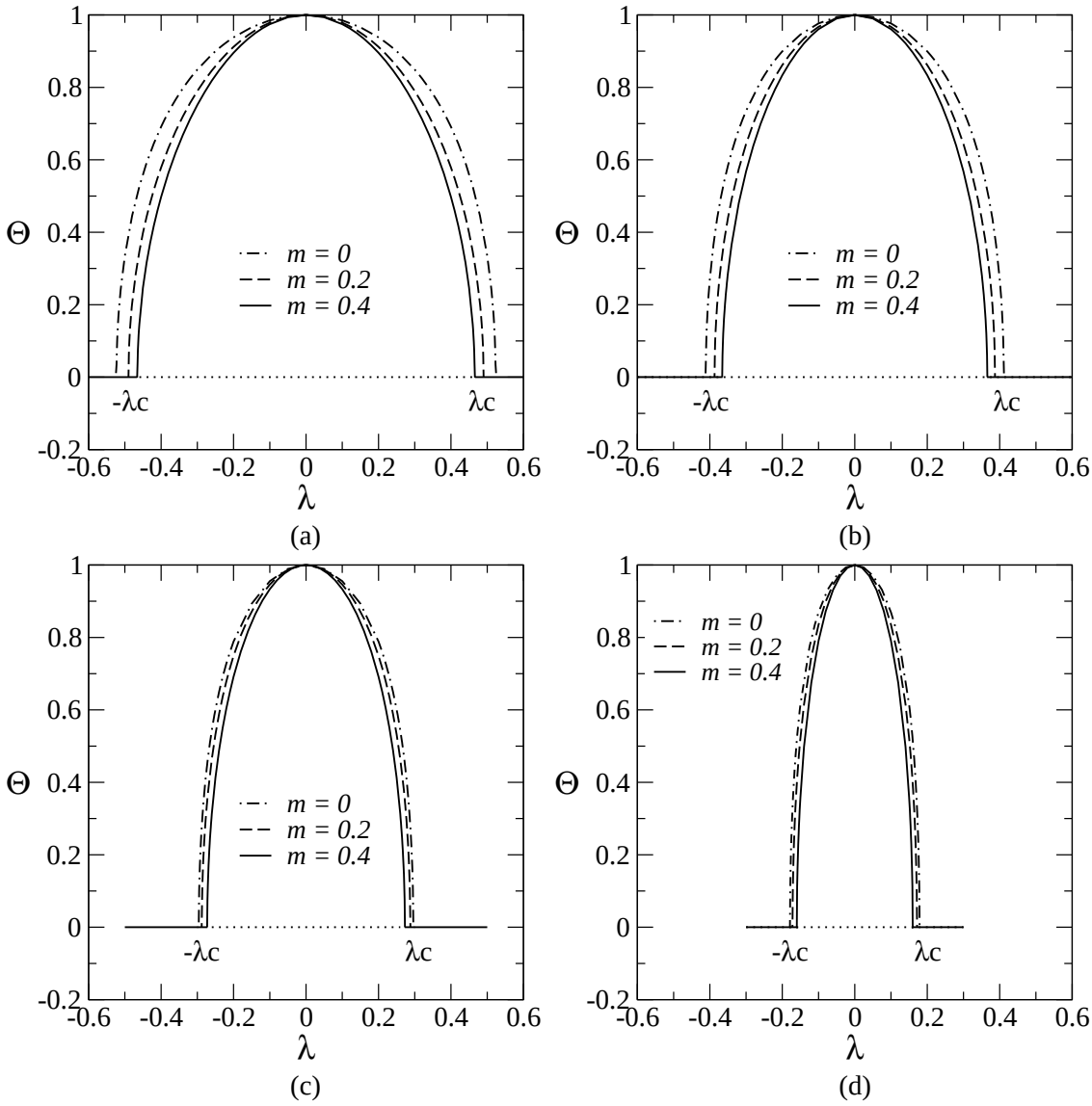

Figure 5.2: Bifurcation diagrams for (a) $\omega = 0.1$, and (b) $\omega = 0.3$, (c) $\omega = 0.5$, and (d) $\omega = 0.7$ and different values of dispersive reflectivity. The negative branches being the mirror images of the positive branches are not shown. According to Eq. (5.4) the gap closes at $\lambda = \pm 0.9$, ± 0.7, ± 0.5 and ± 0.3 in (a)-(d), respectively.

standard model [67] and also single core model equipped with cubic-quintic nonlinearity [54]. To better illustrate the sidelobes, in Figure 5.3(e) the amplitudes of forward-propagating waves (U_1) are plotted in logarithmic scale for $m = 0$ and 0.4. Figure 5.3(e) shows the appearance of sidelobes in soliton profiles as m increases from zero to 0.4. In Section 5.2 the regions where sidelobes appear are found analytically.

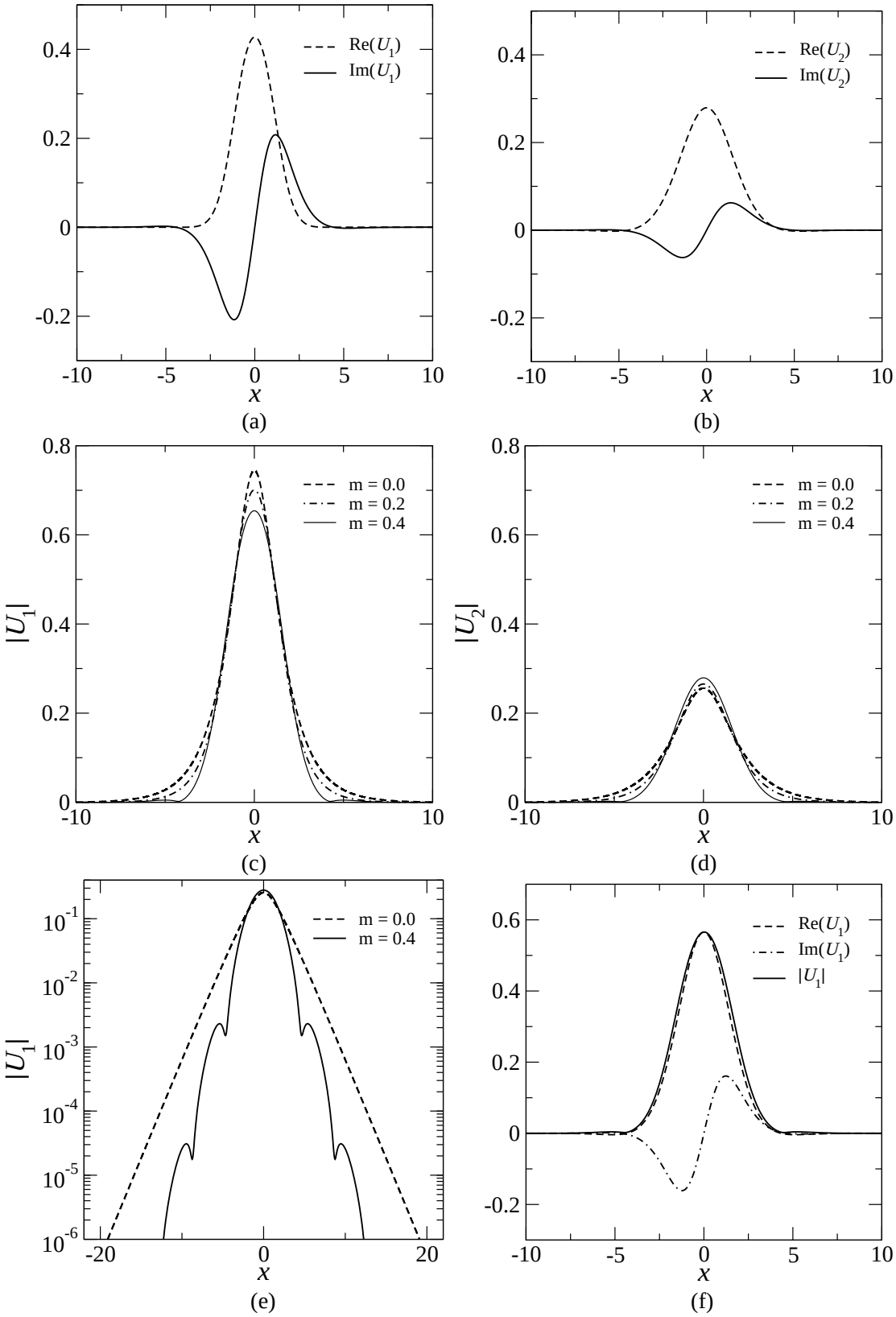

Figure 5.3: Examples of quiescent gap solitons. Asymmetric solution for $m = 0.4$: real and imaginary parts of (a) U_1 and (b) U_2. The effect of dispersive reflectivity on soliton profile: amplitudes of (c) U_1, and (d) U_2. (e) Amplitude of U_1 in logarithmic scale, and (f) Symmetric solution (i.e. $U_1 = U_2$) for $m = 0.4$. In all the above $\omega = 0.5$ and $\lambda = 0.2$.

5.2 Linear Approximation

In references [67] and [54] it was shown that, when the dispersive reflectivity parameter exceeds a certain critical value, sidelobes appear in the solitons' profiles. This is also the case in the model of Eqs. (5.8), as it was shown in Figures 1.3 (c)-(e). Since the amplitudes of the sidelobes are considerably smaller than the soliton itself, the effect of nonlinear terms in Eqs. (5.8) are negligible. Therefore, to analyze the characteristics of the tails of the solitons and sidelobes, we use the linearized equations (5.1). Substituting the symmetry condition (5.7) for quiescent solitons into (5.1) we arrive at

$$\begin{aligned} \omega U_1 + iU_1' - U_1^* + \lambda U_2 - mU_1^{*\prime\prime} &= 0, \\ \omega U_2 + iU_2' - U_2^* + \lambda U_1 - mU_2^{*\prime\prime} &= 0. \end{aligned} \tag{5.10}$$

By rewriting the real and imaginary parts separately, a set of four linear differential equations with real coefficients are obtained,

$$\begin{aligned} (\omega - 1)\, U_{1re} - U_{1im}' + \lambda U_{2re} - mU_{1re}'' &= 0, \\ (\omega + 1)\, U_{1im} + U_{1re}' + \lambda U_{2im} + mU_{1im}'' &= 0, \\ (\omega - 1)\, U_{2re} - U_{2im}' + \lambda U_{1re} - mU_{2re}'' &= 0, \\ (\omega + 1)\, U_{2im} + U_{2re}' + \lambda U_{1im} + mU_{2im}'' &= 0, \end{aligned} \tag{5.11}$$

where $U_{1re,2re}$ and $U_{1im,2im}$ are real and imaginary parts of the forward-propagating waves in core 1 and 2, respectively.

In the case of symmetric solitons, Eqs. (5.11) are further simplified. Letting $U_1 = U_2$, it follows,

$$(\omega + \lambda - 1)\, U_{1re} - U_{1im}' - mU_{1re}'' = 0, \tag{5.12a}$$

$$(\omega + \lambda + 1)\, U_{1im} + U_{1re}' + mU_{1im}'' = 0. \tag{5.12b}$$

It is possible to decouple Eqs. (5.12) into two fourth-order ordinary differential equations (ODEs). To this end, we rewrite (5.12b),

$$U'_{1im} = (\omega + \lambda - 1)\, U_{1re} - mU''_{1re}. \tag{5.13}$$

Taking the derivative with respect to x from Eq. (5.12b) results in

$$(\omega + \lambda + 1)\, U'_{1im} + U''_{1re} + mU'''_{1im} = 0. \tag{5.14}$$

By replacing the first and third order derivative terms in (5.14) from (5.13) we arrive at the following equations,

$$\begin{aligned} \left[(\omega + \lambda)^2 - 1\right] U_{1re} + (1 - 2m)\, U''_{1re} - m^2 U''''_{1re} = 0, \\ \left[(\omega + \lambda)^2 - 1\right] U_{1im} + (1 - 2m)\, U''_{1im} - m^2 U''''_{1im} = 0, \end{aligned} \tag{5.15}$$

where U''''_{1re} is the fourth order derivative. The equations in (5.15) are linear homogeneous fourth order differential equation with constant coefficients that have analytical solutions. We expect the *general solution* of (5.15) to have four independent coefficients to be determined by applying four boundary conditions, i.e. $U_{1re,im}(\pm\infty) = 0$. To find the general solution we start from the characteristic equation of (5.15) which can be obtained by taking the Laplace transform of either of the equations, i.e.

$$\left[(\omega + \lambda)^2 - 1\right] + (1 - 2m)\, S^2 - m^2 S^4 = 0. \tag{5.16}$$

The roots of the characteristic equation (5.16) are,

$$S^2 = \frac{1 - 2m \pm \Gamma}{2m^2}, \tag{5.17}$$

where,

$$\Gamma = \sqrt{1 - 4m + 4m^2\,(\omega + \lambda)^2}. \tag{5.18}$$

Note that in (5.17) m cannot be zero. For the special case of $m = 0$ Eq. (5.16) leads

to

$$\left[(\omega+\lambda)^2-1\right]+S^2=0 \Longrightarrow S=\pm\sqrt{(\omega+\lambda)^2-1}, \tag{5.19}$$

which in turn results in a simple general solution.

The fact that $U_{1re}(x)$ and $U_{1im}(x)$ are even and odd functions of x, respectively, eliminates two of the four unknown coefficients. Using symbolic tools of MATLAB one can obtain a general solution for Eqs. (5.15) which can be simplified to the following,

$$\begin{aligned}
U_1(x) = {} & C_1\left[1+i\frac{1+2m(\omega+\lambda)+\Gamma}{4m(\omega+\lambda+1)}\sqrt{2-4m-2\Gamma}\right]\exp\left(-x\sqrt{\frac{1-2m-\Gamma}{2m^2}}\right) \\
& + C_1^*\left[1+i\frac{1+2m(\omega+\lambda)-\Gamma}{4m(\omega+\lambda+1)}\sqrt{2-4m+2\Gamma}\right]\exp\left(-x\sqrt{\frac{1-2m+\Gamma}{2m^2}}\right) \\
& + C_2\left[1-i\frac{1+2m(\omega+\lambda)+\Gamma}{4m(\omega+\lambda+1)}\sqrt{2-4m-2\Gamma}\right]\exp\left(+x\sqrt{\frac{1-2m-\Gamma}{2m^2}}\right) \\
& + C_2^*\left[1-i\frac{1+2m(\omega+\lambda)-\Gamma}{4m(\omega+\lambda+1)}\sqrt{2-4m+2\Gamma}\right]\exp\left(+x\sqrt{\frac{1-2m+\Gamma}{2m^2}}\right),
\end{aligned} \tag{5.20}$$

where star means complex conjugate, and C_1 and C_2 are arbitrary complex coefficients to be determined by applying the boundary conditions. Clearly, for the right tail of the soliton, i.e. $x>0$, C_2 must vanish. Likewise for $x<0$ which accounts for the left tail, $C_1=0$. It is obvious that after applying the boundary conditions, one arbitrary constant (C_1 for $x>0$ and C_2 for $x<0$) appears in the general solution.

Depending on the sign of $1-4m+4m^2(\omega+\lambda)^2$, Γ may be real or complex. More specifically, for the range of

$$m>\frac{1}{2\left(1+\sqrt{1-(\omega+\lambda)^2}\right)}, \tag{5.21}$$

Γ and consequently the exponents in (5.20) are complex. We note that when the exponents are real-valued, the tails of the solitons decay exponentially. On the other hand when they are complex, sidelobes appear. Therefore inequality (5.21)

determines the region where sidelobes appear. It is worth noting that in the absence of linear coupling, i.e. $\lambda = 0$, Eqs. (5.20) and (5.21) reduce to the ones derived in Ref. [91] for the single-core case. When the inequality (5.21) is satisfied, Eq. (5.20) may be expressed as

$$\begin{aligned} U_1(x) = & A\left[\cos(bx+\varphi) + id\cos(bx+\varphi+\psi)\right]\exp(-ax) \\ & + B\left[\cos(-bx+\varphi) - id\cos(-bx+\varphi+\psi)\right]\exp(ax), \end{aligned} \tag{5.22}$$

where,

$$\begin{aligned} a &= \frac{1}{2m}\sqrt{1-2m+2m\sqrt{1-(\omega+\lambda)^2}}, \\ b &= \frac{1}{2m}\sqrt{-1+2m+2m\sqrt{1-(\omega+\lambda)^2}}, \\ d &= \left(\frac{1-(\omega+\lambda)}{1+\omega+\lambda}\right)^{\frac{1}{4}}, \\ \psi &= \tan^{-1}\left(\frac{1-\sqrt{1-(\omega+\lambda)^2}}{-(\omega+\lambda)} \times \sqrt{\frac{-1+2m\left(1+\sqrt{1-(\omega+\lambda)^2}\right)}{1-2m\left(1-\sqrt{1-(\omega+\lambda)^2}\right)}}\right), \end{aligned} \tag{5.23}$$

are real quantities. The free parameters A, B, and φ can be determined from the exact numerical soliton solution and are related to C_1 and C_2 through $A = 2|C_1|$, $B = 2|C_2|$ and $\varphi = \arg(C_1)$, respectively. Due to the symmetry of the soliton profile C_1 and C_2 are equal.

It should also be noted that the first and second terms of Eq. (5.22) correspond to the right and left soliton tails, respectively. As is shown in Figures 5.4(a) and (b), Eqs. (5.22) and the numerical soliton solution are in excellent agreement and only differ near the soliton's peak where the linear approximation is not valid. Figure 5.4(c) depicts the region within the bandgap, as predicted by (5.21) for various λ, where the sidelobes exist. The numerical results are in complete agreement with the predictions of (5.21).

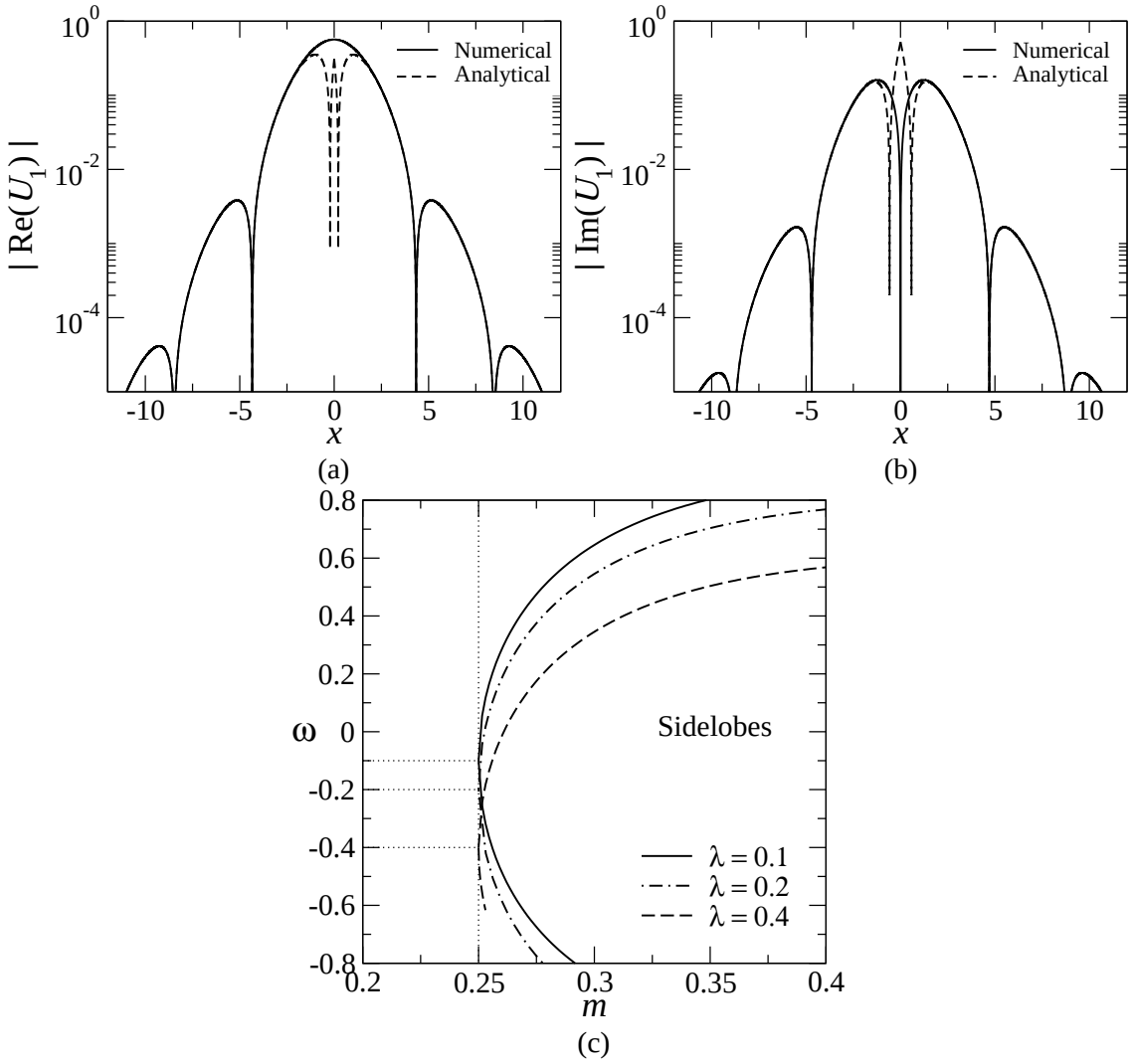

Figure 5.4: Comparison between numerically obtained soliton solutions and Eq. (5.22) for the (a) real and (b) imaginary parts of the symmetric quiescent solitons with $\omega = 0.5$, $\lambda = 0.2$, $m = 0.4$, $A = B = 0.945$ and $\varphi = 1.405$. The rest of the coefficients are calculated using Eqs. (5.23). (c) The region within the photonic bandgap where sidelobes appear in the soliton profiles, predicted by Eq. (5.21).

In the case of asymmetric solitons, i.e. $U_1 \neq U_2$, one may rewrite Eqs. (5.11) in the frequency domain by applying Laplace transform. It results in the following

equation in the matrix form,

$$\begin{bmatrix} \omega-1-ms^2 & -s & \lambda & 0 \\ s & \omega+1+ms^2 & 0 & \lambda \\ \lambda & 0 & \omega-1-ms^2 & -s \\ 0 & \lambda & s & \omega+1+ms^2 \end{bmatrix} \begin{bmatrix} \tilde{U}_{1re} \\ \tilde{U}_{1im} \\ \tilde{U}_{2re} \\ \tilde{U}_{2im} \end{bmatrix} = 0, \quad (5.24)$$

where $\tilde{U}(s)$ is the Laplace transform of $U(x)$. For (5.24) to have non-trivial solutions, the matrix must be singular i.e. with zero determinant. The result is an 8^{th} order polynomial with the following roots,

$$s_i = \pm\sqrt{\frac{\pm\sqrt{4m^2(\omega\pm\lambda)^2-4m+1}-2m+1}{2m^2}},\ i=1,...,8 \qquad (5.25)$$

Note that s_i are eigenvalues of Eqs. (5.11) that can be used to form the general solutions. The manipulation is cumbersome and parametric solvers such as MATLAB or Mathematica may be used. Equations (5.11) admit the following solutions

$$\begin{aligned}
U_1(x) = {} & C_1\left[1+i\frac{1+2m(\omega+\lambda)+\Gamma_1}{4m(\omega+\lambda+1)}\sqrt{2-4m-2\Gamma_1}\right]\exp\left(-\frac{x}{2m}\sqrt{2-4m-2\Gamma_1}\right) \\
& + C_1^*\left[1+i\frac{1+2m(\omega+\lambda)-\Gamma_1}{4m(\omega+\lambda+1)}\sqrt{2-4m+2\Gamma_1}\right]\exp\left(-\frac{x}{2m}\sqrt{2-4m+2\Gamma_1}\right) \\
& + C_2\left[1+i\frac{1+2m(\omega-\lambda)+\Gamma_2}{4m(\omega-\lambda+1)}\sqrt{2-4m-2\Gamma_2}\right]\exp\left(-\frac{x}{2m}\sqrt{2-4m-2\Gamma_2}\right) \\
& + C_2^*\left[1+i\frac{1+2m(\omega-\lambda)-\Gamma_2}{4m(\omega-\lambda+1)}\sqrt{2-4m+2\Gamma_2}\right]\exp\left(-\frac{x}{2m}\sqrt{2-4m+2\Gamma_2}\right) \\
& + C_3\left[1-i\frac{1+2m(\omega+\lambda)+\Gamma_1}{4m(\omega+\lambda+1)}\sqrt{2-4m-2\Gamma_1}\right]\exp\left(+\frac{x}{2m}\sqrt{2-4m-2\Gamma_1}\right) \\
& + C_3^*\left[1-i\frac{1+2m(\omega+\lambda)-\Gamma_1}{4m(\omega+\lambda+1)}\sqrt{2-4m+2\Gamma_1}\right]\exp\left(+\frac{x}{2m}\sqrt{2-4m+2\Gamma_1}\right) \\
& + C_4\left[1-i\frac{1+2m(\omega-\lambda)+\Gamma_2}{4m(\omega-\lambda+1)}\sqrt{2-4m-2\Gamma_2}\right]\exp\left(+\frac{x}{2m}\sqrt{2-4m-2\Gamma_2}\right) \\
& + C_4^*\left[1-i\frac{1+2m(\omega-\lambda)-\Gamma_2}{4m(\omega-\lambda+1)}\sqrt{2-4m+2\Gamma_2}\right]\exp\left(+\frac{x}{2m}\sqrt{2-4m+2\Gamma_2}\right),
\end{aligned} \qquad (5.26a)$$

$$
\begin{aligned}
U_2(x) = {} & C_1\left[1+i\frac{1+2m(\omega+\lambda)+\Gamma_1}{4m(\omega+\lambda+1)}\sqrt{2-4m-2\Gamma_1}\right]\exp\left(-\frac{x}{2m}\sqrt{2-4m-2\Gamma_1}\right)\\
& + C_1^*\left[1+i\frac{1+2m(\omega+\lambda)-\Gamma_1}{4m(\omega+\lambda+1)}\sqrt{2-4m+2\Gamma_1}\right]\exp\left(-\frac{x}{2m}\sqrt{2-4m+2\Gamma_1}\right)\\
& - C_2\left[1+i\frac{1+2m(\omega-\lambda)+\Gamma_2}{4m(\omega-\lambda+1)}\sqrt{2-4m-2\Gamma_2}\right]\exp\left(-\frac{x}{2m}\sqrt{2-4m-2\Gamma_2}\right)\\
& - C_2^*\left[1+i\frac{1+2m(\omega-\lambda)-\Gamma_2}{4m(\omega-\lambda+1)}\sqrt{2-4m+2\Gamma_2}\right]\exp\left(-\frac{x}{2m}\sqrt{2-4m+2\Gamma_2}\right)\\
& + C_3\left[1-i\frac{1+2m(\omega+\lambda)+\Gamma_1}{4m(\omega+\lambda+1)}\sqrt{2-4m-2\Gamma_1}\right]\exp\left(+\frac{x}{2m}\sqrt{2-4m-2\Gamma_1}\right)\\
& + C_3^*\left[1-i\frac{1+2m(\omega+\lambda)-\Gamma_1}{4m(\omega+\lambda+1)}\sqrt{2-4m+2\Gamma_1}\right]\exp\left(+\frac{x}{2m}\sqrt{2-4m+2\Gamma_1}\right)\\
& - C_4\left[1-i\frac{1+2m(\omega-\lambda)+\Gamma_2}{4m(\omega-\lambda+1)}\sqrt{2-4m-2\Gamma_2}\right]\exp\left(+\frac{x}{2m}\sqrt{2-4m-2\Gamma_2}\right)\\
& - C_4^*\left[1-i\frac{1+2m(\omega-\lambda)-\Gamma_2}{4m(\omega-\lambda+1)}\sqrt{2-4m+2\Gamma_2}\right]\exp\left(+\frac{x}{2m}\sqrt{2-4m+2\Gamma_2}\right),
\end{aligned}
\tag{5.26b}
$$

where C_1, C_2, C_3, and C_4 are complex coefficients to be determined from the boundary conditions. The other coefficients are,

$$
\begin{aligned}
\Gamma_1 &= \sqrt{4m^2(\omega+\lambda)^2-4m+1},\\
\Gamma_2 &= \sqrt{4m^2(\omega-\lambda)^2-4m+1}.
\end{aligned}
\tag{5.27}
$$

It should be noted that for the right tail (i.e. $x>0$) $C_{3,4}=0$, and for the left tail $C_{1,2}=0$ for $x<0$. Analyzing Eqs. (5.26) and (5.27), it is found that sidelobes will appear in the solitons' profiles when both Γ_1 and Γ_2 are complex. This occurs when m is in the range

$$
m > max\left\{\frac{1}{2\left(1+\sqrt{1-(\omega+\lambda)^2}\right)}, \frac{1}{2\left(1+\sqrt{1-(\omega-\lambda)^2}\right)}\right\}. \tag{5.28}
$$

When condition (5.28) is met, using the following prescription

$$
\sqrt{P\pm iQ} = \sqrt{\frac{1}{2}\left(P+\sqrt{P^2+Q^2}\right)} \pm i\,\mathrm{sgn}(Q)\sqrt{\frac{1}{2}\left(-P+\sqrt{P^2+Q^2}\right)}, \tag{5.29}
$$

where P and Q are real numbers and sgn() is the sign function, Eqs. (5.26a) and (5.26b) can be expressed in the following forms,

$$\begin{aligned} U_1(x) &= D_1\left[\cos(b_1x+\varphi_1)+ic_1\cos(b_1x+\varphi_1+\psi_1)\right]\exp(-a_1x) \\ &+ D_2\left[\cos(b_2x+\varphi_2)+ic_2\cos(b_2x+\varphi_2+\psi_2)\right]\exp(-a_2x) \\ &+ D_3\left[\cos(-b_1x+\varphi_1)-ic_1\cos(-b_1x+\varphi_1+\psi_1)\right]\exp(a_1x) \\ &+ D_4\left[\cos(-b_2x+\varphi_2)-ic_2\cos(-b_2x+\varphi_2+\psi_2)\right]\exp(a_2x), \end{aligned} \tag{5.30a}$$

$$\begin{aligned} U_2(x) &= D_1\left[\cos(b_1x+\varphi_1)+ic_1\cos(b_1x+\varphi_1+\psi_1)\right]\exp(-a_1x) \\ &- D_2\left[\cos(b_2x+\varphi_2)+ic_2\cos(b_2x+\varphi_2+\psi_2)\right]\exp(-a_2x) \\ &+ D_3\left[\cos(-b_1x+\varphi_1)-ic_1\cos(-b_1x+\varphi_1+\psi_1)\right]\exp(a_1x) \\ &- D_4\left[\cos(-b_2x+\varphi_2)-ic_2\cos(-b_2x+\varphi_2+\psi_2)\right]\exp(a_2x), \end{aligned} \tag{5.30b}$$

where D_1, D_2, D_3, D_4, φ_1 and φ_2 are real arbitrary coefficients that can be determined from the numerical soliton solutions. They are related to C_1 , C_2 , C_3 and C_4 through $D_1 = 2|C_1|$, $D_2 = 2|C_2|$, $D_3 = 2|C_3|$, $D_4 = 2|C_4|$, $\varphi_1 = \arg(D_1)$, and $\varphi_2 = \arg(D_2)$. The symmetry of the soliton's profile dictates that $D_1 = D_3$, and $D_2 = D_4$. The other parameters are all real and are given by

$$a_1 = \frac{1}{2m}\sqrt{1-2m+2m\sqrt{1-(\omega+\lambda)^2}}, \tag{5.31a}$$

$$b_1 = \frac{1}{2m}\sqrt{-1+2m+2m\sqrt{1-(\omega+\lambda)^2}}, \tag{5.31b}$$

$$c_1 = \left(\frac{1-(\omega+\lambda)}{1+\omega+\lambda}\right)^{\frac{1}{4}}, \tag{5.31c}$$

$$a_2 = \frac{1}{2m}\sqrt{1-2m+2m\sqrt{1-(\omega-\lambda)^2}}, \tag{5.31d}$$

$$b_2 = \frac{1}{2m}\sqrt{-1+2m+2m\sqrt{1-(\omega-\lambda)^2}}, \tag{5.31e}$$

$$c_2 = \left(\frac{1-(\omega-\lambda)}{1+\omega-\lambda}\right)^{\frac{1}{4}}, \tag{5.31f}$$

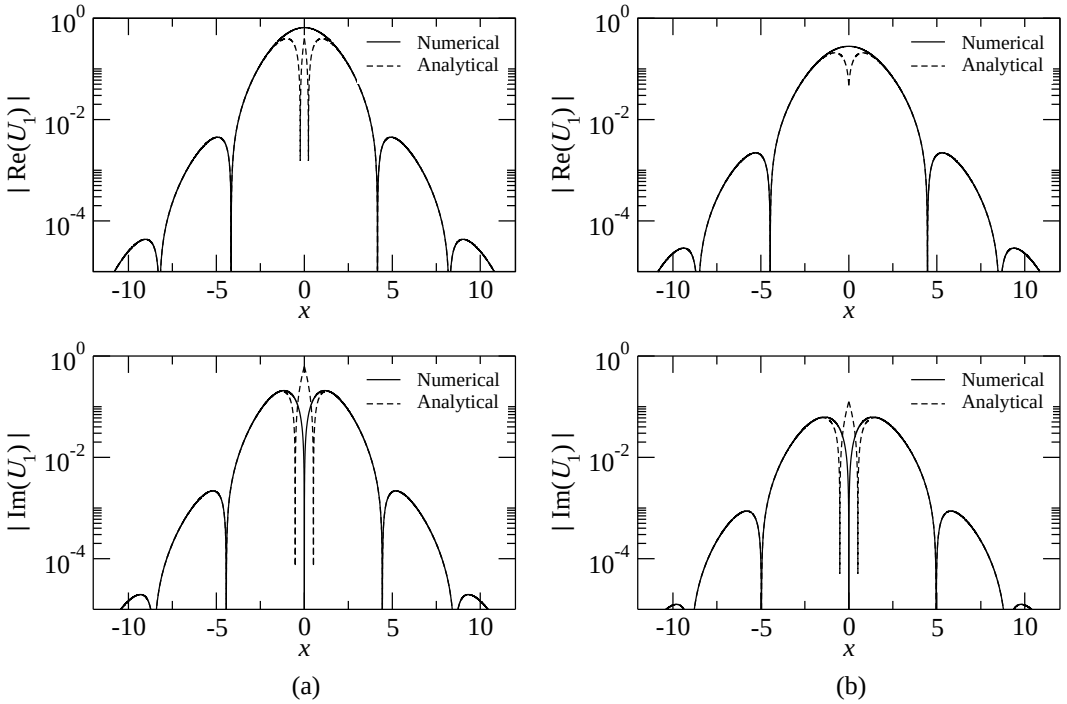

Figure 5.5: Comparison between numerically obtained quiescent asymmetric soliton solution and Eqs. (5.30a) and (5.30b) for $\omega = 0.5$, $\lambda = 0.2$, $m = 0.4$, $D_1 = D_3 = 1.498$, $D_2 = D_4 = 0.616$, $\varphi_1 = 1.453$ and $\varphi_2 = 1.201$. (a) Real part of U_1 , (b) imaginary part of U_1, (c) real part of U_2 and (d) imaginary part of U_2 . The other parameters are calculated using Eqs. (5.31h).

$$\psi_1 = \tan^{-1}\left(\frac{-ia_1\Gamma_1 - b_1\left(1 + 2m\left(\omega + \lambda\right)\right)}{-ib_1\Gamma_1 + a_1\left(1 + 2m\left(\omega + \lambda\right)\right)}\right), \tag{5.31g}$$

$$\psi_2 = \tan^{-1}\left(\frac{-ia_2\Gamma_2 - b_2\left(1 + 2m\left(\omega - \lambda\right)\right)}{-ib_2\Gamma_2 + a_2\left(1 + 2m\left(\omega - \lambda\right)\right)}\right). \tag{5.31h}$$

Figure 5.5 compares soliton solutions obtained by numerically solving Eqs. (5.8) with analytical solutions given in equations (5.30) for $\omega = 0.5$, $\lambda = 0.2$, $m = 0.4$. It is clear that the linear solutions in (5.30) approximate the tails of the solitons extremely well and they only deviate from the numerical solutions in the proximity of the peak of the soliton where the linearized equations (5.10) are not valid.

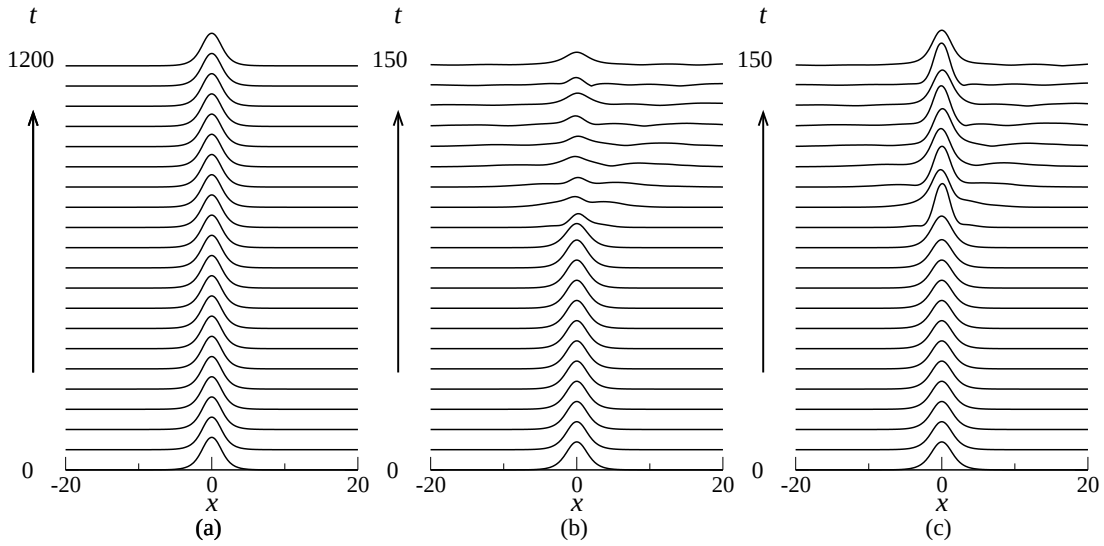

Figure 5.6: Evolution of asymmetric and symmetric solitons corresponding to $\omega = 0.5$, $\lambda = 0.2$ and $m = 0.2$. (a) U_1 component of the stable asymmetric soliton. (b) U_1 and (c) U_2 component of the unstable symmetric soliton for the same parameters.

5.3 Stability

Similar to what explained in Refs. [61] and [77] on the basis of the elementary bifurcation theory, one can conjecture that, in the region where the symmetric and asymmetric solitons coexist (i.e. $|\lambda| < \lambda_c$), the asymmetric solitons are always stable and symmetric ones are unstable. On the other hand, beyond the bifurcation point (i.e. $|\lambda| > \lambda_c$), the symmetric solitons exist on their own and are expected to be stable. To verify these predictions, we have numerically solved Eq. (3.37) using the numerically obtained solutions of (5.8) as initial input. To seed any inherent instability, the stationary solutions were asymmetrically perturbed at $t = 0$. The results of the numerical stability analysis are in complete agreement with the predictions of the bifurcation theory. Examples of the evolution of asymmetric and symmetric solitons are shown in Figure 5.6. As is shown in Figures 5.6(b) and (c), the unstable symmetric soliton sheds some radiation, deforms, and subsequently evolves into a stable asymmetric one.

As was indicated in Section 5.1, the critical value of λ_c at which bifurcation

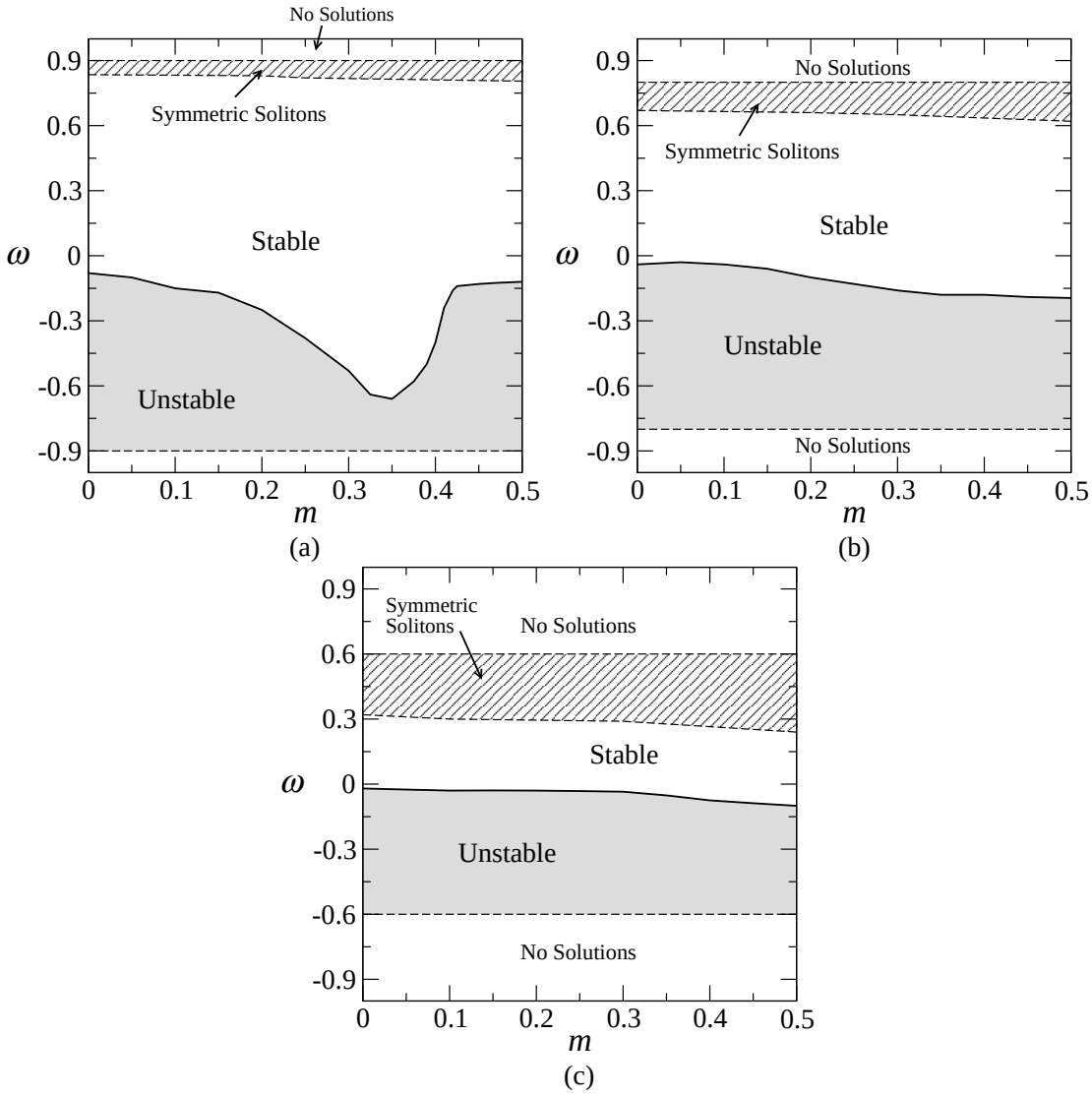

Figure 5.7: Stability regions for quiescent solitons for (a) $\lambda = 0.1$, (b) $\lambda = 0.2$, and (c) $\lambda = 0.4$. The regions where only symmetric types of solutions exist are hatched.

occurs becomes smaller as m increases in the range $0 < m < 0.5$ (refer to Figure 5.2). This means that increasing m enlarges the stable symmetric branch. Our numerical simulations have confirmed this result. This is somewhat analogous to the results of [67] where it was demonstrated that the inclusion of the dispersive reflectivity in the standard single-core model results in the expansion of the stability region.

We have systematically investigated the stability of asymmetric and symmetric

quiescent gap solitons for various values λ and m within the bandgap by simulating their evolution up to $t = 2000$. The results of the numerical stability analysis for the quiescent solitons are displayed in Figures 5.7 (a)-(c) in the plane of (m, ω) for various values of λ. In these figures the hatched areas account for the symmetric solitons that exist on their own and are always stable. Also the regions marked with "No Solution" account for the parameters that fall outside the photonic bandgap (see Eq. (5.4) for bandgap).

As shown in Figures 5.7(a)-(c), it is found that the stabilizing effect of dispersive reflectivity is diminished as λ increases. An interesting feature shown in Figure 5.7 is that, in the case of $\lambda = 0.1$, the stability region is progressively enlarged up to $m \approx 0.35$ and then it shrinks. As for symmetric solitons that coexist with asymmetric counter parts (not shown in Figure 5.7), our analysis shows that they are unaffected by dispersive reflectivity and are always unstable. The instability development does not result in the destruction of gap solitons. Instead, as is shown in Figure 5.6(b) and (c), the unstable solitons shed some radiation and spontaneously rearrange themselves into robust asymmetric quiescent or moving breathers.

5.4 Interaction Dynamics

When two quiescent solitons are placed within a certain range, their tails overlap and causes the solitons to interact. In this section, the interactions of quiescent solitons in the dual-core grating model are systematically studied, relying on the numerical techniques explained in Chapter 4. To this end, we may categorize the interaction problem into the following cases: (a) interactions of two identical quiescent solitons placed $\triangle x$ apart in the same core, with an initial phase difference of $\triangle\varphi$, and (b) interactions of two identical solitons placed $\triangle x$ apart but in opposite cores. The reason we consider identical solitons is that solitons will only interact if their fre-

quency detunings are very close. More importantly launching two different frequency solitons into a grating may be practically limited.

5.4.1 Symmetric Interactions

To study the interactions of quiescent gap solitons, we numerically solve Eqs. (5.8) using the symmetrised split-step Fourier method that was explained in Section 4.4.1 subject to the following initial conditions:

$$\begin{aligned} U_{1,2}(x,0) &= U_{1,2}(x-\frac{\triangle x}{2},0) + U_{1,2}(x+\frac{\triangle x}{2},0)\exp(i\triangle\varphi), \\ V_{1,2}(x,0) &= V_{1,2}(x-\frac{\triangle x}{2},0) + V_{1,2}(x+\frac{\triangle x}{2},0)\exp(i\triangle\varphi), \end{aligned} \tag{5.32}$$

where $U_{1,2}$ and $V_{1,2}$ belong to the stable regions shown in Figure 5.7. In all simulations, we have utilized the absorbing boundary conditions to minimize the reflection of radiation at the boundaries of the computational window.

Through extensive and systematic simulations we have characterized the interactions of solitons and their outcomes. Generally speaking, in the absence of sidelobes, the interaction of solitons is similar to that of nonlinear Schrödinger solitons, i.e. in-phase solitons attract and π-out-of-phase solitons repel. However, when $m \neq 0$, the outcome of the interactions does depend on ω, $\triangle\varphi$ and $\triangle x$. Similar behavior has been reported in gratings written on a single-core equipped with cubic-quintic medium [91].

In the case of $\triangle\varphi = 0$, a number of outcomes are possible. For instance, the interactions can result in the formation of two symmetrically separating solitons (shown in Figure 5.8(a)), the creation of a quiescent soliton (Figure 5.8(b)), repulsion of solitons (Figure 5.8(c)), formation of a temporary bound state that eventually splits into two separating solitons (Figure 5.8(e)) and generation of a quiescent soliton and two moving ones (Figure 5.8(f)). In the case of symmetric solitons (i.e. $U_1 = U_2$ and $V_1 = V_2$), which are only stable when they exist on their own, the interactions

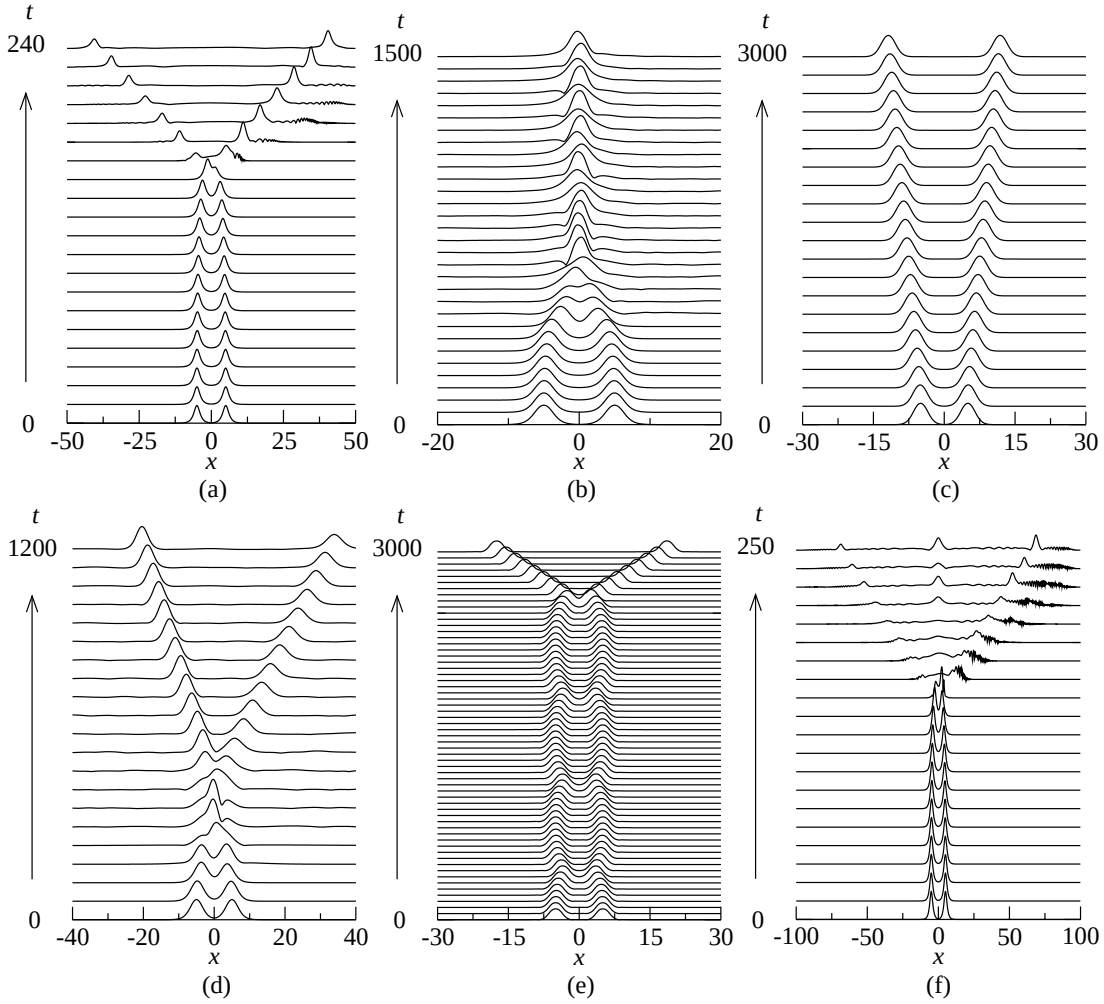

Figure 5.8: Examples of interaction of quiescent in-phase gap solitons. (a) Symmetric separation in region S for $\lambda = 0.1$, $\triangle x = 10$, $\omega = 0.3$, $m = 0.05$, (b) Merger into a quiescent soliton in region M for $\lambda = 0.1$, $\triangle x = 10$, $\omega = 0.5$, $m = 0.25$, (c) Repulsion for $\lambda = 0.1$, $\triangle x = 10$, $\omega = 0.65$, $m = 0.35$, (d) Asymmetric separation in region A in the symmetric region (i.e. initially $U_1 = U_2$ and $V_1 = V_2$) for $\lambda = 0.2$, 10, $\omega = 0.65$, $m = 0.3$, (e) Temporary bound state followed by generation of two separating moving gap solitons for $\lambda = 0.1$, $\triangle x = 10$, $\omega = 0.15$, $m = 0.4$, (f) Generation of a quiescent soliton along with two moving ones for $\lambda = 0.2$, $\triangle x = 10$, $\omega = 0.26$, $m = 0.05$. In all the figures only forward propagating wave in core 1 i.e. U_1 is shown.

may result in their merger into a single quiescent soliton or the formation of two asymmetrically separating solitons (Figure 5.8(d)). The symmetry breaking in Figure 5.8(d) may be attributed to the mismatch between the centers of "phase" and "amplitude" of the two gap solitons [92].

The results of simulations for $\lambda = 0.1$ and 0.2, $\triangle x = 6$ and 10, and $\triangle\varphi = 0$

and π are summarized in Figures 5.9 and 5.10, respectively. The dashed curves in these figures depict the inequality (5.28) which determines the region where sidelobes exist, i.e. the region to the right of the dashed curves (see Figure 5.4(c)). The narrow shaded areas account for the regions where symmetric solutions exist on their own (see Figure 5.7). A noteworthy feature shown in Figures 5.9 and 5.10 is that the outcomes of the interactions are greatly influenced by the presence of sidelobes and initial separation of solitons. More specifically, in the case of symmetric solitons (i.e. the shaded regions), Figures 5.9(a) and (c) show that depending on the value of m, the interactions may result in merger into a single quiescent one or asymmetric separation of solitons. However, when $\triangle x$ is increased to 10 two additional outcomes in the region where solitons have sidelobes are observed, namely repulsion and formation of a temporary bound state that subsequently splits into two separating solitons whose velocities may be different (see Figures 5.9(b) and (d)).

For asymmetric solitons (i.e. $U_1 \neq U_2$ and $V_1 \neq V_2$), in the region where solitons do not have sidelobes (i.e. the region to the left of the dashed curves), the outcomes of the interactions are weakly dependent on the initial separation of gap solitons (cf. 5.9(a) and (b)). On the other hand, the presence of sidelobes drastically alters the character of interactions. In particular, increasing $\triangle x$ from 6 to 10 results in significant shrinkage of the regions R and M and appearance of region B. It is worth noting that in the absence of dispersive reflectivity ($m = 0$), the merger of solitons, which is important for practical applications, occurs in a small range of frequencies. However, the presence of dispersive reflectivity leads to significant expansion of region M. Another interesting feature of Figure 5.9(c) and (d) is that $2 \rightarrow 3$ transformations (region T) occur in the region where solitons do not have sidelobes. More importantly, such transformations are observed even in the absence of dispersive reflectivity (i.e. $m = 0$). This is in sharp contrast with single core FBG models with dispersive reflectivity (e.g. Refs. [72, 91]) where it was reported that

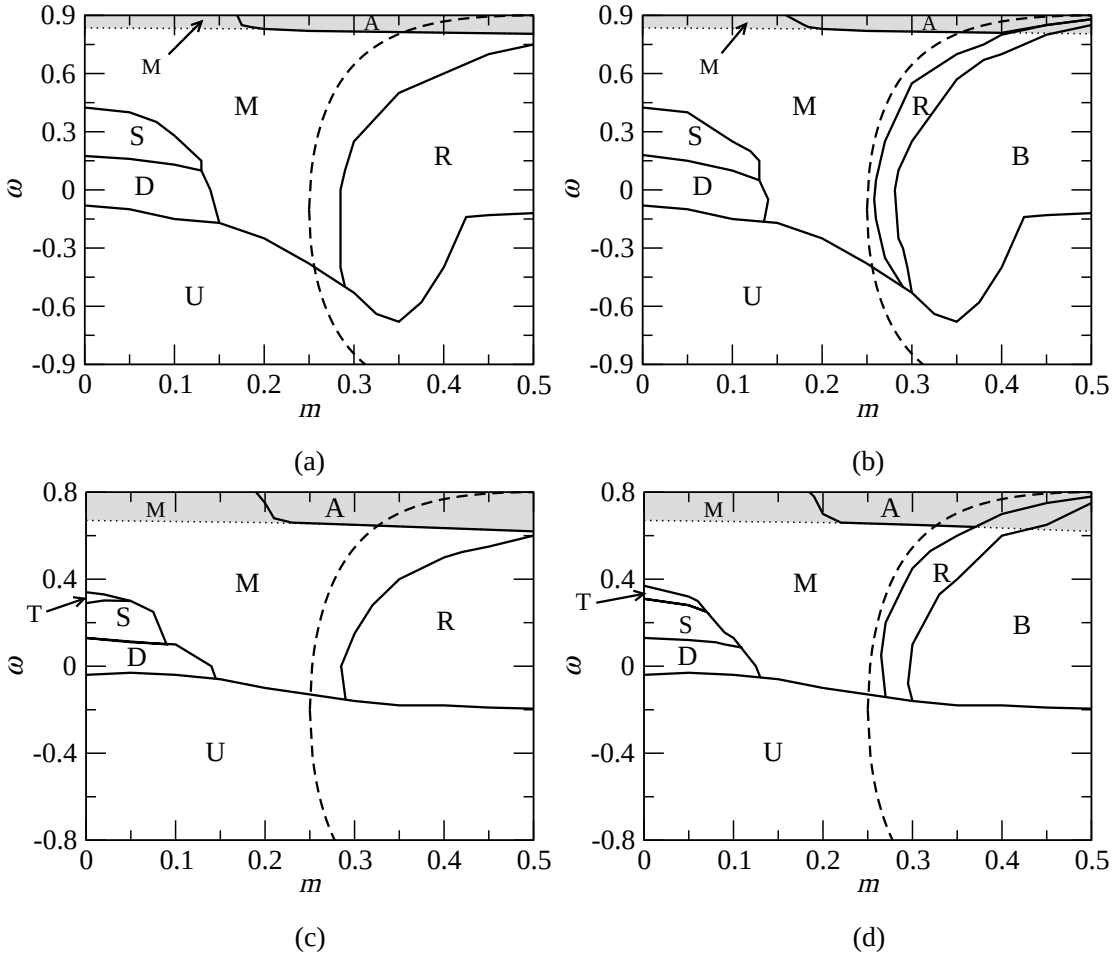

Figure 5.9: Results of the interactions of the in-phase i.e. $\triangle\varphi = 0$ quiescent solitons in the parameter plane of (m, ω) for (a) $\lambda = 0.1$, and $\triangle x = 6.0$, (b) $\lambda = 0.1$, and $\triangle x = 10.0$, (c) $\lambda = 0.2$, and $\triangle x = 6.0$ (d) $\lambda = 0.2$, and $\triangle x = 10.0$. Labels stand for the following outcomes: temporary Bound state following by separation (B), Destruction of the solitons (D), Merger into a single soliton (M), Repulsion of the solitons (R), Symmetric separation (S), and tree soliton generation: a quiescent soliton and two moving ones (T). Region U accounts for the unstable region. Shaded areas show the region where only the symmetric solutions exist. In the region to the right of the dashed curves gap solitons develop sidelobes.

$2 \rightarrow 3$ transformation occurs for moderate to strong dispersive reflectivity. Also, it has previously been shown that in single core FBGs, when $m \neq 0$, interaction or collisions of gap solitons may result in their destruction [72,91]. However, Figure 5.9 shows that in the model of Eqs. (5.8), destruction of solitons can occur even when $m = 0$.

Table 1. Interaction outcomes for $\omega = 0.15$, $m = 0.4$, and $\lambda = 0.1$ and various initial separation.

Initial separation	Outcome
$\Delta x \leq 4.56$	Merger (region M)
$4.56 < \Delta x \leq 6.9$	Repulsion (region R)
$6.9 < \Delta x$	Temporary bound state followed by separation (region B)

Another finding is that at any given ω, m and λ there exists a critical initial separation $\triangle x_{cr}$ below which in-phase gap solitons whether symmetric or asymmetric always attract each other and form a lump. It is highly likely that the resulting lump forms a quiescent soliton, however depending on the soliton parameters the interaction outcome may result in the destruction, or symmetric or asymmetric separation of the solitons. For instance for the parameters of Figure 5.8(c) i.e. $\omega = 0.65$, $m = 0.35$, and $\lambda = 0.1$ the critical separation is 6.99 while for the parameter of Figure 5.8(e) i.e. $\omega = 0.15$, $m = 0.4$, and $\lambda = 0.1$ it is 4.56. For the latter case we have summarized the interaction outcomes for various Δx in table 1. A noteworthy feature is that unlike nonlinear Schrödinger solitons, even in-phase solitons may repel each other depending on Δx.

The outcomes of the interactions of two out-of-phase ($\triangle\varphi = \pi$) quiescent gap solitons are displayed in Figure 5.10. In this case, the most dominant outcome is repulsion of solitons. In the case of solitons without sidelobes, the initial separation of solitons does not have any effect on the outcome of the interactions. In the region where gap solitons have sidelobes the interactions may either result in the repulsion of solitons or formation of a bound state that subsequently splits into two separating solitons (i.e. region B). Similar to the in-phase case, the interaction of solitons with sidelobes is greatly affected by the initial separation. As is shown in Figures 5.10(b) and (d), increasing the separation from 6 to 10 results in the expansion of region R and splitting of region B.

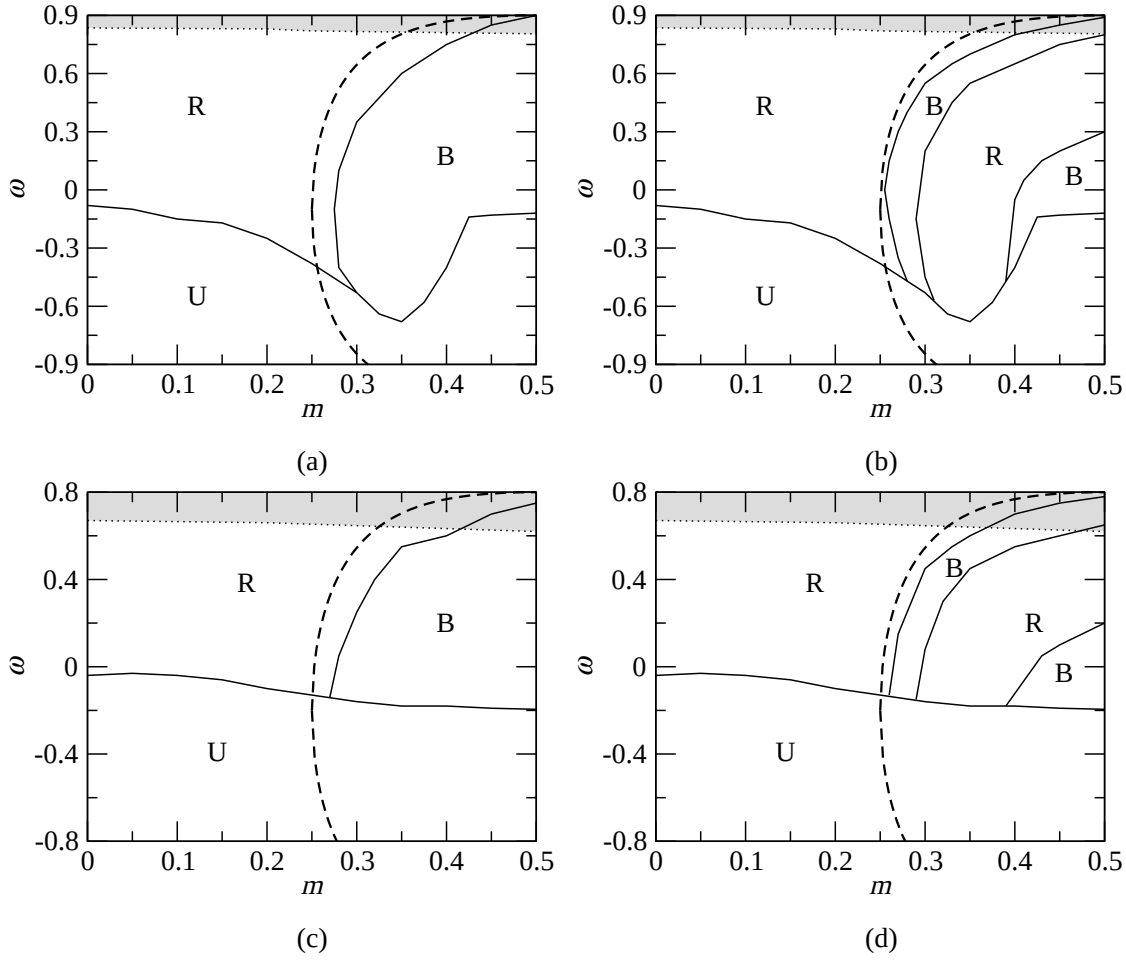

Figure 5.10: Results of the interaction analysis for the out-of-phase ($\triangle\varphi = \pi$) quiescent solitons in the parameter plane of $\omega - m$ for (a) $\lambda = 0.1$, and $\triangle x = 6.0$, (b) $\lambda = 0.1$, and $\triangle x = 10.0$, (c) $\lambda = 0.2$, and $\triangle x = 6.0$ (d) $\lambda = 0.2$, and $\triangle x = 10.0$. The outcomes are: Repulsion of the gap solitons (R), temporary Bound state following by separation of gap solitons (B). Region U accounts for the unstable gap solitons. The dashed line and shades areas are as per Figs. 1.

5.4.2 Asymmetric Interactions

In Section 5.4.1 the interactions of two identical asymmetric or symmetric quiescent solitons whose larger (smaller) components were in the same core i.e. $\{U_{1,2}\}_{left} = \{U_{1,2}\}_{right}$, and $\{V_{1,2}\}_{left} = \{V_{1,2}\}_{right}$ (the subscripts "left" and "right" correspond to the left and right solitons in Figure 5.8) were investigated. In this section we consider another initial configuration where the solitons are mirror images of each other i.e. $\{U_1, V_1\}_{left} = \{U_2, V_2\}_{right}$, and $\{U_2, V_2\}_{left} = \{U_1, V_1\}_{right}$. As a result,

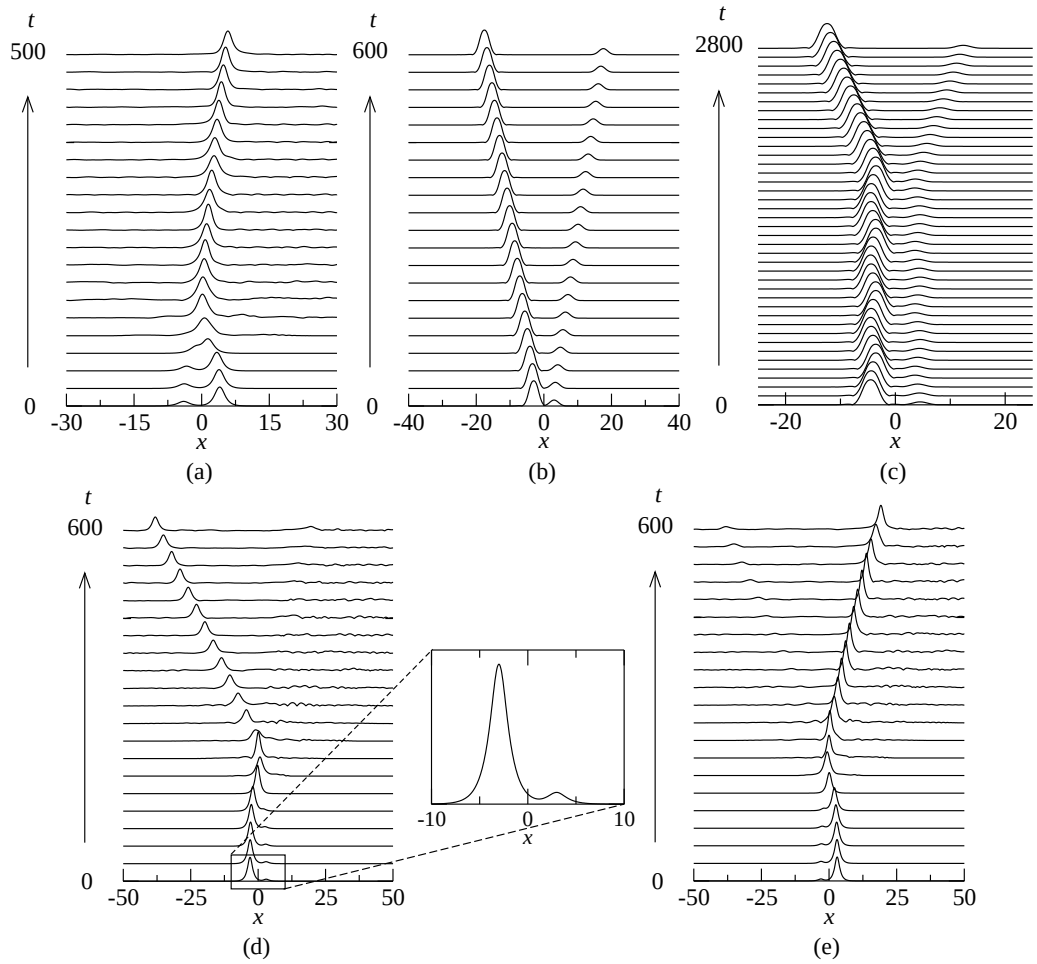

Figure 5.11: Examples of asymmetric interaction of in-phase quiescent solitons. (a) Merger into a single moving for $\lambda = 0.2$, $\triangle x = 8$, $\omega = 0.0$, $m = 0.1$, (b) repulsion of solitons for $\lambda = 0.2$, $\triangle x = 6$, $\omega = 0.15$, $m = 0.4$, (c) temporary bound state followed by separation of solitons for$\lambda = 0.1$, $\triangle x = 9$, $\omega = 0.15$, $m = 0.46$. (d) and (e) show U_1 and U_2 components for $\lambda = 0.1$, $\triangle x = 6$, $\omega = 0.0$, $m = 0.05$, respectively. The inset in (d) shows the initial setup.

the amplitudes of the interacting solitons in each core will be different. In the case of $\triangle\varphi = 0$, the simulations demonstrate that the interactions may result in asymmetric separation of solitons, repulsion, merger into a moving or quiescent soliton, and formation of temporary bound state followed by symmetric or asymmetric separation of solitons. Some examples are shown in Figure 5.11.

In Figures 5.11(a)-(c) only U_1 component i.e. forward-propagating wave in the first core is shown. Figure 5.11(a) shows how the two solitons merge into a single slow

moving one; a transition that causes energy loss in the form of radiation. Figures 5.11(d) and (e) show U_1 and U_2 components for the case of asymmetric separation, respectively. In the latter, as inferred from Figures 5.11(d) and (e), after the interactions the soliton in core 1 has a higher velocity. It should be noted that because one of the pulses is smaller (specially when λ is small) we need to put the two pulses closer to each other compared to the case of symmetric interactions for the solitons to interact.

It is found that in contrast to the results found in the symmetric interaction case (cf. Figure 5.9), destruction, and $2 \rightarrow 3$ transformation do not occur, when interacting pulses are not identical. For π-out-of-phase solitons, the outcomes are similar to the ones discussed in Section 5.4.1 except for the region B where the temporary bound state is always followed by asymmetric separation of solitons.

5.5 Potential Applications of Quiescent Solitons

The existence and stability of gap solitons have been considered theoretically in various nonlinear systems such as photonic bandgap crystals and FBGs. However, these types of gap solitons have not been observed experimentally yet. As was mentioned earlier in this chapter, the slowest reported gap soliton travels at 16% of the speed of light in vacuum [18].

Gap solitons are potential candidates for reaching zero group velocity, a phenomenon that is of significant importance. For instance, one of the most important potential applications of zero-velocity solitons is the ability to capture (and store) light pulses, i.e. optical memories. One may also categorize very-slowly moving gap solitons ($v \ll 1$ in normalized units) under these applications, e.g. optical delay lines. Therefore, it is crucial to investigate the characteristics of quiescent gap solitons. To have a better picture, we describe a conceptual design of an optical memory here:

in the simplest form, an optical memory may consist of two coupled Bragg gratings which are a few centimeters long. In theory a "memory cell" needs only to be wide enough to hold a quiescent soliton. Therefore, such device can potentially hold many memory cells. The questions are: how do we write to these memory cells and how do we recover the optical signal?

One method of generating quiescent solitons is through the collision of two moving ones. This is described in details in the next chapter. There are, however, other approaches that have been proposed and experimented in photonic crystals. For instance, it has been shown that in resonance photonic crystals it is possible to trap (or store) optical pulses in a local defect [101, 102]. Experimental results given in the same reports also show how the stored pulse can be recovered using another out-of-phase pulse. In principle, this may be the building block of on-chip optical memories. Same idea has been used in reference [103] to trap gap solitons in FBGs. There, the authors have studied the interaction of solitons with defects in fiber gratings and showed that it is possible under certain soliton parameters and defect strength to capture moving gap solitons. It is also suggested that such grating defects can be imposed and controlled externally via electrostriction (which in turn suggests that optical sensing is also another possible application). One may note that grating nonuniformities are inevitable in making such defects. This is where the dispersive reflectivity parameter may come into play to examine the effect of such nonuniformities on the performance of the memory.

The interaction outcomes given in Figures 5.9 and 5.10 for in-phase and out-of-phase gap solitons are useful to engineer the length of each memory cell, for example to prevent interactions of gap solitons in adjacent cells. Also, the same recovery technique used in resonance photonic crystals [101, 102] can be applies to the model studied in this thesis. More specifically, as will be also presented for the case of moving gap solitons in the next chapter, out-of-phase solitons generally repel each

other. So, to release the non-moving gap soliton from a memory cell, one approach is to launch another pulse (moving gap soliton) into the coupled FBG, at the properly chosen parameters. Of course much theoretical research is yet to be done before any experiment of this sort becomes possible.

Chapter 6

Moving Gap Solitons

Gap solitons in general, unlike NLS solitons, may have any velocity between zero to the speed of light in the medium ($0 \leq v \leq c$ where c is the speed of light in the medium) [20]. In the previous chapter the dynamics of quiescent ($v = 0$) gap solitons have been investigated. This chapter addresses the dynamics of the general case of moving gap solitons. In general when $v \neq 0$, unlike the quiescent gap solitons, there are no symmetry conditions. Therefore, we need to solve the general nonlinear coupled mode equations, i.e.

$$\begin{aligned}
&iu_{1t} + iu_{1x} + \left(\frac{1}{2}|u_1|^2 + |v_1|^2\right) u_1 + v_1 + \lambda u_2 + mv_{1xx} = 0,\\
&iv_{1t} - iv_{1x} + \left(\frac{1}{2}|v_1|^2 + |u_1|^2\right) v_1 + u_1 + \lambda v_2 + mu_{1xx} = 0,\\
&iu_{2t} + iu_{2x} + \left(\frac{1}{2}|u_2|^2 + |v_2|^2\right) u_2 + v_2 + \lambda u_1 + mv_{2xx} = 0,\\
&iv_{2t} - iv_{2x} + \left(\frac{1}{2}|v_2|^2 + |u_2|^2\right) v_2 + u_2 + \lambda v_1 + mu_{2xx} = 0.
\end{aligned} \tag{6.1}$$

The first section of this chapter is dedicated to finding the moving soliton solutions of Eqs. (6.1). In this section linear forms of NLCMEs are also solved analytically leading to approximate solutions of moving soliton tails. In Sections 6.2 and 6.3 the stability and collision dynamics of both symmetric and asymmetric moving solitons

are investigated.

6.1 Moving Soliton Solutions

As mentioned in Chapter 5, in general there are no known analytical solutions to the NLCMEs (6.1), even in the absence of dispersive reflectivity. Therefore, we rely on numerical techniques to find soliton solutions, whether quiescent or moving. For quiescent solitons, as discussed in the previous chapter, we apply the relaxation algorithm directly to the NLCMEs. In the case of moving solitons however, it makes sense to transform Eqs. (6.1) into the reference frame moving with the soliton velocity v. This means that solutions of the following form are searched for,

$$\begin{aligned} u_{1,2}(X,t) &= U_{1,2}(X,t)\exp(-i\Omega t), \\ v_{1,2}(X,t) &= V_{1,2}(X,t)\exp(-i\Omega t), \end{aligned} \tag{6.2}$$

where $\{X,t\} = \{x - vt, t\}$ are the new coordinates in the moving reference frame. It should be noted that v is normalized to the speed of light in the fiber (i.e. c_0/n_0 with n_0 being the average refractive index of the fiber) so that $v = 1$ means a soliton with the speed of light. Ω is the detuning frequency of the soliton in the new moving coordinates which is related to its counterpart in the laboratory frame, i.e. ω, through

$$\Omega(k) = \omega(k) - vk, \tag{6.3}$$

where k is the wave number [77]. Substituting Eqs. (6.2) into (6.1) and applying chain rule for the partial derivatives, coupled mode equations in the moving reference

frame are obtained,

$$\begin{aligned}
&\Omega U_1 + i\,(1-v)\,U_{1X} + \left(\frac{1}{2}\,|U_1|^2 + |U_1|^2\right) U_1 + V_1 + \lambda U_2 + mV_{1XX} = 0,\\
&\Omega V_1 - i\,(1+v)\,V_{1X} + \left(\frac{1}{2}\,|V_1|^2 + |U_1|^2\right) V_1 + U_1 + \lambda v_2 + mU_{1XX} = 0,\\
&\Omega U_2 + i\,(1-v)\,U_{2X} + \left(\frac{1}{2}\,|U_2|^2 + |V_2|^2\right) U_2 + V_2 + \lambda u_1 + mV_{2XX} = 0,\\
&\Omega V_2 - i\,(1+v)\,V_{2X} + \left(\frac{1}{2}\,|V_2|^2 + |U_2|^2\right) V_2 + U_2 + \lambda V_1 + mU_{2XX} = 0, \qquad (6.4)
\end{aligned}$$

where the subscripts X denote derivative with respect to X.

It is also relevant to translate the dispersion relation (5.3) into the new moving coordinates in order to find the transformed edges of the bandgap. Substituting Eq. (6.3) into the dispersion relation (5.3), the transformed relation is obtained,

$$(\Omega + vk)^2 = \left(1 - mk^2\right)^2 + \lambda^2 + k^2 \pm 2\lambda\sqrt{(1-mk^2)^2 + k^2}. \qquad (6.5)$$

Alternatively, following the same approach explained in Section 5.1, it is possible to derive Eq. (6.5) directly from the linearized form of Eqs. (6.4). To this end, we first linearize Eqs. (6.4) which take the following form,

$$\begin{aligned}
&\Omega U_1 + i\,(1-v)\,U_{1X} + V_1 + \lambda U_2 + mV_{1XX} = 0,\\
&\Omega V_1 - i\,(1+v)\,V_{1X} + U_1 + \lambda v_2 + mU_{1XX} = 0,\\
&\Omega U_2 + i\,(1-v)\,U_{2X} + V_2 + \lambda u_1 + mV_{2XX} = 0,\\
&\Omega V_2 - i\,(1+v)\,V_{2X} + U_2 + \lambda V_1 + mU_{2XX} = 0. \qquad (6.6)
\end{aligned}$$

Plane wave solutions are sought for in the form of $U_{1,2}, V_{1,2} \sim exp\,(ikX - i\Omega t)$. Substituting the latter into Eqs. (6.6) we arrive at the following equations in the

matrix form,

$$\begin{bmatrix} \Omega - k(1-v) & 1-mk^2 & \lambda & 0 \\ 1-mk^2 & \omega + k(1+v) & 0 & \lambda \\ \lambda & 0 & \Omega - k(1-v) & 1-mk^2 \\ 0 & \lambda & 1-mk^2 & \Omega + k(1+v) \end{bmatrix} \begin{bmatrix} U_1 \\ V_1 \\ U_2 \\ V_2 \end{bmatrix} = 0. \quad (6.7)$$

For (6.7) to have non-trivial solutions the determinant of the square matrix must be zero which results in the dispersion relation in (6.5).

The transformed linear gap spectrum can be obtained by solving for the roots of $\partial\Omega/\partial k = 0$. The latter results in the following third order polynomial of k^2,

$$4m^4k^6 - m^2\left(8m + v^2 - 4\right)k^4 + \left[4m(m-1) + v^2(2m-1) + 1\right]k^2 - v^2 = 0, \quad (6.8)$$

with the following real-valued roots:

$$k_0^2 = \frac{(4m - v^2 - 2 + f_1)^2 + 3v^2 f_1}{12m^2 f_1}, \quad (6.9)$$

where,

$$f_1 = \left(\sqrt{f_2} + 3v\sqrt{3(4m-1)}\right)^{2/3}$$
$$f_2 = (12m-1)\left(-v^4 + 5v^2 - 4\right) + 16m^2\left(3v^2 + 6 - 4m\right) + \left(v^2 - 1\right)\left(v^4 + 6v^2 - 4\right). \quad (6.10)$$

Substituting the roots $\pm k_0$ from Eq. (6.9) back into the dispersion relation in (6.5) we arrive at the following bandgap,

$$|\Omega| \leq \sqrt{k_0^2 + (1 - mk_0^2)^2} - v|k_0| - |\lambda|. \quad (6.11)$$

Inequality (6.11) shows that in the moving coordinates, the bandgap is dependent on

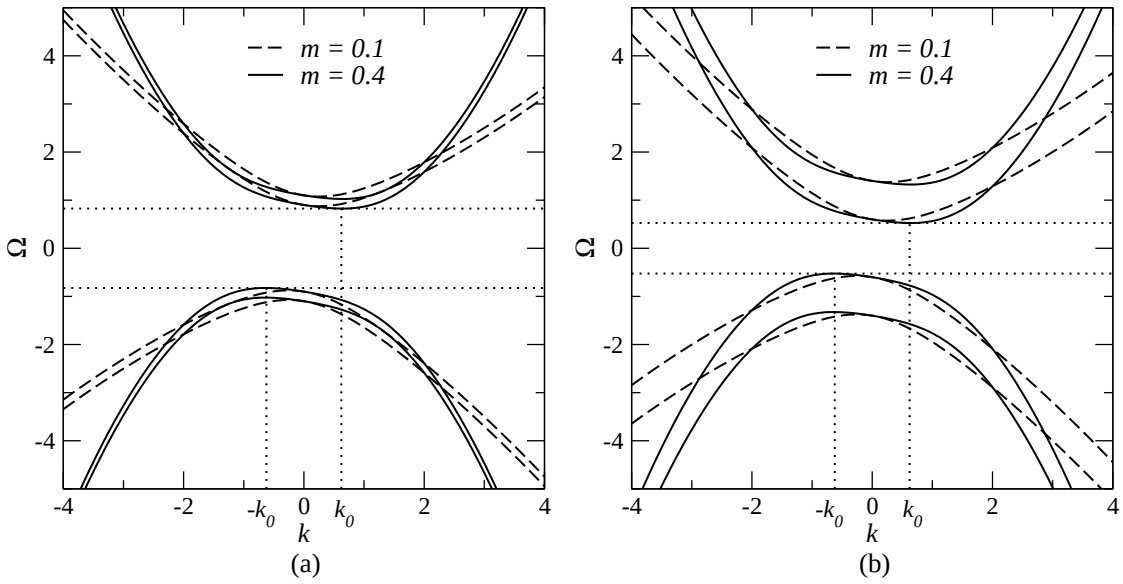

Figure 6.1: Dispersion curves in the reference frame moving with the velocity of $v = 0.2$ for $m = 0.1$ and 0.4, and (a) $\lambda = 0.1$, (b) $\lambda = 0.4$. Doted lines indicate the edges of the bandgap for $m = 0.4$.

m. More specifically, with increase of m the bandgap in the moving frame shrinks. In the absence of dispersive reflectivity Eq. (6.8) takes the form of

$$\left(1 - v^2\right) k^2 - v^2 = 0 \Longrightarrow k_0^2 = \frac{v^2}{1 - v^2}, \tag{6.12}$$

leading to the bandgap of the standard dual-core model in the moving coordinates, i.e.

$$|\Omega| \leq \sqrt{1 - v^2} - |\lambda| \,. \tag{6.13}$$

Four branches of dispersion relation (6.5) are shown in Figure 6.1 for $v = 0.2$ and various values of m and λ. The dotted lines in Figures 6.1(a)-(b) indicate the edges of bandgap for $m = 0.4$. It is worth noting that according to Eqs. (6.9) k_0^2 do not depend on λ. For example in both Figures 6.1(a) and (b) $k_0 = \pm 0.623$. From Eq. (6.11) the bandgap for Figure 6.1(a) and (b) are obtained to be $|\Omega| \leq 0.825$ and $|\Omega| \leq 0.525$, respectively.

It is found that the model of Eqs. (6.4) supports two types of symmetric ($U_1 = U_2$,

$V_1 = V_2$) and asymmetric ($U_1 \neq U_2$, $V_1 \neq V_2$) moving gap solitons. As explained in Chapter 5, we are only interested in the range $0 < m < 0.5$ for which it is found that moving gap solitons fill the entire bandgap.

Similar to the quiescent solutions, it is found that for given Ω and v there exists a critical coupling coefficient λ_c beyond which only symmetric solutions exist. For values of $\left|\lambda\right| < \lambda_c$ symmetric and asymmetric moving gap solitons are found to co-exist in the model. Asymmetry parameter Θ defined in Eq. (5.9) may be used in the moving case too, to show the bifurcation of solutions at λ_c. Bifurcation graphs are plotted numerically in Figures 6.2(a) and (b) in the plane of (λ, Θ) for different values of Ω and v. The horizontal lines in Figures 6.2(a) and (b) account for symmetric solutions (i.e. $\Theta = 0$), and the dotted-horizontal lines correspond to the symmetric solitons that co-exist with asymmetric ones. Also in these figures the edges of the solution space (which correspond to the edges of bandgap) are: (a) $\lambda = \pm 0.875$, ± 0.866, ± 0.825, and (b) $\Omega = \pm 0.395$, ± 0.362, ± 0.265 for $m = 0.1$, 0.2, and 0.4, respectively.

An interesting feature seen in Figures 6.2(a) and (b) is that the bifurcation points (λ_c) depend on m. More specifically, with increase of dispersive reflectivity parameter, λ_c decreases. This phenomenon is illustrated in Figure 6.2(c) where λ_c is plotted versus m for $v = 0.2$ and various frequencies.

According to Eq. (6.11) the location of edges of bandgap in the moving reference frame depends on m and v. This is illustrated in Figure 6.2(d) where bandgap edges Ω_0 are plotted in the plane of (m, Ω) for $\lambda = 0.1$ and various values of soliton velocity. Similarly, edges of bandgap are displayed in Figure 6.2(e) in the plane of (v, Ω) for $\lambda = 0.1$ and various values of dispersive reflectivity. Note that in both Figures 6.2(d) and (e) the corresponding bandgap edges in the lab frame are $|\omega_0| = 0.9$ (bandgap does not depend on m).

As discussed in Section 5.2, in the case of quiescent solitons, above a certain

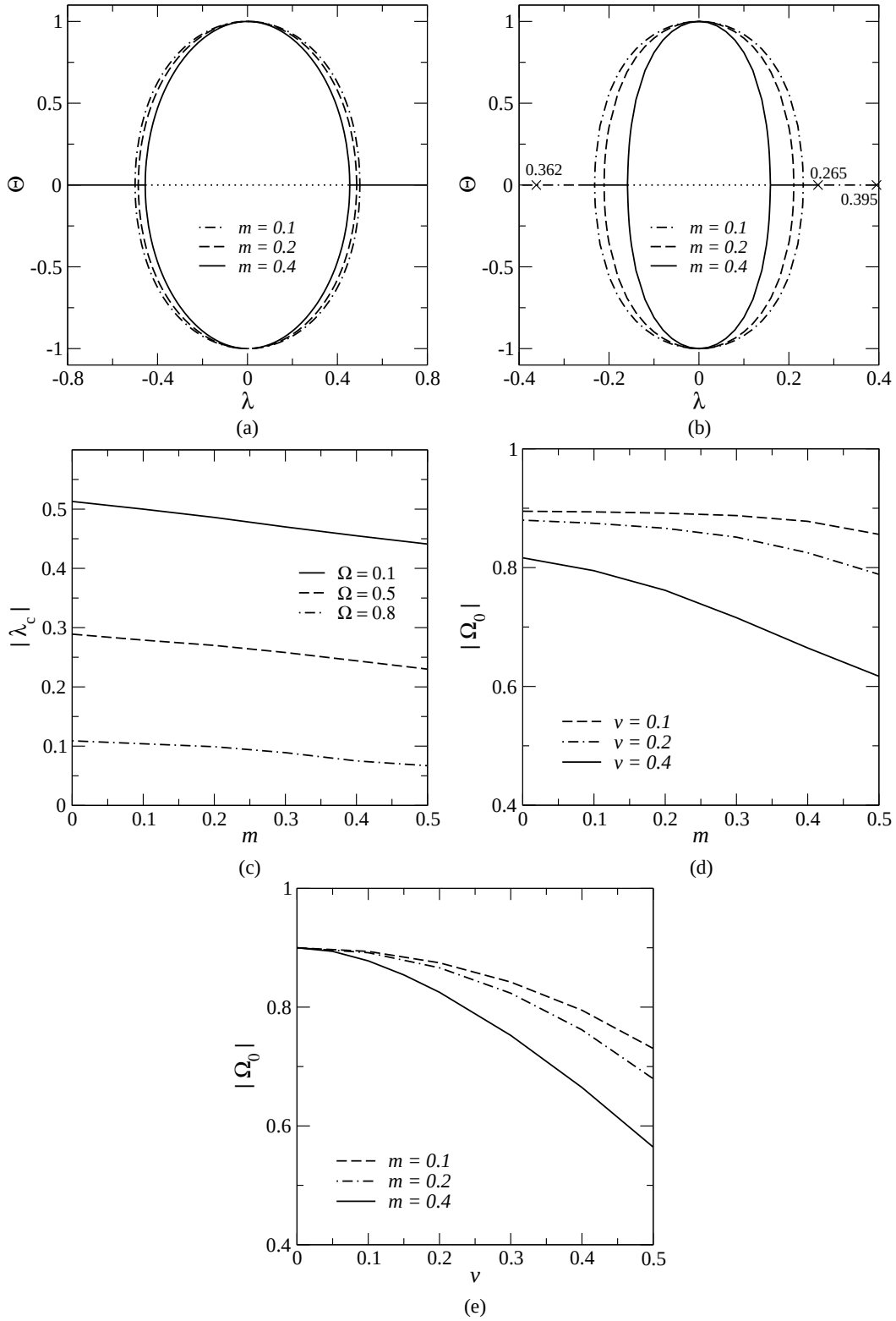

Figure 6.2: Bifurcation diagrams for (a) $\Omega = 0.1$, $v = 0.2$ and (b) $\Omega = 0.5$, $v = 0.4$, and various values of m. Dotted lines in both figures depict symmetric solitons that co-exist with asymmetric counterparts. In Figure (b) values of λ corresponding to the edges of bandgap for various values of m are marked. (c) Change of bifurcation point with respect to m for $v = 0.2$ and various values of Ω. Location of bandgap edges versus (d) dispersive reflectivity and (e) soliton velocity, according to Eq. (6.11) for $\lambda = 0.1$.

threshold of dispersive reflectivity solitons develop sidelobes. By analyzing gap soliton in the linear region, i.e. soliton tails, we also obtained the condition given in inequality (5.28) that is met when sidelobes appear. Similar phenomenon is seen for moving gap solitons. However, linear analysis of asymmetric moving gap soliton tails is not possible. This is explained in the next subsection. Therefore, we have

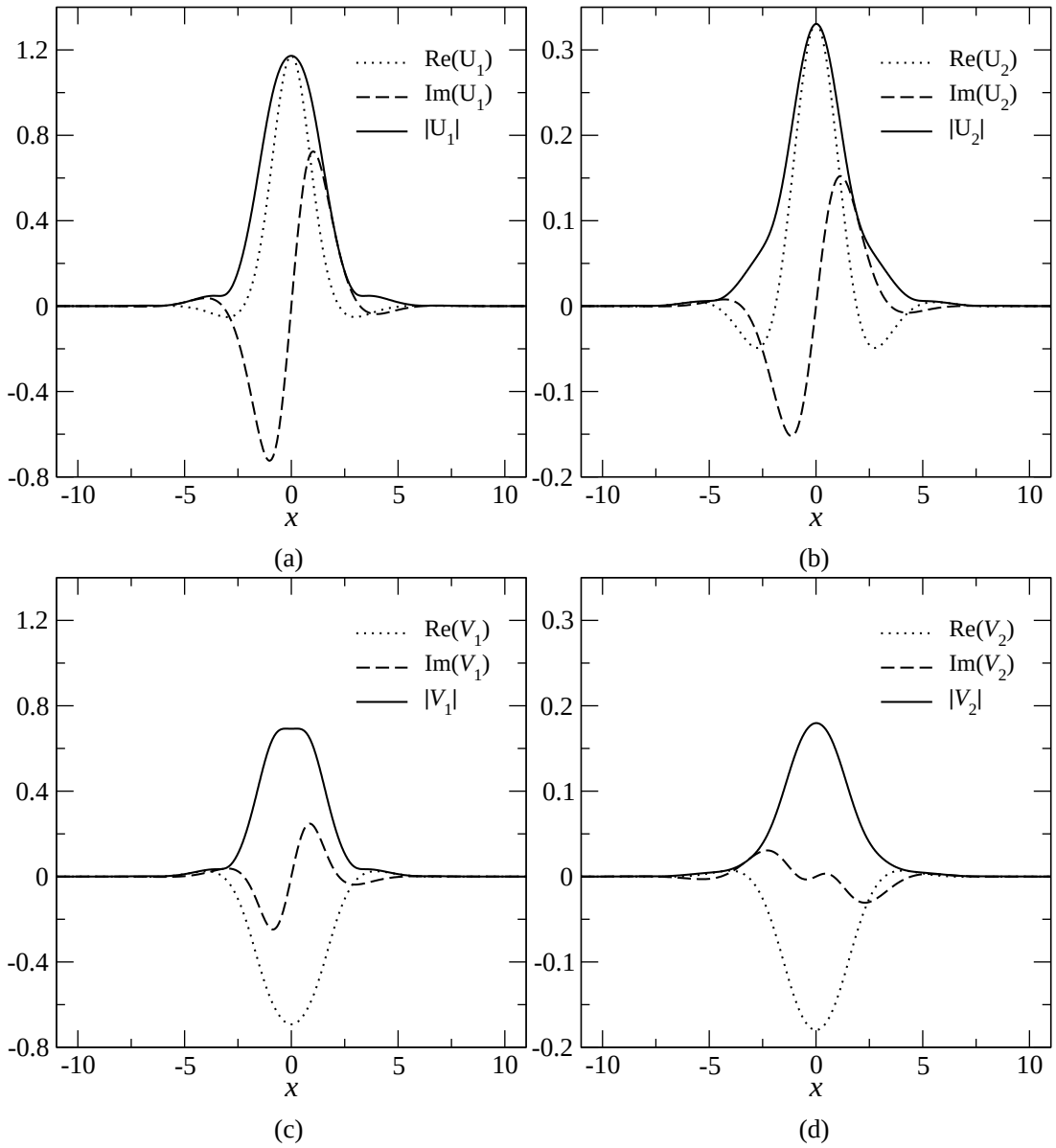

Figure 6.3: Real and imaginary parts and amplitudes of an example moving soliton with sidelobes. (a) to (d) in order: forward- and backward-propagating waves in core 1 and 2 for $m = 0.45$, $v = 0.35$, $\Omega = -0.1$, and $\lambda = 0.25$.

to find the sidelobe regions numerically. The components of a moving soliton with sidelobes are shown in Figure 6.3(a)-(d), respectively.

In determining the regions where solitons develop sidelobes, it is important to note that real and imaginary parts of forward or backward propagating waves in either of the cores may have oscillations in their tails even in the region where no sidelobes exist. This is due to the fact that the real and imaginary parts are not in-phase, i.e. the oscillations cancel each other in calculating the soliton amplitude, i.e. $|U_{1,2}|$ and $|V_{1,2}|$. For instance Figure 6.4(a) shows an example of an asymmetric moving soliton for $m = 0.1$, $v = 0.2$, $\Omega = 0.35$, and $\lambda = 0.2$ where no sidelobes exist. To have a better resolution of the trailing parts oscillations, Figure 6.4(b) displays the real part, imaginary part, and amplitude of U_1 in logarithmic scale for the same parameters as in Figure 6.4(a). As shown in Figure 6.4(b) real and imaginary parts have oscillations in their tails while there are no sidelobes may be usedin the soliton profile. Therefore to examine the existence of sidelobes numerically, we look for the

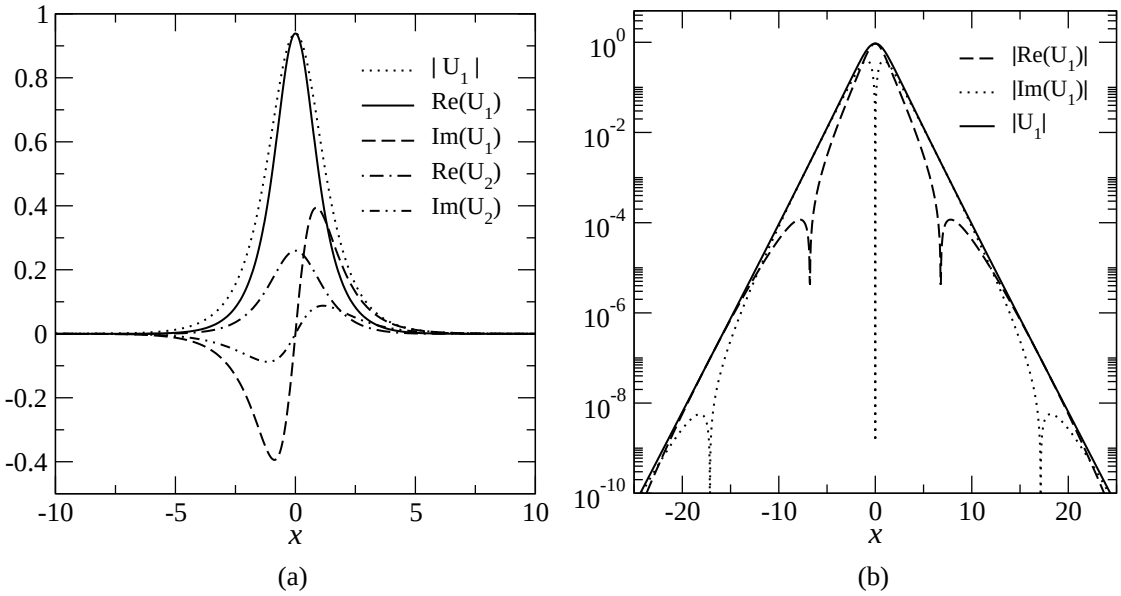

Figure 6.4: (a) Real and imaginary parts of forward-propagating waves in cores 1 and 2 i.e. U_1 and U_2 for $m = 0.1$, $v = 0.2$, $\Omega = 0.35$, and $\lambda = 0.2$ (asymmetric soliton). (b) Real, imaginary and amplitude of U_1 in logarithmic scale for the same parameters.

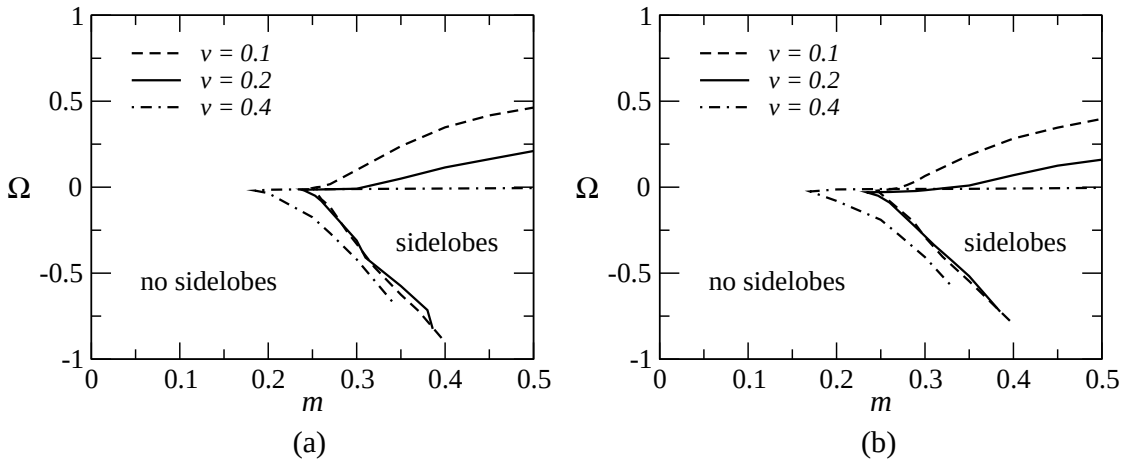

Figure 6.5: Generation of sidelobes as a result of dispersive reflectivity for (a) $\lambda = 0.1$, (b) $\lambda = 0.2$ and various values of soliton velocity.

nontrivial roots of $\partial |U_1| / \partial x$ or other wave components (sidelobes appear in all of the four $U_{1,2}$ and $V_{1,2}$ components simultaneously).

Using the technique explained above, we identified the sidelobe regions in the plane of (m, Ω) for various values of coupling and soliton velocity. The outcomes are shown in Figures 6.5(a) and (b). The analysis shows that for faster solitons, specifically $v \geq 0.4$, no sidelobes appears in the upper half of the bandgap.

6.1.1 Analysis of Tail of Solitons

In Section 5.2 linear forms of coupled mode equations (5.1) (or (6.6)) were solved for the special case of quiescent solitons where the symmetry conditions $v_{1,2} = -u^*_{1,2}$ reduced the number of equations and consequently the number of unknowns to half of the general case. In the case of symmetric quiescent gap solitons equations further simplified into half. In the general case, i.e. $v \neq 0$, we need to deal with a system of eight coupled ODEs. More specifically, splitting the real and imaginary parts in Eq.

(6.6), we arrive at the following system of equations,

$$\begin{aligned}
\Omega U_{1re} - (1-v)\, U'_{1im} + V_{1re} + \lambda U_{2re} - m V''_{1re} &= 0,\\
\Omega U_{1im} + (1-v)\, U'_{1re} + V_{1im} + \lambda U_{2im} + m V''_{1im} &= 0,\\
\Omega V_{1re} + (1+v)\, V'_{1im} + U_{1re} + \lambda U_{1re} + m U''_{1re} &= 0,\\
\Omega V_{1im} - (1+v)\, V'_{1re} + U_{1im} + \lambda U_{1im} + m U''_{1im} &= 0,\\
\Omega U_{2re} - (1-v)\, U'_{2im} + V_{2re} + \lambda U_{1re} + m V''_{2re} &= 0,\\
\Omega U_{2im} + (1-v)\, U'_{2re} + V_{2im} + \lambda U_{1im} + m V''_{2im} &= 0,\\
\Omega V_{2re} + (1+v)\, V'_{2im} + U_{2re} + \lambda U_{2re} + m U''_{2re} &= 0,\\
\Omega V_{2im} - (1+v)\, V'_{2re} + U_{2im} + \lambda U_{2im} + m U''_{2im} &= 0,
\end{aligned} \tag{6.14}$$

where prime stands for derivative with respect to X and,

$$\begin{aligned}
U_1 &= U_{1re} + iU_{1im},\\
U_2 &= U_{2re} + iU_{2im},\\
V_1 &= V_{1re} + iV_{1im},\\
V_2 &= V_{2re} + iV_{2im}.
\end{aligned} \tag{6.15}$$

All the coefficients are constant and the equations are homogenous. However, different set of coefficients result in different types of solutions that may deviate from the soliton tails.

In the case of symmetric moving gap solitons the order of the ODEs, i.e. the number of equations in (6.14) can be halved by applying the symmetry conditions.

Substituting $U_1 = U_2$ and $V_1 = V_2$ in Eqs. (6.14) it obtains,

$$\begin{aligned}
(\Omega+\lambda)\,U_{1re} - (1-v)\,U'_{1im} + V_{1re} + mV''_{1re} &= 0,\\
(\Omega+\lambda)\,U_{1im} + (1-v)\,U'_{1re} + V_{1im} + mV''_{1im} &= 0,\\
(\Omega+\lambda)\,V_{1re} + (1+v)\,V'_{1im} + U_{1re} + mU''_{1re} &= 0,\\
(\Omega+\lambda)\,V_{1im} - (1+v)\,V'_{1re} + U_{1im} + mU''_{1im} &= 0.
\end{aligned} \tag{6.16}$$

In what follows we solve the special case of Eqs. (6.16).

Characteristic equation of the system of (6.16) can be found by substituting $U_{1,2}, V_{1,2} \sim e^{\Gamma X}$ where Γ is a complex number. In matrix form it can be expressed as follows,

$$\begin{bmatrix}
\Omega+\lambda & -(1-v)\,\Gamma & 1+m\Gamma^2 & 0\\
(1-v)\,\Gamma & \Omega+\lambda & 0 & 1+m\Gamma^2\\
1+m\Gamma^2 & 0 & \Omega+\lambda & (1+v)\,\Gamma\\
0 & 1+m\Gamma^2 & -(1+v)\,\Gamma & \Omega+\lambda
\end{bmatrix}
\begin{bmatrix}
U_{1re}\\ U_{1im}\\ V_{1re}\\ V_{1im}
\end{bmatrix} = 0. \tag{6.17}$$

For Eqs. (6.17) to have nontrivial solutions the square matrix must be singular which results in the following equation,

$$\begin{aligned}
m^4\Gamma^8 + 2m^2\left(2m-1+v^2\right)\Gamma^6 + \left(1+4mv^2+6m^2+v^4-4m-2v^2-2m^2\left(\lambda+\Omega\right)^2\right)\Gamma^4\\
+\left(\left(\lambda+\Omega\right)^2\left(2+2v^2-4m\right)+2v^2+4m-2\right)\Gamma^2 + \left(\left(\lambda+\Omega\right)^2-1\right)^2 = 0.
\end{aligned} \tag{6.18}$$

Because the polynomial in (6.18) is a fourth order polynomial of Γ^2, its roots are complex conjugates of each other. It is worth noting that for $m = 0$ Eq. (6.18) simplifies to a fourth-order polynomial,

$$\left(v^2-1\right)^2\Gamma^4 + 2\left(\left(\lambda+\Omega\right)^2\left(1+v^2\right)+v^2-1\right)\Gamma^2 + \left(\left(\lambda+\Omega\right)^2-1\right)^2 = 0, \tag{6.19}$$

leading to four complex roots,

$$\Gamma^2 = -\frac{(\Omega+\lambda)^2(v^2+1)+v^2-1\pm 2\sqrt{(\Omega+\lambda)^2 v^2\left[(\Omega+\lambda)+v^2-1\right]}}{(1-v^2)^2}. \tag{6.20}$$

For $v=0$, Eq. (6.20) simplifies to Eq. (5.19).

In general, it is possible for any set of soliton parameters to find the roots of Eq. (6.18) and form the general solution of Eqs. (6.16), by applying boundary conditions. Equations (6.16) admit the following general solutions,

$$\begin{aligned}
U_{1re}(X) &= \sum_{n=1}^{8}\Psi_n \exp(\Gamma_n X),\\
U_{1im}(X) &= \sum_{n=1}^{8}\Psi_n\Gamma_n \exp(\Gamma_n X)\left\{a_1\Gamma_n^6+b_1\Gamma_n^4+c_1\Gamma_n^2+d_1\right\},\\
V_{1re}(X) &= \sum_{n=1}^{8}\Psi_n \exp(\Gamma_n X)\left\{a_2\Gamma_n^6+b_2\Gamma_n^4+c_2\Gamma_n^2+d_2\right\},\\
V_{1im}(X) &= \sum_{n=1}^{8}\Psi_n\Gamma_n \exp(\Gamma_n X)\left\{a_3\Gamma_n^6+b_3\Gamma_n^4+c_3\Gamma_n^2+d_3\right\},
\end{aligned} \tag{6.21}$$

where Γ_n are the roots of Eq. (6.18) and Ψ_n are complex coefficients to be satisfied through boundary conditions, i.e.

$$\begin{aligned}
U_{1re,im}(\pm\infty) &= 0,\\
V_{1re,im}(\pm\infty) &= 0.
\end{aligned} \tag{6.22}$$

In obtaining Eqs. (6.21) we also used MATLAB symbolic tools. Applying the boundary conditions (6.22) to Eqs. (6.21), it is found that U_{1re} and V_{1re} must be real and even functions of X. Similarly U_{1im} and V_{1im} must be real and odd functions

of X. Thus, Ψ_n coefficients take the following form,

$$\begin{cases} \Psi_{2j} = 0, \Psi_3 = \Psi_1^*, \Psi_7 = \Psi_5^* & X > 0 \\ \Psi_{2j-1} = 0, \Psi_4 = \Psi_2^*, \Psi_8 = \Psi_6^* & X < 0 \end{cases} \tag{6.23}$$

where $j = 1, .., 4$. This reduces the total number of unknowns in Eqs. (6.21) to four arbitrary constants. The rest of the coefficients in Eqs. (6.21) are:

$$\begin{aligned}
a_1 &= m^4 \beta_1^{-1}, \\
b_1 &= 2 * m^2 \left(v^2 + 2m - 1\right) \beta_1^{-1}, \\
c_1 &= \left[\left(3\left(\lambda + \Omega\right)^2 + 1\right) v^2 + \left(\left(\lambda + \Omega\right)^2 - 1\right)(1 - 2m)\right] \beta_1^{-1}, \\
d_1 &= \left[v^4 + 2\left(2m - 1\right) v^2 - m^2 \left(\left(\lambda + \Omega\right)^2 - 5\right) - 4m + 1\right] \beta_1^{-1}, \\
a_2 &= m^4 \left(1 + v\right) \beta_2^{-1}, \\
b_2 &= m^2 \left(1 + v\right) \left(2v^2 + 3m - 2\right) \beta_2^{-1}, \\
c_2 &= \left[v^2 \left(1 + v\right) \left(v^2 + 3m - 2\right) - \left(-1 + 3m + 3m^2 \left(\left(\lambda + \Omega\right)^2 - 1\right)\right) v \right. \\
&\quad \left. + m^2 \left(3 - \left(\lambda + \Omega\right)^2\right) - 3m + 1\right] \beta_2^{-1} \\
d_2 &= \left[\left(\left(\lambda + \Omega\right)^2 + 1\right) v^3 + \left(3\left(\lambda + \Omega\right)^2 + 1\right) v^2 - \left(m - 1\right) \left(3\left(\lambda + \Omega\right)^2 - 1\right) v \right. \\
&\quad \left. - \left(m - 1\right) \left(\left(\lambda + \Omega\right)^2 - 1\right)\right] \beta_2^{-1} \\
a_3 &= m^4 \left(v^2 + 2v + 1 - m\right) \beta_3^{-1} \\
b_3 &= \left[\left(v^2 + 2v + m\right) 2v^2 + \left(2m - 1\right) 4v - \left(\left(\lambda + \Omega\right)^2 + 3\right) m^2 + 6m - 2\right] m^2 \beta_3^{-1} \\
c_3 &= \left[v^6 + 2v^5 + \left(3m - 1\right) v^4 + 4\left(2m - 1\right) v^3 + \left(4\left(1 - \left(\lambda + \Omega\right)^2\right) m^2 + 2m - 1\right) v^2 + \right. \\
&\quad \left. \left(4\left(3 - \left(\lambda + \Omega\right)^2\right) m^2 - 8m + 2\right) v - \left(3 + \left(\lambda + \Omega\right)^2\right) m^3 + 8m^2 - 5m + 1\right] \beta_3^{-1} \\
d_3 &= \left\{\left(3 + \left(\lambda + \Omega\right)^2\right) v^4 + 4\left(1 + \left(\lambda + \Omega\right)^2\right) v^3 + \left[\left(3 - 7\left(\lambda + \Omega\right)^2\right) m + 6\left(\lambda + \Omega\right)^2 - 2\right] v^2 + \right. \\
&\quad \left. \left(1 - \left(\lambda + \Omega\right)^2\right) \left(6m - 4\right) v + \left(-1 + \left(\lambda + \Omega\right)^2\right) \left[\left(1 + \left(\lambda + \Omega\right)^2\right) m^2 - 3m + 1\right]\right\} \beta_3^{-1}
\end{aligned} \tag{6.24}$$

where,

$$\beta_1 = 2v\left(\lambda+\Omega\right)\left(\left(\lambda+\Omega\right)^2-1\right),$$
$$\beta_2 = 2v\left(\lambda+\Omega\right)\left(m\left(\lambda+\Omega\right)^2-\left(v+1\right)^2\right),$$
$$\beta_3 = 2v\left(\left(\lambda+\Omega\right)^2-1\right)\left(m\left(\lambda+\Omega\right)^2-\left(v+1\right)^2\right). \qquad (6.25)$$

By properly choosing the four arbitrary constants that appear in (6.21) (i.e. Ψ_{2j-1} for $X>0$ and Ψ_{2j} for $X<0$), one can obtain the analytical expressions for the tails of the gap solitons. As is shown in Figures 6.6(a) and (b), real and imaginary parts of the analytical solutions obtained from Eqs. (6.21) and the exact numerical soliton solutions are in excellent agreement, except in the proximity of soliton's peak where the linear approximation does not hold.

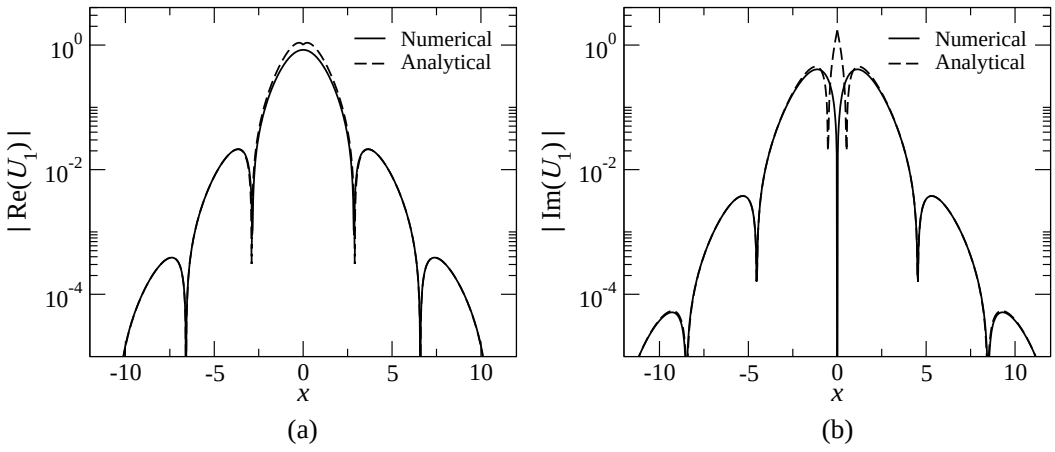

Figure 6.6: Comparison of numerically obtained soliton solutions with analytical solutions obtained from Eqs. (6.21); (a) real and (b) imaginary parts of a symmetric gap soliton for $\Omega = 0.4$, $\lambda = 0.2$, $m = 0.35$, and $v = 0.2$. Eq. (6.18) was solved numerically. The complex coefficients were found using a curve fitting algorithm: $\Psi_1 = 0.6288 - 0.4042i$, $\Psi_3 = 0.6288 + 0.4042i$, $\Psi_5 = -0.1260 + 0.6701i$, $\Psi_7 = -0.1260 - 0.6701i$.

6.2 Stability of Moving Solitons

We have investigated the stability of moving gap solitons in the model of Eqs. (6.4) through systematic numerical analysis. To this end, Eqs. (6.4) are numerically solved using the relaxation algorithm that was explained in Section 4.2. The obtained pulses are then propagated in the structure via the symmetrised split-step Fourier method described in Section 4.4.1. The results are displayed in Figures 6.7(a)-(f) where stable regions for different values of v and λ are shown in the plane of (m, Ω). As it can be inferred from Figure 6.7, for $m = 0$ i.e. standard dual-core model, the asymmetric moving solitons with $\Omega \lesssim 0$ are unstable. The case of $m = 0$ has also been studied in reference [77] where it has been reported that moving asymmetric solitons are always stable where they exist. The results displayed in Figure 6.7 not only agree well with the results of reference [77], but also generalize the model by including all frequencies of the bandgap.

One important finding is that with increase of dispersive reflectivity parameter the stability region expands into the negative values of Ω. This is true for higher velocity solitons too as shown in Figures 6.7(e)-(f). This is yet another confirmation of the stabilizing effects of dispersive reflectivity. Similar to the quiescent solitons, in the moving case increase of λ decreases the stabilizing effects of dispersive reflectivity. For instance with increase of λ from 0.1 to 0.2 in Figures 6.7(e) and (f) the stable region slightly shrinks to approximately $\Omega \gtrsim 0$ for the whole range of $m < 0.5$.

According to bifurcation theory it is known that for given Ω, m and v, above critical coupling λ_c, the symmetric solutions that exist on their own are always stable. The numerical stability analysis confirms the predictions of the bifurcation theory. The regions where symmetric solutions exist on their own are shown in Figures 6.7(a)-(f). It should be noted that unstable symmetric solutions that co-exist with asymmetric ones are not shown in these figures.

In obtaining the stable regions, we have used two methods. The common method

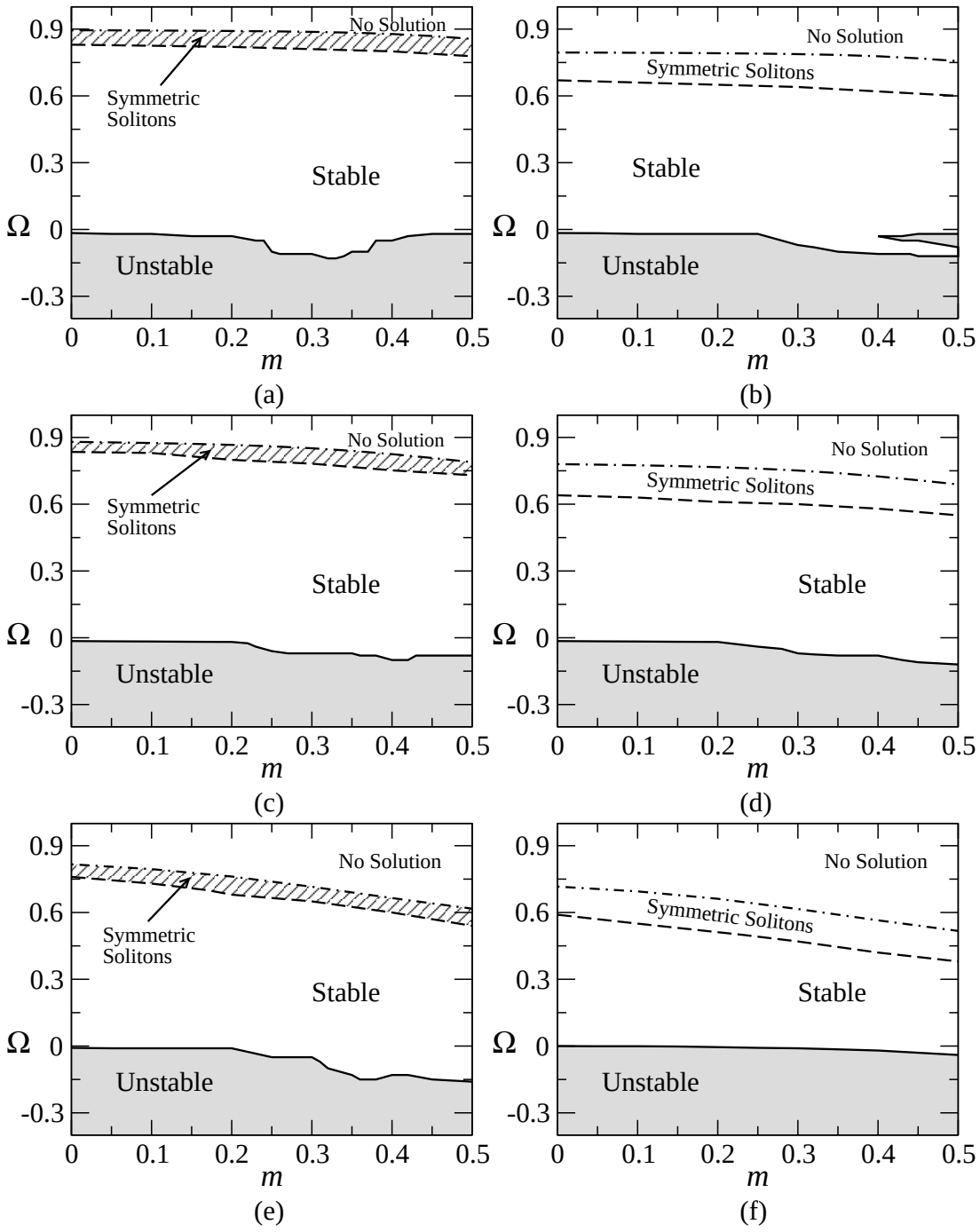

Figure 6.7: Stability diagrams for moving solitons in the plane of (m, Ω) for different coupling coefficients λ, and soliton velocities v; (a) $\lambda = 0.1$ and $v = 0.1$, (b) $\lambda = 0.2$ and $v = 0.1$, (c) $\lambda = 0.1$ and $v = 0.2$, (d) $\lambda = 0.2$ and $v = 0.2$, (e) $\lambda = 0.1$ and $v = 0.4$, (f) $\lambda = 0.2$ and $v = 0.4$. The dashed lines depict bifurcation points. The narrow hatched regions correspond to the symmetric solutions that exist on their own. Edges of the bandgap in the moving reference plane are shown by dash-dotted curves (cf. Figures 6.2(c)-(e)).

is to examine the stability of solitons against perturbations. However, this approach makes it difficult to distinguish the stability of pulses for the parameters very close to the stability borders. More specifically, perturbations cause velocity change in both stable and unstable solitons that are close to the stability border, particularly when longer propagation time is needed. Thus, it is somewhat inaccurate to identify the stability borders using this approach. The same difficulty was experienced in the quiescent case. More specifically, perturbed stable quiescent solitons that are close to the stability border may become moving as a result of the perturbation.

The other method that is used in this thesis is to examine the oscillations of the solitons peak during propagation in the absence of the perturbations. In this case the numerical noise is enough to trigger any instability. For instance, maximum amplitude of U_1 component for $\Omega = -0.1$, $\lambda = 0.1$, $m = 0.1$, and $v = 0.2$ which falls in the unstable region (cf. Figure 6.7(c)) is shown in Figure 6.8(a). With increase of frequency to $\Omega = +0.05$ the soliton is in the stable region. Maximum amplitude of U_1 for the stable soliton is shown in Figure 6.8(b). It is obvious that the oscillations of the soliton's peak in Figure 6.8(a) amplifies as the soliton propagates in the medium, suggesting that the soliton is unstable. On the other hand the soliton's peak is at

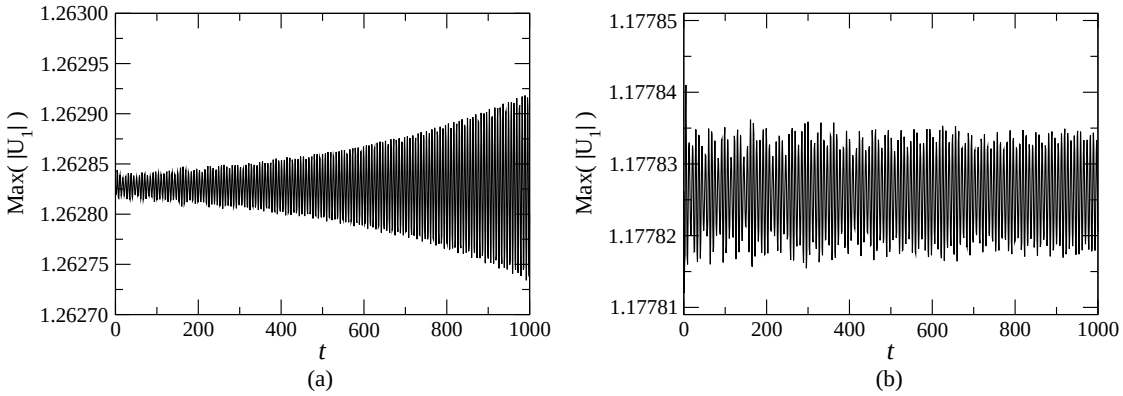

Figure 6.8: Evolution of maximum amplitudes of forward-propagating waves in core 1 (U_1) for moving asymmetric solitons. (a) An unstable soliton for $\Omega = -0.1$, $\lambda = 0.1$, $m = 0.1$, and $v = 0.2$, and (b) stable soliton for the same parameters but $\Omega = +0.05$. Perturbations are not used.

a steady state in Figure 6.8(b), suggesting that the soliton is stable. Also, periodic changes of the soliton's peak, i.e. breathing, can be seen in Figure 6.8(b). It should be noted that the increase in the oscillations of the peak amplitude happen in all of the components.

Similar to the quiescent solitons, the development of instability in the moving solitons generally does not lead to the destruction of the solitons. Instead, whether symmetric or asymmetric they spontaneously rearrange themselves into robust asymmetric ones. During the rearrangement solitons generally shed some radiation and the energy loss causes the soliton to either reduce its velocity or frequency or both depending on the parameters. It is possible to approximately determine the parameters of the emerging robust solitons via curve fitting, however the emerging solitons generally undergo fluctuations, i.e. breather, which makes it hard to make any accurate estimate of the new parameters.

Examples of the evolution of unstable asymmetric and symmetric moving solitons are shown in Figures 6.9(a) and (b), respectively. In these figures U_1 and U_2 components are shown at the same time for better comparison. As shown in Figure 6.9(a) the asymmetric solitons gain velocity as they propagate and as a result shed some radiations. The emerging fast moving solitons then undergo breathing. Similarly, the symmetric solitons in Figure 6.9(b) lose some energy while propagate along the fiber. They quickly transform into asymmetric robust ones which subsequently undergo breathing.

6.3 Collisions of Moving Solitons

Interactions and collisions of solitons are of great interest and have been studied in various contexts [93–95]. This is, in part, due to the fact that the outcomes of such interactions provide further insights into the nonlinear dynamics of the system which

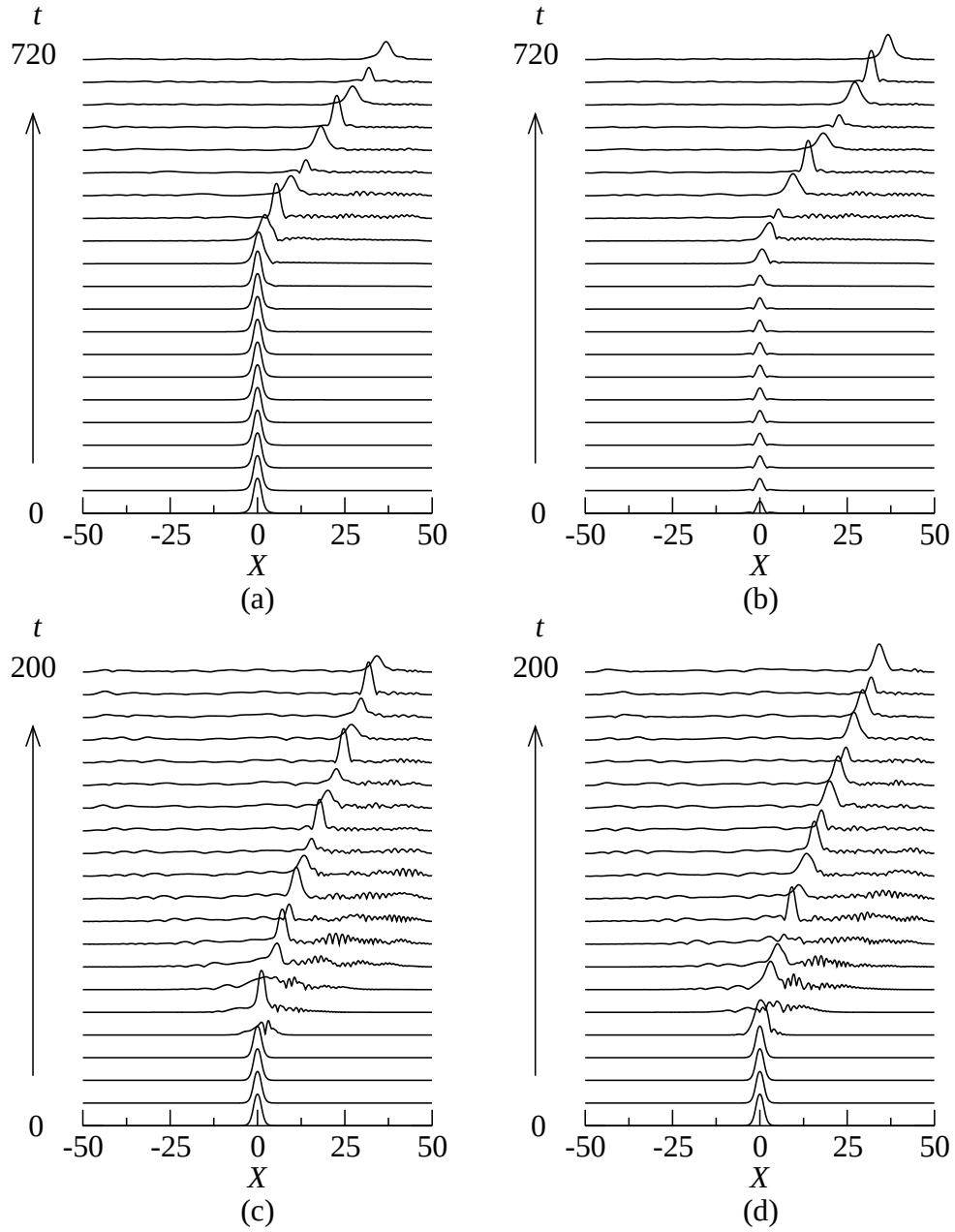

Figure 6.9: Evolution of (a) U_1 and (b) U_2 components of an unstable asymmetric moving gap soliton. (c) and (d): evolution of U_1 and U_2 components of a symmetric moving gap soliton. Other parameters in all the above are: $\Omega = -0.4$, $\lambda = 0.4$, $m = 0.25$, and $v = 0.2$. The above symmetric and asymmetric solitons co-exist in the system.

can be used to manipulate light for various applications. A major challenge in the slow light applications is the generation of stationary or quiescent gap solitons. One of the proposed methods is through the collisions of counter-propagating moving gap

solitons which at certain parameters result in the merger of the gap solitons into a single non-moving one [66, 92, 96, 97].

To study the collisions of moving gap solitons, we have propagated stable identical counter-propagating solitons numerically throughout the plane of (m, Ω) for different values of λ and v, subject to the following initial conditions:

$$\begin{aligned} U_p(X,0) &= U_{p,v}(X - \frac{\triangle X}{2}, 0) + U_{p,-v}(X + \frac{\triangle X}{2}, 0)\exp(i\triangle\varphi), \\ V_p(X,0) &= V_{p,v}(X - \frac{\triangle X}{2}, 0) + V_{p,-v}(X + \frac{\triangle X}{2}, 0)\exp(i\triangle\varphi), \end{aligned} \tag{6.26}$$

where $\triangle X$ and $\triangle\varphi$ are initial separation and phase difference of the two colliding solitons. $p = 1, 2$ correspond to the first and second cores. Also, $\{U_{p,v}, V_{p,v}\}$ correspond to the forward-propagating soliton with the velocity of v. Similarly $\{U_{p,-v}, V_{p,-v}\}$ correspond to the backward-propagating soliton with the velocity of v.

One interesting result, which was found by systematically changing ΔX in many simulations, is that the initial separation has negligible effect on the character of interactions. This is found for collisions of both symmetric and asymmetric gap solitons.

We have studied two cases of in-phase ($\Delta\varphi = 0$) and out-of-phase ($\Delta\varphi = \pi$) collisions. Figures 6.10(a)-(f) show examples of collisions of in-phase counter-propagating identical solitons for various parameters. Through systematic simulations we have found that collision of two moving symmetric or asymmetric gap solitons leads to one of five possible outcomes: it may result in the passage of solitons through each other (Figure 6.10(a) and (e)), merger into a single quiescent or moving soliton (Figure 6.10(b)), elastic bounce (Figure 6.10(c)), creation of a single quiescent and two moving solitons (Figure 6.10(d)), and destruction of both solitons (Figure 6.10(f)).

It is found that in the region where solitons bounce off each other, they generally maintain their energies and consequently their velocities and frequencies after the particle like collision. In contrast the passage of solitons through each other is

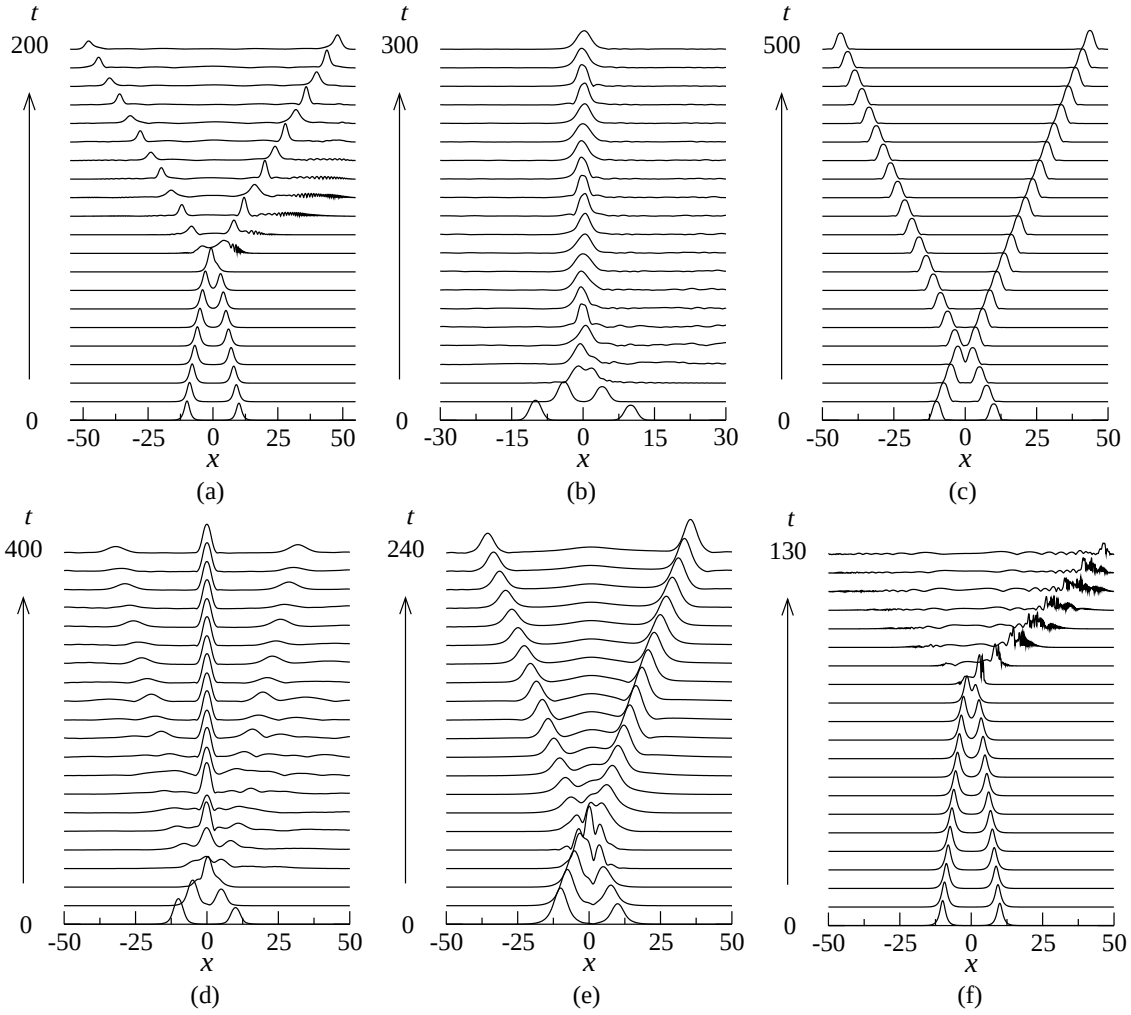

Figure 6.10: Examples of collisions of stable identical counter-propagating in-phase moving gap solitons. (a) Passage of asymmetric solitons through each other for $\Omega = 0.2$, $\lambda = 0.1$, $m = 0.1$, and $v = 0.1$, (b) Merger of asymmetric solitons into a quiescent one for $\Omega = 0.1$, $\lambda = 0.1$, $m = 0.3$, and $v = 0.2$, (c) Elastic collision of asymmetric solitons for $\Omega = 0.0$, $\lambda = 0.2$, $m = 0.45$, and $v = 0.1$, (d) Generation of a quiescent soliton along with two moving ones for $\Omega = 0.55$, $\lambda = 0.2$, $m = 0.4$, and $v = 0.2$, and (e) Symmetric separation in the symmetric region where $u_1 = u_2$ and $v_1 = v_2$ for $\Omega = 0.65$, $\lambda = 0.2$, $m = 0.42$, and $v = 0.2$. (f) Destruction of asymmetric solitons for $\Omega = 0.08$, $\lambda = 0.2$, $m = 0.05$, and $v = 0.1$. Only forward-propagating wave in core 1 i.e. U_1 is shown.

generally not elastic, giving rise to the emission of radiation (e.g. Figure 6.10(a)). Similarly merger of solitons, as is shown in Figure 6.10(b), generally result in radiation loss and the emerging quiescent or moving soliton has less power than the two initial solitons combined. The amount of radiation varies based on the soliton

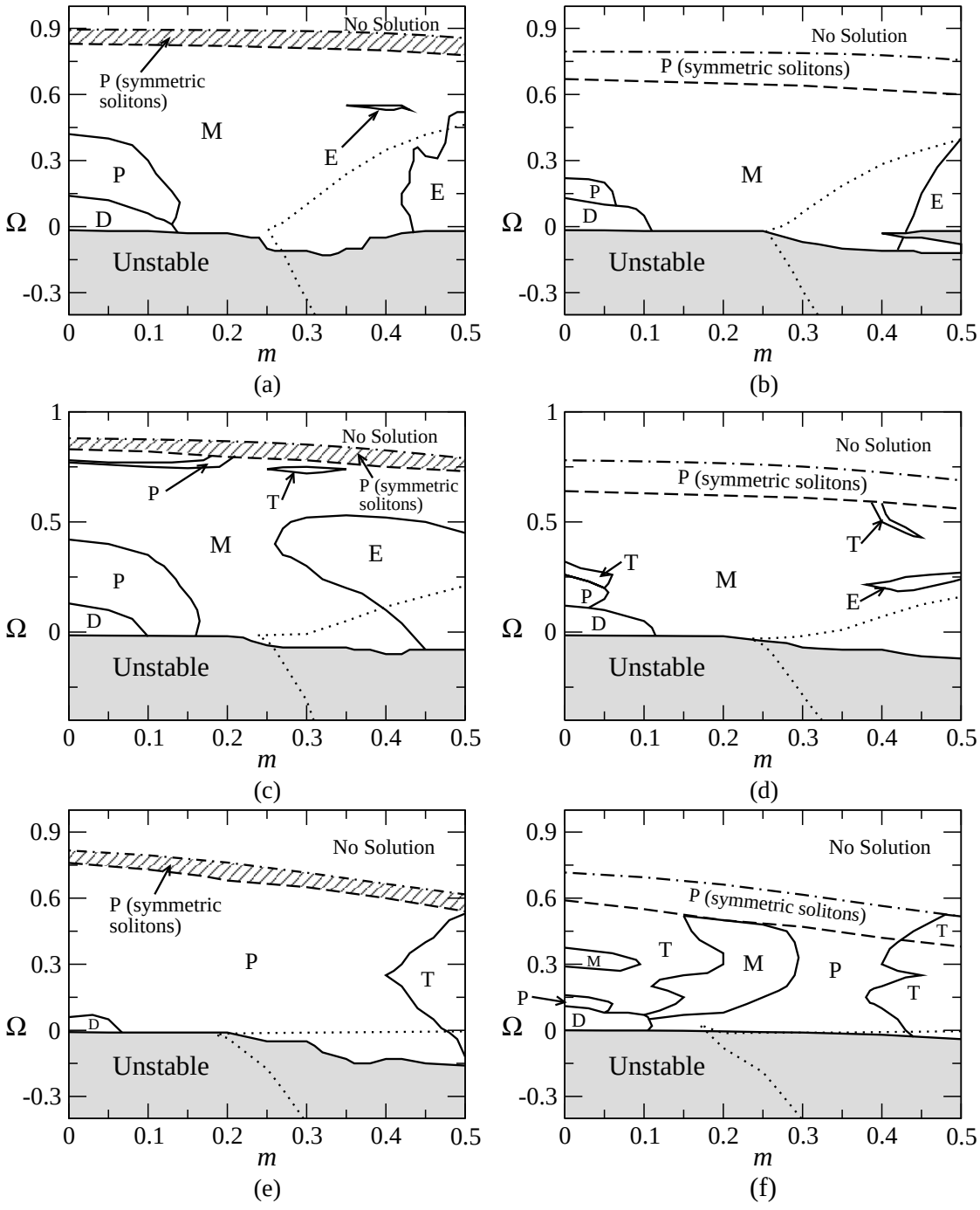

Figure 6.11: Outcomes of the interactions of in-phase moving gap solitons in the plane of (m, Ω) for (a) $\lambda = 0.1$ and $v = 0.1$, (b) $\lambda = 0.2$ and $v = 0.1$, (c)$\lambda = 0.1$ and $v = 0.2$, and (d) $\lambda = 0.2$ and $v = 0.2$, (e) $\lambda = 0.1$ and $v = 0.4$, (f) $\lambda = 0.2$ and $v = 0.4$. Labels stand for: Destruction (D), Elastic bounce (E), Merger (M), Passage of solitons through each other (P), three solitons generation i.e. generation of two moving and one quiescent solitons (T). The dashed lines show the bifurcation points i.e. the border between symmetric and asymmetric solutions. The dash-dotted lines show bandgap edges in the moving reference frame. Regions in which sidelobes appear are determined by dotted lines.

parameters.

In the case of in-phase gap solitons, the outcomes of interactions are summarized in Figures 6.11(a)-(f) for various λ and v in the plane of (m, Ω). The dotted curves in these figures show the regions where sidelobes appear in the soliton profile. One striking finding is that with increase of velocity of solitons from 0.1 to 0.2 a region appears in which collisions result in the generation of two moving solitons and a quiescent one (region T). With further increase of velocity to 0.4, as shown in Figure 6.11(e) and (f), region T significantly expands. Also, region P, where solitons pass through each other, expands largely with increase of soliton velocity from 0.2 to 0.4. As shown in Figures 6.11(d) and (f) $2 \rightarrow 3$ transformation happens even in the absence of dispersive reflectivity, i.e. standard coupled mode system. This is the first time that three gap soliton generation is reported as a result of in-phase collision of moving solitons in the $m = 0$ case, suggesting that this is a feature of the model.

As shown in Figure 6.11, collisions of stable symmetric solutions where $U_1 = U_2$ and $V_1 = V_2$ (cf. Figure 6.7), usually result in the passage of solitons through each other except for small regions for fast moving solitons.

Outcomes of out-of-phase symmetric and asymmetric gap solitons, i.e. when $\Delta\varphi = \pi$, generally fall into two categories: gap solitons with small or no sidelobes symmetrically bounce off each other. This is similar to the collisions of out-of-phase nonlinear Schrodinger (NLS) solitons. On the other hand for larger values of m, i.e. regions specified in Figure 6.5 where sidelobes appear, it is seen that gap solitons repel each other and lose some energy by decreasing their velocities after the collision.

6.4 Potential Applications Of Moving Solitons

The ability to delay optical pulses by slowing down the light inside a grating has a number of potential applications: optical buffers, delay lines, and all-optical mem-

ories, to name a few, which may be used in high speed optical communication systems. For example, a configuration has been proposed in reference [104] for optical memories, which consists of a fiber ring incorporating a phase-sensitive amplifier to compensate for the ring losses. It has been shown that such storage devices are physically realizable and can store up to 10 Mbits of data indefinitely, which may be useful for interchange and routing buffers [105].

Generating slowly moving gap solitons is a challenge of its own. A method was proposed recently to create very slow gap solitons with the help of grating-assisted couplers [100]. The proposal involves many design complexities, however gap solitons with velocities as low as 4% of the speed of light in vacuum were numerically reported. The results of the soliton-soliton collision that were presented in Figures 6.11 may also be used to overcome the problem of creating slow optical pulses. For instance, the velocity of the resulting moving gap solitons can be controlled by properly choosing the parameters: they may have faster, slower or even zero velocities (refer to Figures 6.10).

In reference [96] it was shown that to get a quiescent soliton from an inelastic collision of faster gap solitons, the initial velocities of solitons must be less than 20% of the group velocity, which has not been experimentally observed yet. However, figure 6.11(f) shows the collision outcomes for $v = 0.4$, i.e. fast initial solitons, which lead into the generation of quiescent gap solitons in region M.

One of the key slow-light applications of gap solitons is their use in all-optical switching (or logic gates), which is an integral part of future communication networks. All-optical AND gates, for instance, were first proposed in the concept of gap solitons by Lee and Ho [99]. The proposed method was based on two orthogonally polarized gap solitons that form a coupled system, described through coupled NLS equations. They showed that the coupled pulses launched simultaneously into the grating propagate through the nonlinear periodic medium while individual pulses

undergo strong grating-induced reflection (i.e. an AND operation), because their frequency lies within the bandgap. Same principle was also used a few years later in fiber Bragg gratings and the all-optical AND gate was experimentally demonstrated to have a switching contrast of 17dB (i.e. the ratio of output power in ON and OFF states) [98]. One advantage of optical logic gates over their semiconductor counterparts is shorter response time (or propagation delay). For example current NAND gates have propagation delays in the order of a few to hundreds of ns, while the logic operation in [98] is done as soon as the pulses travel through the grating which is of the order of sub-ns for an 8-cm long grating.

Similarly, one potential application for the model that we studied in this thesis is optical switching. For instance, by controlling m in Figure 6.11(c) at fixed frequencies (say $\Omega = 0.45$), it is possible to control the outcomes of the soliton-soliton collision between the two regions of merger (M) and elastic bounce (E). More specifically, in region M the incident pulses will (theoretically) remain inside the grating, while in the region E they will bounce off each other and appear at the output ports. This could be used in optial routing applications or even optical Add-Drop components.

Chapter 7

Summary

7.1 Conclusions

The existence, stability and interactions of gap solitons in Kerr-type nonlinear grating-assisted fiber couplers were studied. In this thesis we incorporated the dispersive reflectivity parameter (m), which accounts for the grating nonuniformities, into the nonlinear coupled mode equations to generalize the model. The effects of the dispersive reflectivity on the profiles, stability and interactions of gap solitons in the system were investigated in details.

Analytical expressions of the bandgap were derived in both laboratory and moving frames. We showed that when $0 < m < 0.5$ bandgap is independent of m, however for $m > 0.5$ the bandgap shrinks with increase of m. It was also found that above a certain value of dispersive reflectivity solitons develop sidelobes, regardless of their types.

In terms of the types of solutions, the system was found to support two families of symmetric and asymmetric gap solitons that fill the entire photonic bandgap. By obtaining bifurcation diagrams we showed that for given parameters the two types of solutions bifurcate at certain coupling coefficient (λ_c). More specifically, for values

of coupling coefficient greater than λ_c symmetric solutions exist on their own, while below λ_c the two types of symmetric and asymmetric gap solitons can exist at the same time. The bifurcation theory predicts that asymmetric solitons are stable where they exist, while symmetric ones are only stable where they exist on their own.

For better insights into the characteristics of the model, gap solitons in the system were studied in two separate cases of quiescent and moving ones. In the quiescent case linear forms of coupled mode equations were solved analytically for both types of symmetric and asymmetric solitons. This led to the analytical forms of the tails of the quiescent gap soliton, where due to smaller amplitudes the nonlinear effects are negligible. From the linear analysis we also found the condition for solitons to have sidelobes. We showed that the obtained analytical solutions agree well with the exact numerical solutions except in the peak region of the soliton where nonlinearity comes into play. This is a significant achievement that can be useful in optical switching applications.

We also tried the same linear analysis for the case of moving gap solitons. The system of linear CMEs in the case of asymmetric moving solitons has not been solved yet and analytical solutions remain unknown. However, in the case of symmetric moving solitons, we were able for the first time to solve the linear system analytically, resulting in excellent approximate solutions for the symmetric moving solitons tails.

The stability of symmetric and asymmetric gap solitons were investigated using systematic numerical simulations. Whether quiescent or moving, we found that when $m = 0$ asymmetric gap solitons are stable for $\omega \gtrsim 0$. However with increase of m stable region expands into negative frequencies. Symmetric solitons, on the other hand, are stable only if they exist on their own. The results were found to be in excellent agreement with the predictions drawn from the bifurcation theory.

It is concluded that dispersive reflectivity generally results in the stabilization of the gap solitons and the expansion of the stability region. We also found that as

the coupling coefficient λ increases the stabilization effect of dispersive reflectivity is reduced. The stabilizing effect of dispersive reflectivity was also verified using bifurcation theory. More specifically, we found that as m increases λ_c decreases which broadens the region where symmetric stable gap solitons exists.

Interactions of quiescent solitons in the model were studied using systematic numerical analysis. In the case of in-phase solitons, it was found that the interactions may result in various outcomes such as merger into a single quiescent soliton, destruction of solitons, formation of a bound state that eventually breaks up into two separating solitons, formation of two moving and one quiescent soliton and repulsion of solitons. A key finding was that destruction and $2 \rightarrow 3$ transformation can occur even if dispersive reflectivity is absent. To the best of our knowledge, such outcomes have not been reported in the other models of gap solitons in the absence of dispersive reflectivity. Therefore, one can conclude that these outcomes are specific to this model and arise as a result of the coupling between the gratings.

We also considered the effect of the initial separation on the outcome of the interactions. It was found that, for both in-phase and π-out-of-phase cases, when gap solitons do not have sidelobes in their profiles the outcome of interactions are weakly dependent on the initial separation. On the other hand, the interactions of gap solitons with sidelobes are strongly dependent on the initial separation.

In the case of moving gap solitons, we found that collisions feature rich dynamics. In-phase collisions of moving solitons were investigated and several outcomes were identified among which merger of the solitons into a single quiescent and $2 \rightarrow 3$ transformation are the most interesting ones. It was shown that three soliton generation is more likely to happen when coupling coefficient is stronger. Slow symmetric solitons were found to pass through each other in inelastic collisions while faster ones may generate three solitons for larger dispersive reflectivity.

Colliding out-of-phase solitons were generally found to repel each other. Another

finding was that when dispersive reflectivity is weak the collisions are usually elastic while for strong dispersive reflectivity solitons lose energy in the form of radiation during and after the collisions.

7.2 Future Work

There are areas that we identified throughout this thesis which may be further investigated in the form of new research projects. Here we briefly point these areas out.

One interesting finding in the study of the collisions of moving gap solitons was that quiescent gap solitons may be generated as a result of the collisions under controlled conditions. In this thesis we investigated in-phase and out-of-phase collisions of pulses with identical velocities and frequencies. In practice, the colliding pulses may become slightly out of phase or have unequal velocities or slightly different frequencies. Collisions of such solitons give more insight into the system's dynamics.

In this thesis we considered identical nonuniformities in the two cores using the same dispersive reflectivity parameter. However, in reality due to the random nature of nonuniformities, dispersive reflectivity may vary from one core to the other. Therefore, one may solve the coupled mode equations incorporating m_1 and m_2 accounting for different nonuniformities in the cores. This will add one more parameter to the system of equations and may result in new features of gap soliton interactions in the model.

Bibliography

[1] K. Porsezian, V.C. Kuriakose, "*Optical Solitons Theoretical and Experimental Challenges*," Lecture Notes in Physics **613** (2003).

[2] W. G. French, J. B. MacChensey, P. B. O'Conor, and G. W. Tasker, "Low-loss optical waveguides with pure fused SiO2 cores," *Bell Syst. Tech. J.* **53**, 951 (1974).

[3] T. Miya, Y. Terunuma, T. Hosaka, and T. Miyashita, "Ultimate low-loss single-mode fibre at 1.55 μm," *Electron. Lett.* **15**, 106 (1979).

[4] G. P. Agrawal, "*Nonlinear Fiber Optics*," Academic Press, 4th Edition (2007).

[5] A. R. Chraplyvy and R. W. Tkach, "Terabit/Second Transmission Experiments," *IEEE J. Quantum Elec.* **34** (11), 2103 (1998).

[6] J. S. Russell, "Report on Waves," *Report of the Fourteenth meeting of the British Association for the Advancement of Science*, York, 311 (1844).

[7] N. J. Zabusky, M. D. Kruskal, "Interaction of 'solitons' in a collisionless plasma and the recurrence of initial states," *Phys. Rev. Lett.* **15** (6), 240 (1965).

[8] Clifford S. Gardner, John M. Greene, Martin D. Kruskal, and Robert M. Miura, "Method for Solving the Korteweg-deVries Equation," *Phys. Rev. Lett.* **19**, 1095 (1967).

[9] M. J. Ablowitz and H. Segur, "*Solitons and the Inverse Scattering Transform*," SIAM, Philadelphia (1981).

[10] Wikipedia, "Nonlinear Schrödinger Equation," http://en.wikipedia.org/wiki/Nonlinear _Schrödinger_equation.

[11] A. Hasegawa and F. Tappert, "Transmission of stationary nonlinear optical pulses in dispersive dielectric fibers. I. Anomalous dispersion," *Appl. Phys. Lett.* **23**, 142 (1973).

[12] A. Hasegawa and F. Tappert, Transmission of stationary nonlinear optical pulses in dispersive dielectric bers. II. Normal dispersion," *Appl. Phys. Lett.* **23**, 171 (1973).

[13] L. F. Mollenauer, R. H. Stolen, and J. P. Gordon, "Experimental observation of picosecond pulse narrowing and solitons in optical fibers," Phys. Rev. Lett. **45**, 1095 (1980).

[14] H. G. Winful, J. H. Marburger and E. Garmire, "Theory of bistability in nonlinear distributed feedback structures," *Appl. Phys. Lett.* **35**, 379 (1979).

[15] W. Chen and D. L. Mills, "Gap solitons and the nonlinear optical response of superlattices," *Phys. Rev. Lett.* **58**, 160 (1987).

[16] B.A. Malomed, R.S. Tasgal, "Vibration modes of a gap soliton in a nonlinear optical medium," *Phys. Rev.* E **49**, 5787 (1994).

[17] I.V. Barashenkov, D.E. Pelinovsky, E.V. Zemlyanaya, "Vibrations and Oscillatory Instabilities of Gap Solitons," *Phys. Rev. Lett.* **80**, 5117 (1998).

[18] J. T. Mok, C. M. de Sterke, I. C. M. Litter and G. J. Eggleton, "Dispersionless slow light using gap solitons," *Nature Phys.* **2**, 775 (2006).

[19] C. M. de Sterke, J. E. Sipe, "Gap Solitons," *Prog. Opt.* **33**, 203 (1994).

[20] A.B. Aceves and S. Wabnitz, "Self-induced transparency solitons in nonlinear refractive periodic media," *Phys. Lett.* A **141**, 37 (1989).

[21] D. N. Christodoulides and R. I. Joseph, "Slow Bragg solitons in nonlinear periodic structures," *Phys. Rev. Lett.* **62**, 1746 (1989).

[22] P. St. J. Russell, "Bloch wave analysis of dispersion and pulse propagation in pure distributed feedback structures," *J. Mod. Opt.* **38**, 1599 (1991).

[23] A. De Rossi, C. Conti, and S. Trillo, "Stability, Multistability, and Wobbling of Optical Gap Solitons," *Phys. Rev. Lett.* **81**, 85 (1998).

[24] B.J. Eggleton, R.E. Slusher, C.M. De Sterke, P. A. Krug, and J. E. Sipe, "Bragg Grating Solitons," *Phys. Rev. Lett.* **76**, 1627 (1996).

[25] B.J. Eggleton, C.M. De Sterke, and R.E. Slusher, "Nonlinea pulse propagation in Bragg gratings," *J. Opt. Soc. Am. B* **14**, 2980 (1997).

[26] B. B. Baizakov, V. V. Konotop and M. Salerno, "Regular spatial structures in arrays of Bose–Einstein condensates induced by modulational instability," *J. Phys. B: At. Mol. Opt. Phys.* **35,** 5105 (2002).

[27] E. A. Ostrovskaya and Y. S. Kivshar, "Matter-wave gap solitons in atomic band-gap structures," *Phys. Rev. Lett.* **90**, 160407 (2003).

[28] V. A. Brazhnyi and V. V. Konotop, "Theory of Nonlinear Matter Waves in Optical Lattices," *Mod. Phys. Lett.* **18**, 627 (2004).

[29] B. Eiermann, T. Anker, M. Albeiz, M. Taglieber, P. Treutlin, K. P. Marzlin and M. K. Oberthaler, "Bright Bose-Einstein gap solitons of atoms with repulsive interaction," *Phys. Rev. Lett.* **92** 230401 (2004).

[30] A. Gubeskys, B. A. Malomed and I. M. Merhasin, "Two-component gap solitons in two- and one-dimensional Bose-Einstein condensates," *Phys. Rev.* A **73** 023607 (2006).

[31] R. Kashyap, "*Fiber Bragg Gratings*," Academic Press (1999).

[32] W. H. Loh, R. I. Laming, N. Robinson, A. Cavaciuti, F. Vaninetti, C. J. Anderson, M. N. Zervas, and M. J. Cole, "Dispersion compensation over distances in excess of 500 km for 10 Gb/s systems using chirped fiber gratings," IEEE *Photon. Technol. Lett.* **8**, 944 (1996).

[33] Krug P. A., Stephens T., Dhosi G., Yoffe G., Ouellette F. and Hill P., "Dispersion compensation over 270 km at 10 Gbit/s using an offset-core chirped fibre Bragg grating," *Electron. Lett.* **31**, 1091 (1995).

[34] S. Radic, N. George and G. P. Agrawal, "Theory of low-threshold optical switching in nonlinear phase-shifted periodic structures," *J. Opt. Soc. Am.* B **12**, 671 (1995).

[35] M. Aslund, L. Poladian, J. Canning, C. M. de Sterke, "Add-Drop Multiplexing By Dispersion Inverted Interference Coupling," *J. Lightwave Technol.* **20**, 1585 (2002).

[36] Y. J. Rao, "In-fibre Bragg grating sensors," *Measurement Science and Technology* **8**, 355 (1999).

[37] G. P. Agrawal, "*Applications of Nonlinear Fiber Optics*," 2nd Edition, Academic Press (2008).

[38] M. N. Zervas, "*Fiber Bragg Gratings for Optical Fiber Communications,*" Wiley, Hoboken, NJ, (2001).

[39] H. G. Winful and G. D. Cooperman, "Self-pulsing and chaos in distributed feedback bistable optical devices," *Appl. Phys. Lett.* **40**, 298 (1982).

[40] S. M. Jensen, "The nonlinear coherent coupler," *IEEE J . Quantum Electron.* **18**, 1580 (1982).

[41] A. W. Snyder, Y. Chen, "Nonlinear fiber couplers: switches and polarization beam splitters," *Optics Lett .* **14**, 517 (1989).

[42] A. Mecozzi, S. Trillo, S. Wabnitz, and B. Daino, *Optics Lett.* **12**, 275 (1987); S. Trillo, S. Wabnitz, W. C. Banyai, N. Finlayson, C. T. Seaton, G. I. Stegman, and R. H. Stolen, I*EEE J . quantum Electron.* **25**, 104 (1989).

[43] A. Yariv, P. Yeh, "*Optical Waves in Crystals: Propagation and Control of Laser Radiation*," Wiley (1984).

[44] D. Marcuse, "Directional couplers made of nonidentical asymmetric slabs. Part II: Grating-assisted couplers," *J. Lightwave Technol.* **5** (2), 268 (1987).

[45] J. Atai and Y. Chen, "Nonlinear couplers composed of different nonlinear cores," *J. Appl. Phys.* **72**, 24 (1992).

[46] J. Atai and Y. Chen, "Nonlinear mismatches between two cores of saturable nonlinear couplers," *IEEE J. Quantum Elec.* **29** (1), 242 (1993).

[47] Yijiang Chen, "Grating-assisted Nonlinear Couplers," *J. Modern Opt.* **38** (9), 1731 (1991).

[48] S. S. Orlov, A. Yariv, and S. van Essen, "Coupled-mode analysis of fiber-optic add drop filters for dense wavelength-division multiplexing," *Opt. Lett.* **22**, 688 (1997).

[49] Y. J. Chen and A. W. Snyder, "Grating-assisted couplers," *Opt. Lett.* **16**, 217 (1991).

[50] A. S. Kewitsch, G. A. Rakuljic, P. A. Willems, and A. Yariv, *Opt. Lett.* **23**, 106 (1998).

[51] J. Capmany, P. Munoz, D. Pastor, "Optimum Design and Performance Evaluation of an All-Fiber Add-Drop Multiplexer Based on a Grating Coupler," *IEEE Selected Topics in Quantum Elec.* **5** (5), 1392 (1999).

[52] David K. Cheng, *"Field and Wave Electromagnetics*," 2nd Edition, Addison-Wesley (2004).

[53] G. Boudebs, S. Cherukulappurath, H. Leblond, J. Troles, F. Smektala, and F. Sanchez, "Experimental and theoretical study of higher-order nonlinearities in Chalcogenide glasses," *Opt. Comm.* **219**, 427 (2003).

[54] S. Dasanayaka and J. Atai, "Stability of Bragg grating solitons in a cubic-quintic nonlinear medium with dispersive reflectivity," *Physics Letters A* **375**, 225 (2010).

[55] G. Keiser, "*Optical Fiber Communication*s," 3rd edition, McGraw Hill (2000).

[56] J. Gowar, "*Optical Communication Systems*," Prentice Hall (1993).

[57] P. N. Butcher, D. Cotter, "*The Elements of Nonlinear Optics*," Cambridge University Press, Cambridge (1990).

[58] D. Marcuse, "*Theory of Dielectric Optical Waveguides*," Academic Press, 2nd ed., Chap. 3 (1991).

[59] D. Taverner, N. G. R. Broderick, D. J. Richardson, R. I. Laming, and M. Ibsen, "Nonlinear self-switching and multiple gap-soliton formation in a fiber Bragg grating," *Opt. Lett.* **23**, 328 (1998).

[60] C. M. de Sterke, B. J. Eggleton, and P. A. Krug, "High-intensity pulse propagation in uniform gratings and grating superstructures," *J. Lightwave Technol.* **15** 1494 (1997).

[61] Y. J. Tsofe and B. A. Malomed, "Quasisymmetric and Asymmetric Gap Solitons in Linearly Coupled Bragg Gratings With a Phase Shift," *Phys. Rev. E* **75**, 56603 (2007).

[62] S. Radic, N. George, and G. P. Agrawal "Low-threshold optical switching in non-uniform, nonlinear, distributed feedback structures," *Opt. Photon. News* **6** (12), 18 (1995).

[63] B. J. Eggleton, P. A. Krug, L. Poladian, and F. Ouellette, "Long periodic superstructure Bragg gratings in optical fibres," *Electron. Lett.* **30**, 1620 (1994).

[64] E. N. Tsoy and C. M. de Sterke, "Propagation of Nonlinear Pulses in Chirped Fiber Gratings," *Phys. Rev.* E **62**, 2882 (2000).

[65] C. M. de Sterke, "Wave Propagation Through Nonuniform Gratings with Slowly Varying Parameters," *J. Lightwave Technol.* **17** (11), 2405 (1999).

[66] N. M. Litchinitser, B. J. Eggleton, C. M. de Sterke, A. B. Aceves, and G. P. Agrawal, "Interaction of Bragg solitons in fiber gratings," *J. Opt. Soc. Am.* B **16**, 18 (1999).

[67] J. Atai and B. A. Malomed, "Gap solitons in Bragg Gratings with Dispersive Reflectivity," *Phys. Lett. A* **342**, 404 (2005).

[68] N. G. R. Broderick and C. M. de Sterke, "Theory of grating superstructures," *Phys. Rev.* E **55**, 3634 (1997).

[69] D. Janner, G. Galzerano, G. Della Valle, P. Laporta, and S. Longhi, "Slow light in periodic superstructure Bragg gratings," *Phys. Rev.* E **72**, 056605 (2005).

[70] M. Gnan, G. Bellanca, H. M. H. Chong, P. Bassi and R. M. De la Rue, "Modelling of Photonic Wire Bragg Gratings," *Opt. Quantum Electron.* **38**, 133 (2006).

[71] K. Levy and B. A. Malomed, "Stability and collisions of traveling solitons in Bragg-grating superstructures," *J. Opt. Soc. Am.* B **25**, 302 (2008).

[72] D. R. Neill, J. Atai, and B. A. Malomed, "Dynamics and Collisions of Moving Solitons in Bragg Gratings with Dispersive Reflectivity," *J. Opt. A: Pure Appl. Opt.* **10**, 085105 (2008).

[73] B. H. Baratali and J. Atai, "Gap solitons in Dual-Core Bragg Gratings with Dispersive Reflectivity," *J. Opt.* **14**, 065202 (2012).

[74] B. H. Baratali and J. Atai, "Dynamics of interacting solitons in dual core Bragg gratings with dispersive reflectivity," *J. Appl. Phys.* **115**, 153112 (2013).

[75] S. Dasanayaka, "Soliton Dynamics in Uniform and Non-uniform Bragg Gratings with Cubic-Quintic Nonlinearity," PhD Thesis, Page 24, Faculty of Engineering and Information Technologies, University of Sydney (2013).

[76] J. Atai and B. A. Malomed, "Families of Bragg-grating solitons in a cubic-quintic medium," *Phys. Lett.* A **284**, 247 (2001).

[77] W. Mak, B.A. Malomed and P. L. Chu, "Solitary waves in coupled nonlinear waveguides with Bragg gratings," *J. Opt. Soc. Am.* B **15**, 1685 (1998).

[78] V. Pereyra, "PASVA3: An adaptive finite-difference FORTRAN program for first order nonlinear, ordinary boundary problems," *Codes for Boundary Value Problems in Ordinary Differential Equations. Lecture Notes in Computer Science* **76**, 67 (1979) Springer-Verlag.

[79] S. S. Rao, *"Applied Numerical Methods for Engineers and Scientists,"* Prentice Hall, 1st Edition (2001).

[80] Xin-Hua Wang, "*Finite Element Methods for Nonlinear Optical Waveguides - Advances in nonlinear optics Volume 2,*" CRC Press (1996).

[81] V. E. Zakharov and A. B. Shabat, "Exact theory of two-dimensional self-focusing and one-dimensional self-modulation of waves in nonlinear media," *Soviet Physics - JETP* **34**, 62 (1972).

[82] Q. Chang, E. Jia, and W. Sun, "Different schemes for solving the generalized nonlinear Schrödinger equation," *Journal of Computational Physics* **148**, 397 (1999).

[83] T. R. Taha and M. J. Ablowitz, "Analytical and Numerical Aspects of Certain Nonlinear Evolution Equations. II. Numerical, Nonlinear Schrodinger Equation," *J. Comp. Phys.* **55**, 203 (1984).

[84] J. W. Cooley and J. W. Tukey, "An Algorithm for the Machine Calculation of Complex Fourier Series," *Math. Comput.* **19**, 297 (1965).

[85] R. H. Hardin and F.D. Tappert, "Applications of the split-step Fourier method to the numerical solution of nonlinear and variable coefficient wave equations," *SIAM Rev.* **15**, 423 (1973).

[86] R. A. Fisher and W. K. Bischel, "Numerical studies of the interplay between self-phase modulation and dispersion for intense plane-wave laser pulses," *Appl. Phys. Lett.* **23**, 661 (1973); *J. Appl. Phys.* **46**, 4921 (1975).

[87] Z. Toroker and M. Horowitz, "Optimized split-step method for modeling nonlinear pulse propagation in fiber Bragg gratings," *J. Opt. Soc. Am.* B **25**, 448 (2008).

[88] J. A. Fleck, J. R. Morris, and M. D. Feit, "Time-dependent propagation of high energy laser beams through the atmosphere," *Appl. Phys.* **10**, 129 (1976).

[89] E. Süli and D. Mayers, "*An Introduction to Numerical Analysis*," Cambridge University Press (2003).

[90] S.D. Gedney, "An anisotropic perfectly matched layer absorbing media for the truncation of FDTD latices," *Ant. and Prop., IEEE Trans.* **44** (12), 1630 (1996).

[91] S. Dasanayaka and J. Atai, "Interactions of solitons in Bragg gratings with dispersive reflectivity in a cubic-quintic medium," *Phys. Rev. E* **84**, 026613 (2011).

[92] L. Khaykovich and B. A. Malomed, "Deviation from one dimensionality in stationary properties and collisional dynamics of matter-wave solitons," *Phys. Rev.* A **74**, 023607 (2006).

[93] W. Królikowski and S.A. Holmstrom, "Fusion and Birth of Spatial Solitons Upon Collision," *Opt. Lett.* 22, **369** (1997).

[94] J. Meier, G.I. Stegeman, Y. Silberberg, R. Morandotti, and J.S. Aitchison, "Nonlinear Optical Beam Interactions in Waveguide Arrays," *Phys. Rev. Lett.* **93**, 093903 (2004).

[95] Y. Chen and J. Atai, "Parametric spatial solitary waves," *Opt. Lett.* **19**, 1287 (1994).

[96] W. C. K. Mak, B. A. Malomed, and P. L. Chu, "Formation of a standing-light pulse through collision of gap solitons," *Phys. Rev. E* **68**, 026609 (2003).

[97] D. R. Neill and J. Atai, "Collision dynamics of gap solitons in Kerr media," *Phys. Lett.* A **353**, 416 (2006).

[98] D. Taverner, N. G. R. Broderick, D. J. Richardson, M. Ibsen, and R. I. Laming, "All-optical AND gate based on coupled gap-soliton formation in a fiber Bragg grating," *Opt. Lett.* **23** (4), 259 (1998).

[99] S. Lee and S. T. Ho, "Optical switching scheme based on the transmission of coupled gap solitons in nonlinear periodic dielectric media," *Opt. Lett.* **18** (12), 962 (1993).

[100] R. Shnaiderman, Richard S. Tasgal, and Y. B. Band, "Creating very slow optical gap solitons with a grating-assisted coupler," *Opt. Lett.* **36** (13), 2438 (2011).

[101] I. V. Mel'nikova and J. S. Aitchison, "Gap soliton memory in a resonant photonic crystal," *Appl. Phys. Lett.* **87,** 201111 (2005).

[102] I.V. Mel'nikov, A. Knigavko, J.S. Aitchison, and C.A. Merchant, "Generation of slow intense optical solitons in a resonance photonic crystal," Eur. Phys. J. Special Topics **160**, 301 (2008).

[103] William C. K. Mak, Boris A. Malomed, and Pak L. Chu, "Interaction of a soliton with a local defect in a fiber Bragg grating," *J. Opt. Soc. Am.* B **20** (4), 725 (2003).

[104] G. Bartolini, R.-D. Li, P. Kumar, W. Riha and K. V. Reddy, "1.5 μm phase-sensitive amplifier for high-speed communications," *Optical Fiber Communication Conference*, Vol. 4, OSA Technical Digest Series, Washington D.C., 202 (1994).

[105] A. Mecozzi, W. L. Kath, P. Kumar, and C. G. Goedde, "Long-term storage of a soliton bit stream by use of phase-sensitive amplification," *Optics Lett.* **19** (24), 2050 (1994).